CONSTRUCTION OF SEDIMENT BUDGETS IN LARGE SCALE DRAINAGE BASINS: THE CASE OF THE UPPER INDUS RIVER

A Thesis Submitted to the College of

Graduate Studies and Research

in Partial Fulfillment of the Requirements

for the Degree of Doctor of Philosophy

in the Department of Geography and Planning

University of Saskatchewan

Saskatoon

By

Khawaja Faran Ali

PERMISSION TO USE

In presenting this thesis in partial fulfillment of the requirements for a Postgraduate degree from the University of Saskatchewan, I agree that the Libraries of this University may make it freely available for inspection. I further agree that permission for copying of this thesis in any manner, in whole or in part, for scholarly purposes may be granted by the professors who supervised my thesis work or, in their absence, by the Head of the Department or the Dean of the College in which my thesis work was done. It is understood that any copying or publication or use of this thesis or parts thereof for financial gain shall not be allowed without my written permission. It is also understood that due recognition shall be given to me and to the University of Saskatchewan in any scholarly use which may be made of any material in my thesis.

Requests for permission to copy or to make other uses of materials in this thesis in whole or part should be addressed to:

Head of the Department of Geography and Planning

University of Saskatchewan

Saskatoon, Saskatchewan S7N 5C8

Canada

ABSTRACT

High rates of soil loss and high sediment loads in rivers necessitate efficient monitoring and quantification methodologies so that effective land management strategies can be designed. Constructing a sediment budget is a useful approach to address these issues. Quantifying a sediment budget using classical field-based techniques, however, is labour intensive and expensive for poorly gauged, large drainage basins. The availability of global environmental datasets in combination with GIS techniques provides an opportunity for studying large basins. Following this approach, a framework is presented for constructing sediment budgets for large, data-sparse drainage basins, which is applied to the mountainous upper Indus River basin in northern Pakistan. The methodological framework consists of five steps: (1) analyzing hydro-climatological data for dividing the drainage basin into characteristic regions, and calculating sediment yields; (2) investigation of major controls on sediment yields; (3) identification and mapping of sediment source areas by spatially distributed modelling of erosional processes; (4) spatially distributed modelling of sediment yields; and (5) carrying out the sediment budget balance calculation at the basin outlet. Further analysis carried out on the Indus data has enabled a better understanding of sediment dynamics in the basin.

Analysis of the available hydro-climatological data indicates that the basin can be subdivided into three characteristic regions based on whether runoff production and subsequent sediment generation is controlled by temperature (Region 1, upper, glacierized sub-basins), precipitation caused by the monsoon and western disturbances (Region 3, lower sub-basins), or a combination of the two (Region 2, middle reach sub-basins). It is also demonstrated that contrary to the

conventional model, the specific sediment yield increases markedly with drainage area along the Indus River. An investigation of major controls on specific sediment yield in the basin indicates that percent snow/ice cover is a major land cover control for specific sediment yield. Spatially distributed erosion modelling predictions indicate that 87% of the annual gross erosion takes place in the three summer months with greatest erosion potential concentrated in sub-basins with high relief and a substantial proportion of glacierized area. Lower erosion rates can be explained by the arid climate and low relief on the Tibetan Plateau, and by the dense vegetation and lower relief in the lower monsoon sub-region. The model predicts an average annual erosion rate of 3.2 mm a^{-1} or 868 Mt a^{-1}. Spatially distributed sediment yield predictions made with coupled models of erosion and sediment delivery indicate that the Indus sub-basins generally show an increase of sediment delivery ratio with basin area. The predicted annual basin sediment yield is 244 Mt a^{-1} and the overall sediment delivery ratio in the basin is calculated as 0.28. The long-term mean annual sediment budget, based on mass balance, is characterized by a gross erosion of 762.9, 96.7 and 8.4 Mt, and a gross storage of 551.4, 66.1, and 6.5 Mt in the upper, middle, and lower regions of the basin, respectively. The sediment budget indicates that the major sources of eroded sediment are located in the Karakoram, in particular in the Hunza basin. Substantial sediment storage occurs on the relatively flat Tibetan Plateau and the Indus River valley reach between Partab Bridge and Shatial. The presented framework for sediment budget construction requires relatively few data, mostly derived from global datasets. It therefore can be utilized for other ungauged or poorly gauged drainage basins of the world.

ACKNOWLEDGEMENT

First and foremost, I would like to thank my supervisor Dr. Dirk de Boer for years of guidance, mentoring, and encouragement. Without his invaluable help, I could never have completed this dissertation. I am grateful to my committee members, Dr. Alec Aitken, Dr. Xulin Guo, Dr. Lawrence Martz, and Dr. Charles Maulè for their assistance and guidance and for devoting their valuable time to serve on my Ph.D. program. I also wish to express my gratitude to my fellow students and staff in the Department of Geography and Planning for their help in my research.

Finally I am deeply grateful to my parents, my wife (Aisha) and kids (Hamza and Talha). Without their love, support and encouragement, none of my achievements would have been possible.

TABLE OF CONTENTS

Page

LIST OF TABLES

LIST OF FIGURES

CHAPTER 1 – INTRODUCTION

1.1 Research Background

1.1.1 Sediment Budgets

High mountain regions like the Himalayas are characterized by a high rate of denudation, reaching values to 6 mm a^{-1} (Cornwell *et al*., 2003), with river systems like the Ganges-Brahmaputra and the Indus acting as the conduits for sediment transfer. High erosion rates and high sediment loads in these rivers present challenges to resource management, and necessitate the design of effective monitoring and quantification methodologies. Sediment budgeting is emerging as an essential prerequisite for the development of effective sediment management and control strategies (Walling and Horowitz, 2005). Sediments budgets are a useful and powerful conceptual framework for examining the relationships between sources, sinks, fluvial transport and sediment yield, and investigating how these relationships are affected by changes in land use, climate, seismicity and isostatic adjustment (Wasson, 2002). Reid and Dunne (1996, p. 3) have defined a sediment budget as "an accounting of the sources and disposition of sediment as it travels from its point of origin to its eventual exit from a drainage basin." A detailed sediment budget accounts for rates and processes of erosion and sediment transport on hillslopes and in channels, for temporary storage of sediment, and for weathering of sediment while in transport or

storage (Dietrich *et al*., 1982). Figure 1.1 below presents a flowchart that indicates the typical relationship between sediment mobilization, production, deposition, and yield.

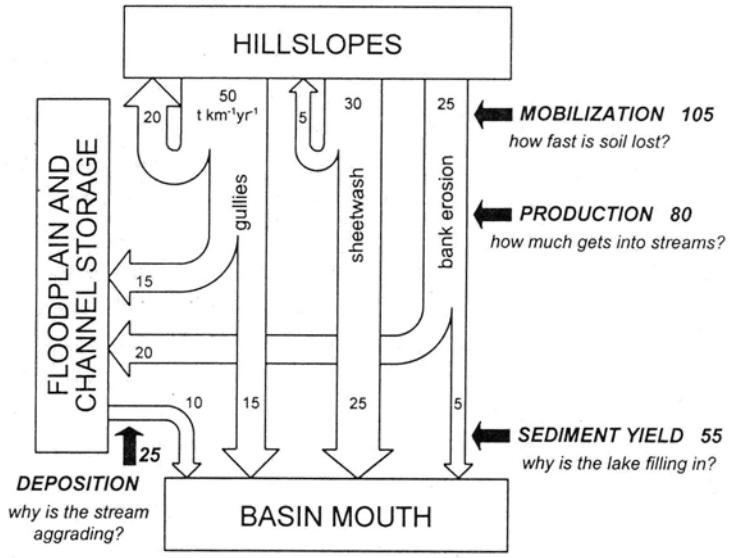

Figure 1.1 A flowchart indicating typical relationship between sediment mobilization, production, deposition, and yield (after Reid and Dunne, 1996)

The sediment budget equation in the form:

$$I = O + \Delta S \tag{1.1}$$

where I is input, O is output, and ΔS is the change of storage, can describe the routing of clastic and dissolved sediment over a specified time increment and with respect to a particular storage reservoir (Slaymaker, 1993).

Sediment budgets are useful tools for addressing a number of scientific and management problems that involve predicting changes in erosion and sedimentation in response to changes on the slopes and in the channel system as a result of changes in land use and climate (Reid and Dunne, 2003; Walling and Collins, 2008; Trimble, 2009). Sediment budgets are not an alternative to monitoring; however, budgeting can complement monitoring programs, whereas monitoring can be used to refine budget estimates. Moreover, empirical results from sediment budgeting studies may be transferred to other watersheds with similar climate, geology, soils, and land use. Sediment budgeting is a more comprehensive technique than sediment yield estimation (Sutherland and Bryan, 1991) because sediment yield is sometimes not responsive to storage, erosion rate, or land use changes in the drainage basin (Trimble, 1999). According to Phillips (1991), sediment budget is the most sensitive indicator of a basin response to environmental change and considered to be the single most important piece of information about a fluvial system.

1.1.2 Techniques for Constructing Sediment Budgets

According to Reid and Dunne (1996), efficient budget construction incorporates the following seven steps in a typical conventional method: 1) careful definition of the problem to be addressed; 2) collection of background information; 3) subdivision of the project area into uniform sub-areas; 4) interpretation of aerial photographs; 5) field work; 6) data analysis; and 7) checking of results. Conventional sediment budget construction techniques include: 1) field studies with experimental plots to establish basic principles and measure rates of erosion; 2) measuring sediment loads at catchment outlets and then relating them to soil erosion using

sediment delivery ratios; and 3) using anthropogenic (^{137}Cs) and naturally-occurring (^{210}Pb) radioactive elements. There is, however, no widely accepted or generally applicable procedure for establishing a comprehensive sediment budget for a drainage basin, because it has proved difficult to adapt traditional measurement techniques to address the spatial and temporal variability associated with the operation of sediment mobilization and transfer processes at the drainage basin scale (Walling and Collins, 2008). Sediment budget construction requires identification of erosion processes and their controls, and estimation of process rates. This task of quantifying and relating the major processes responsible for the generation and transportation of sediment is difficult because the processes are often slow and highly variable in time and space (Dietrich and Dunne, 1978). Field-based methodologies are more suited to small scale drainage basins (e.g., Dietrich and Dunne, 1978; Kelsey, 1980; Swanson *et al.*, 1982; Roberts and Church, 1986; Rawat, 1987; Campbell *et al*., 1988; Sutherland and Bryan, 1991; Phillips, 1991; Slaymaker, 1993; Trimble, 1999; and Bartley *et al*., 2007). Field-based studies of sediment budgets are frequently hampered by the limited availability of data, both in terms of quality and quantity, which raises the question of the representativeness of the dataset for larger or smaller basins over longer periods of time (De Boer and Ali, 2002). Integration of GIS and remote sensing has emerged as a useful tool for studying large basins (e.g. Lu and Higgitt, 1999; Gupta *et al*., 2002) and it provides new insights in sediment budgets (Wasson, 2002). The emerging GIS and remote sensing techniques in combination with fine resolution global datasets can prove to be very useful for sediment budget studies (Ali and De Boer, 2003; Ramos-Scharrón and MacDonald, 2007; Rustomji *et al*., 2008).

1.1.3 Need of Research in Sediment Budgets

Basin scale sediment budgets involve a wide variety of erosional, depositional and transport processes over varying spatial and time scales. Field observations over a wide range of timescales and modeling of sediment fluxes are required for a clear understanding of how erosional and depositional landscapes are linked by the sediment-routing system (Slaymaker, 2006; Allen, 2008). Sediment budget studies have mostly dealt with relatively small drainage basins ranging from a few hectares to a few hundred square kilometers (Phillips, 1991). Reid and Dunne (1996) have cited studies that encompass basin areas ranging from 38 to 21,000 km^2. The expense and logistical problems associated with the construction of sediment budgets for large river basins pose quite a few challenges, including identification and quantification of sediment source areas, measurement of river loads, and data sparsity. While identification of sediment sources in often difficult, aerial photography, field mapping or fingerprinting methods and tracer techniques can complement field inspection and give some valuable information for small catchment scale studies (Coleman and Scatena, 1986; Schmidt and Ergenzinger, 1994; Peart and Walling, 1986; 1988; Symader and Strunk, 1993). Quantification of sediment sources, however, remains a major challenge in constructing a sediment budget for a large river basin (Brown *et al*., 2009; Wilkinson *et al*., 2009). A few sediment budget studies carried out for large river basins have reflected upon these difficulties, including Parker (1988), Kesel *et al*. (1992), Holmes Jr. (1997), Rondeau *et al*. (2000), Wasson (2003), Shi and Zhang (2005), Garzanti *et al*. (2006) Wang *et al*. (2007), and Xu (2008). For example, the sequence of daily sediment stations provides a unique database for the Missouri River where concurrent records are available since 1940s. Even with this good quality data, however, natural variability provides substantial

uncertainty in terms of the sediment budget (Parker, 1988). This requires attention to devising simplified methods, models or means of estimating erosion and sediment yield in large drainage basins.

Another important aspect is the diversity of locations of sediment budget studies. Sutherland and Bryan (1991) have noticed that sediment budgets have been mostly developed for North American catchments, particularly for the west coast region of the United States like Dietrich and Dunne (1978), Kelsey (1980), Lehre (1982), Roberts and Church (1986), and Slaymaker (1993). More such budgets are required, particularly in dryland and mountain regions where they are currently under-represented (Wasson, 2002). The attributes of high mountainous rivers make them more challenging for studying their sediment dynamics (Schmidt and Ergenzinger, 1994).

According to Bordas and Walling (1988), many past studies have focused on either the erosional processes operating within a basin or the sediment yield at its outlet. There is a need to integrate the two and to establish sediment budgets that attempt to quantify the relationships between the various components of the erosion-transport-deposition system in the drainage basin. From a management perspective, it is therefore essential to consider the sediment system in its entirety, as opposed to focusing on the downstream fluxes (Walling and Collins, 2008).

1.2 Study Area: The Upper Indus River Basin

The Indus River is one of the longest rivers in southern Asia (Ahmad, 1993; Meadows and Meadows, 1999), with a total length of 2880 km and a drainage area of 912,000 km^2 extending

across portions of Pakistan, India, China and Afghanistan (Figure 1.2). The upper Indus basin upstream of Tarbela Dam is 1125 km long, with a drainage area of 219,830 km^2. The Indus River rises in the Tibetan Plateau at an elevation of 5486 m on Mount Kailash (Jain *et al*., 2007), follows a well-defined valley parallel to the geologic strike, and descends down to the Arabian Sea. Much of its flow originates in the mountains of the Karakoram and Himalayas. The major Indus tributaries include the Shyok, Shigar, and Gilgit in the upper, glacierized portion; the Astore in the middle reaches; and the Gorband, Brandu, and Siran in the lower, monsoon-affected portion. Major tectonic activity, culminating in the Himalayan orogeny during the mid-Eocene, has shaped the high relief and complex geologic structures observed in the upper Indus basin today (Molnar and Tapponnier, 1975; Miller, 1984). These young mountain ranges of extreme ruggedness and high elevations are subject to exceptionally rapid degradation by a combination of processes (Searle, 1991; Shroder, 1993; Collins and Hasnain, 1995). Widespread mass movements generated by tectonic instability, rapid weathering due to the severe climatic conditions, heavy snowfall resulting in a spring snowmelt, the action of glaciers, and catastrophic outburst floods from landslide-, moraine-, and glacier-dammed lakes are major factors in the high sediment yield observed in the basin (Ferguson, 1984; Hewitt, 1998; 2009; Shroder and Bishop, 1998). The lower, southern part of the basin experiences heavy monsoon rainfall, and rivers in this part of the basin carry large amounts of sediment associated with flash floods. Ali and De Boer (2007) provide a detailed account of the physiography, geology and tectonics, and climate of the basin. The Indus is the oldest Himalayan river known and it has not changed its course like the Ganges-Brahmaputra River Systems (Clift, 2002).

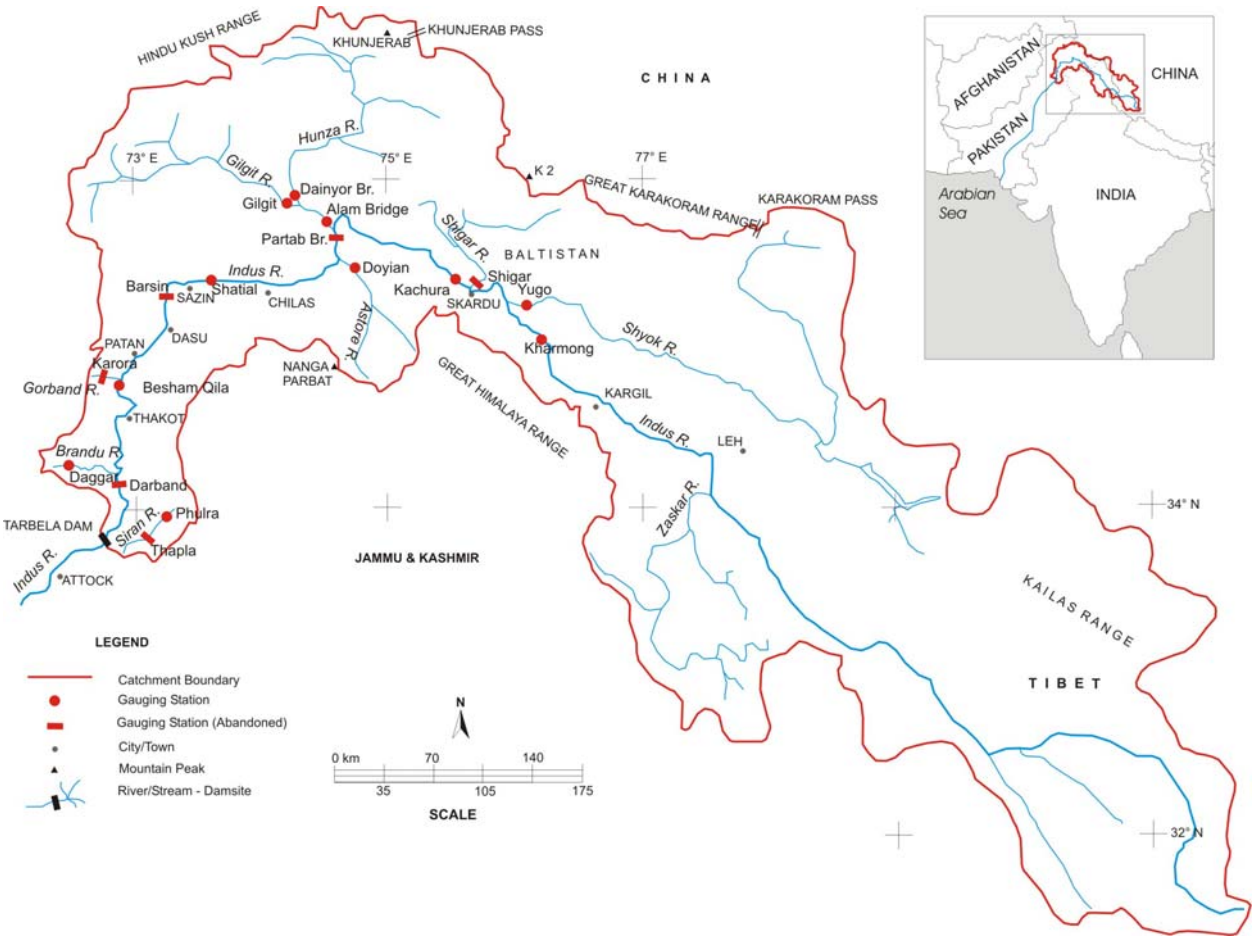

Figure 1.2 The upper Indus River basin

1.3 Research Objectives

The overall objective of this study is to develop a framework for constructing sediment budgets in large data-sparse drainage basins and apply it to the upper Indus River basin. The upper Indus represents a unique high mountainous data-sparse large river basin that still exists in its natural condition without any major human impacts and has not received much attention in the past. In view of the recent energy and water crisis in Pakistan where most of the planned

water storage and hydro power projects are located in the upper Indus basin, a sediment budget study seems to be timely and desirable. In order to address the relevant research needs and gaps in sediment budgets construction of large scale drainage basins raised in section 1.1.3, these are the aims of this study.

- To delineate spatial patterns and variation of suspended sediment yields in the upper Indus River basin based on hydro-climatological database
- To establish major controls on specific sediment yields in the basin based on numerous variables derived from global geo-spatial datasets and construction of multiple regression models for predicting sediment yields
- To develop a spatially distributed model of erosion and sediment yields in the basin
- To construct a detailed sediment budget as an accounting of the sources and disposition of sediment in the basin based on mass balance approach

1.4 Research Methodology

Sediment budget construction requires a clear understanding of sediment dynamics in the drainage basin. To gain this understanding, this study has utilized multiple data types and sources including the available hydrological records, erosion rates in the basin compiled from literature, and the recent work in the Indus basin by Ali and De Boer (2007; 2008; in review). It is argued that data sparsity of large scale drainage basins can be addressed by using simplification of plot-scale processes and utilizing global datasets available at coarser scales so that sediment budgets

can be constructed in an erosion-transport-deposition context by integrating remote sensing and GIS along with the hydrological records.

The methological framework for constructing a long-term mean annual sediment budget for the upper Indus River presented in this study consists of five distinct steps.

(1) Processing and analysis of the hydro-climatological database for dividing the drainage basin into characteristic regions and calculating sediment yields.
(2) Investigation of major controls on sediment yield and constructing multiple regression models for predicting sediment yields.
(3) Identification, mapping and quantification of sites that act as sources of sediment from spatially distributed modelling of erosion.
(4) Spatially distributed modelling of sediment yield by coupling models of erosion and sediment delivery ratios.
(5) Carrying out the sediment budget balance calculation at the basin outlet based on a mass balance approach by analyzing the amount of sediment contributed by different tributaries, on a watershed-by-watershed basis.

1.5 Thesis Structure

A schematic representation of data flow and processing is shown in Figure 1.3 which illustrates the thesis structure in terms of the division of the thesis into various chapters and their connection with each of the research objectives and methodological steps.

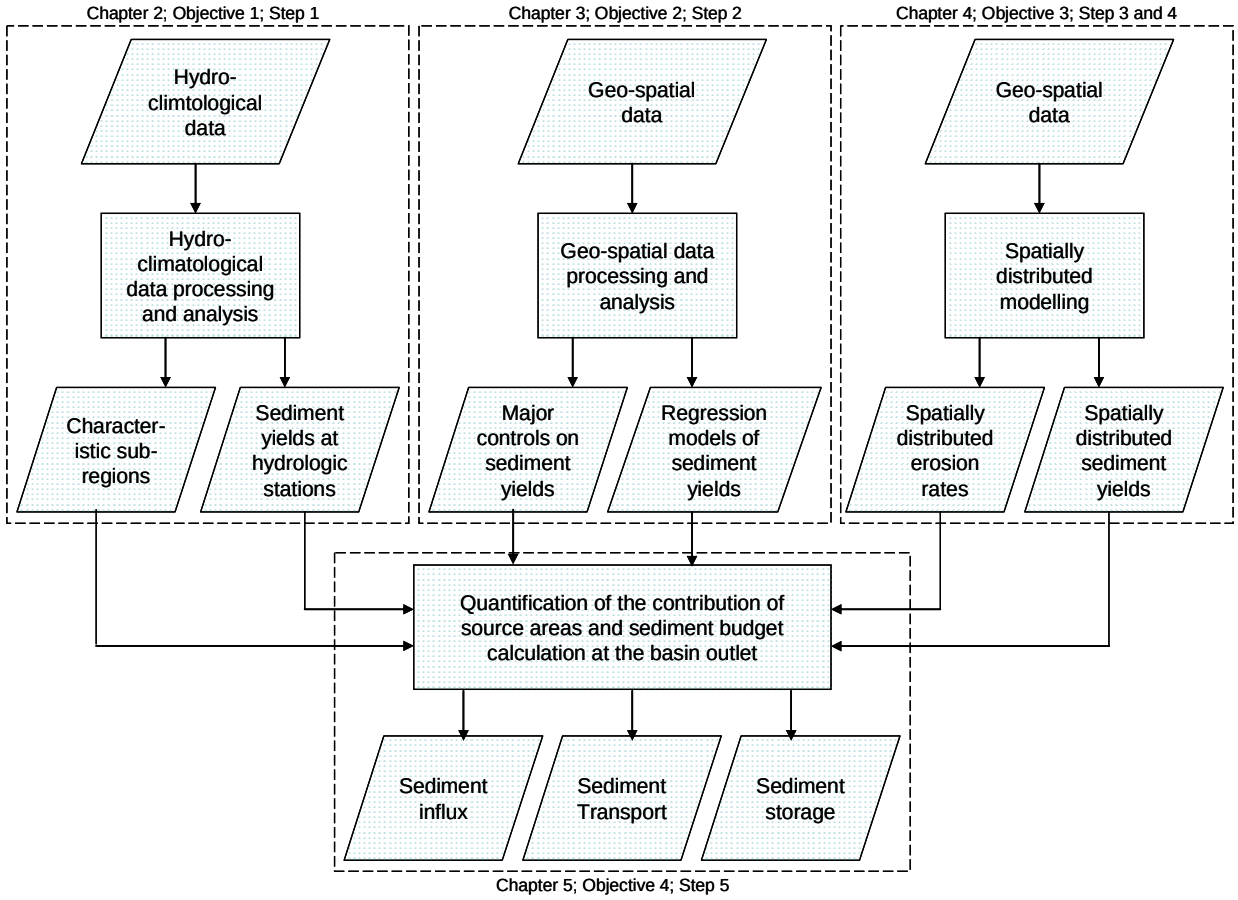

Figure 1.3 Thesis structure

Chapter 1 is the introduction where a general review of the pertinent literature is presented, as well as the research objectives, study area, and the thesis structure. The literature review gives an overview of sediment budgets, their usefulness and research needs, and emphasizes that the models, integrating remote sensing data, offer a feasible approach to sediment budget construction for large data-sparse drainage basins.

Chapter 2 addresses the first research objective of investigating spatial patterns and variation of suspended sediment yields in the upper Indus River basin based on a relatively small hydrological database. This chapter marks the completion of hydro-climatological data analysis and detailed study of the physiography of the basin resulting into the division of the basin into three characteristic regions. Moreover, the analysis of regression coefficients of sediment rating curves is carried out, magnitude frequency characteristics of sediment transport have been investigated, and relationships between specific sediment yield and basin area are developed.

Chapter 3 concerns the major controls on specific sediment yields in the basin and addresses the second objective of this study. Twenty nine variables are derived from global geo-spatial datasets available in the public domain and their correlation with specific sediment yield in the basin is investigated. Reduction of scatter is obtained by basin grouping technique and multiple regression models are constructed for estimating sediment yield in the basin. The models of specific sediment yield presented in this study link hydrological variables and environmental characteristics on a regional scale, and allow the prediction of specific sediment yield at ungauged sites within the basin. The models, however, do not explain all the observed variation in specific sediment yield in the basin, which emphasizes the importance of and need for physically-based, spatially distributed models. The understanding of the major controls of specific sediment yield in the basin obtained in this chapter is used in the next step in the study (chapter 4) to develop a physically-based, spatially distributed model for estimating specific sediment yield in different parts of the basin, and subsequently to construct a detailed sediment budget for comprehensive accounting of the sources and disposition of sediments in the basin (Ali and De Boer, 2003).

In chapter 4, spatially distributed modelling of erosion is presented at 1-km spatial scale, and monthly and annual time scales. Spatially distributed sediment yields are then predicted by coupling models of sediment yield and sediment delivery. Chapter 5 aims at overcoming the limitations of present sediment budgeting techniques and presents a methodological framework for constructing sediment budgets for large data-sparse drainage basins. Finally, to illustrate the practical applicability of the proposed methodological framework, it is implemented for the upper Indus River basin.

In chapter 6, the results and conclusions of each manuscript are summarized, the limitations of the present research are discussed, and recommendations for future work relating to this thesis are given.

1.6 References

Ahmad, N. (1993), *Water Resources of Pakistan and Their Utilization.* Shahid Nazir, Lahore, Pakistan.

Ali, K. F., and D. H. De Boer (2003), Construction of sediment budgets in large scale drainage basins: the case of the upper Indus River, in *Erosion Prediction of Ungauged Basins (PUBs): Integrating Methods and Techniques*, edited by D. H. De Boer et al., *IAHS Publ*., *279*, 206–215.

Ali, K. F., and D. H. De Boer (2007), Spatial patterns and variation of suspended sediment yield in the upper Indus River basin, northern Pakistan, *J. Hydrol.*, *334*, 368–387, doi: 10.1016/j.hydrol.2006.10.013.

Ali, K. F., and D. H. De Boer (2008), Factors controlling specific sediment yield in the upper Indus River basin, northern Pakistan, *Hydrol. Processes*, *22*, 3102–3114, doi: 10.1002/hyp.6896.

Ali, K. F., and D. H. De Boer (in review), Spatially distributed erosion and sediment yield modeling in the upper Indus River basin

Allen, P. A. (2008), From landscapes into geological history, *Nature*, *451*, 274–276, doi:10.1038/nature06586.

Bartley, R., A. Hawdon, D. A. Post, and C. H. Roth, (2007), A sediment budget for a grazed semi-arid catchment in the Burdekin basin, Australia, *Geomorphology*, *87*, 302 – 321.

Bordas, M. P., and D. E. Walling (Eds.) (1988), *Sediment Budgets*, Proc. Porto Algere Symp., December 1988, *IAHS Publ*., 174.

Brown, A. G., C. Carey, G. Erkens, M. Fuchs, T. Hoffmann, J–J. Macaire, K–M, Moldenhauer, and D. E. Walling (2009), From sedimentary records to sedimentary budgets: Multiple approaches to catchment sediment flux, *Geomorphology*, *108*, 35–47.

Campbell, B. L., R. J. Loughran, and G. L. Elliot (1988), A method of determining sediment budgets using caesium–137, In *Sediment Budgets*, edited by M. P. Bordas and D. E. Walling, *IAHS Publ*., *174*, 171–179.

Clift, P. D. (2002), A brief history of the Indus River, in *The Climatic and Tectonic Evolution of the Arabian Sea Region*, edited by P. D. Clift et al., *Geological Society, London, Special Publications*, *195*, 237–258, doi: 10.1144/GSL.SP.2002.195.01.13.

Coleman, D. J., and F. N. Scatena (1986), Identification and evaluation of sediment sources, in: *Drainage Basin Sedimentary Delivery*, edited by R.F. Hadley, *IAHS Publ., 159*, 3–18.

Collins, D. N., and S. I. Hasnain (1995), Runoff and sediment transport from glacierized basins at the Himalayan scale, in *Effects of Scale on Interpretation and Management of Sediment and Water Quality*, edited by W. R. Osterkamp, *IAHS Publ*., *226*, 17–25.

Cornwell, K., D. Norsby, and R. Marston (2003), Drainage, sediment transport, and denudation rates on the Nanga Parbat Himalaya, Pakistan, *Geomorphology*, *55*, 25–43.

De Boer, D.H., and K. F. Ali (2002), Sediment budgets and self-organization in a cellular landscape model, in *The Structure, Function and Management Implications of Fluvial Sedimentary Systems*, edited by F. J. Dyer et al., IAHS Publ., *276*, 365–372.

Dietrich, W. E., and T. Dunne (1978), Sediment budget for a small catchment in mountainous terrain, *Geomorphology*, *29*, 191–206.

Dietrich, W. E., T. Dunne, N. F. Humphrey, and L. M. Reid, (1982), Construction of sediment budgets for drainage basins: in *Sediment Budgets and Routing in Forested Drainage Basins*, edited by F. J. Swanson et al., pp. 5–23, U.S.D.A. Forest Service General Technical Report PNW–141.

Ferguson, R. I. (1984), Sediment load of the Hunza River, in *The International Karakoram Project*, edited by K. J. Miller, Cambridge University Press, Cambridge, 580–598.

Garzanti, E., S. Andò, G. Vezzoli, A. A. A. Megid, and A. E. Kammar (2006), Petrology of Nile River sands (Ethiopia and Sudan): Sediment budgets and erosion patterns, *Earth and Planetary Science Letters*, *252*(3–4), 327–341.

Gupta, A., L. Hock, H. Xiaojing, and C. Ping (2002), Evaluation of part of the Mekong River using satellite imagery, Geomorphology, *44*, 221–239.

Hewitt, K. (1998), Catastrophic landslides and their effects on the upper Indus streams, Karakoram Himalaya, northern Pakistan, *Geomorphology*, *26*, 47–80.

Hewitt, K. (2009), Catastrophic rock slope failures and late Quaternary developments in the Nanga Parbat–Haramosh Massif, Upper Indus basin, northern Pakistan, *Quaternary Science Reviews*, *28*, 1055–1069.

Holmes, Jr., R. R. (1997), Suspended-Sediment Budget for the Kankakee River Basin, 1993-95, U.S. Geological Survey Open File Report 97–120, Urbana, Illinois.

Jain, S. K., P. K. Agarwal, and V. P. Singh (2007), *Hydrology and Water Resources of India*, Springer, Dordrecht.

Kelsey, H. M. (1980), A sediment budget and analysis of geomorphic process in Van Duzen River basin, north coastal California, 1941–1957, *Geological Society of America Bulletin Part I*, *91*, 190–195.

Kesel, R. H., E. G. Yodis, and D. J. McCraw (1992), An approximation of the sediment budget of the lower Mississippi River prior to human modification, *Earth Surface Processes and Landforms*, *17*, 711–722.

Lehre, A. K. (1982), Sediment budget of a small coast range drainage basin in North-Central California, in *Sediment Budgets and Routing in Forested Drainage Basins*, edited by F. J. Swanson et al., pp. 67–77, USDA Forest Service, General Technical Report PNW-141.

Lu, X. X., and D. L. Higgitt (1999), Sediment yield variability in the Upper Yangtze, China, *Earth Surf. Processes and Landforms*, *24*, 1077–1093.

Meadows, A., and P. S. Meadows (Eds.) (1999), *The Indus River: Biodiversity, Resources, Humankind*, Oxford University Press, Karachi, Pakistan.

Miller, K. J. (Ed.) (1984), *The International Karakoram Project*, Cambridge University Press, Cambridge.

Molnar, P., and P. Tapponnier (1975), Cenozoic tectonics of Asia: Effects of a continental collision, *Science*, *189*, 419–426.

Parker, R. S. (1988), Uncertainties in defining the suspended sediment budget for large drainage basins, in *Sediment Budgets*, edited by M. P. Bordas and D. E. Walling, *IAHS Publ*., *174*, 523–532.

Peart, M. R., and D. E. Walling (1986), Fingerprinting sediment source: The example of a drainage basin in Devon, UK, in *Drainage Basin Sedimentary Delivery*, edited by R. F. Hadley, *IAHS Publ., 159*, 41–55.

Peart, M. R., and D. E. Walling (1988), Techniques for establishing suspended sediment sources in two drainage basins in Devon, UK: A comparative assessment, in *Sediment Budgets*, edited by M. P. Bordas and D. E. Walling, *IAHS Publ., 174*, 269–279.

Phillips, J. D. (1991), Fluvial sediment budgets in North Carolina Piedmont, *Geomorphology*, *4*(3/4), 231–242.

Ramos-Scharrón C. E., and L. H. MacDonald (2007), Development and application of a GIS-based sediment budget model, *Journal of Environmental Management*, *84*(2), 157–172.

Rawat, J. S. (1987), Modelling of water and sediment budget: concepts and strategies, in *Geomorphological Models - Theoretical and Empirical Aspects*, edited by F. Ahnert, pp. 147–159, Catena Supplement 10, Catena Verlag, Cremlingen.

Reid, L. M., and T. Dunne (1996), *Rapid Evaluation of Sediment Budgets*, Catena Verlag GMBH, Reiskirchen, Germany.

Reid, L.M., and T. Dunne (2003), Sediment budgets as an organizing framework in fluvial geomorphology, in Tools in Fluvial Geomorphology, edited by G. M. Kondolf et al., pp. 463–499, Wiley, Chichester.

Roberts, R. G., and M. Church (1986), The sediment budget in severely disturbed watersheds, Queen Charlotte Ranges, British Columbia, *Can. J. For. Res.*, *16*, 1092–1106.

Rondeau, B., D. Cossa, P. Gagnon, and L. Bilodeau (2000), Budget and source of suspended sediment transport in St. Lawrence River in Canada, *Hydrol. Processes*, *14*(1), 21–36.

Rustomji, P., G. Caitcheon, P. Hairsine (2008), Combining a spatial model with geochemical tracers and river station data to construct a catchment sediment budget, *Water Resour. Res*., *44*, W01422, doi:10.1029/2007WR006112.

Schmidt, K. -H., and P. Ergenzinger (1994), Recent developments and perspectives in mountain river research, in *Dynamics and Geomorphology in Mountain Rivers*, edited by P. Ergenzinger and K. Schmidt, pp. 3–14, Springer-Verlag, Berlin, Germany.

Searle, M. P. (1991), *Geology and Tectonics of the Karakoram Mountains*, Wiley, New York.

Shi, C., and D. D. Zhang (2005), A sediment budget of the lower Yellow River, China, over the period from 1855 to 1968, *Geografiska Annaler, Series A: Physical Geography*, *87*(3), 461–471, doi:10.1111/j.0435-3676.2005.00271.x.

Shroder, J. F. (Ed.) (1993), *Himalaya to the Sea: Geology, Geomorphology and the Quaternary*, Routledge, Chichester.

Shroder, J. F. and M. P. Bishop (1998), Mass movement in the Himalaya: new insights and research directions, *Geomorphology*, *26*, 13–35.

Slaymaker, O. (1993), The sediment budget of the Lillooet River basin, British Columbia, *Physical Geography*, *14*(3), 304–320.

Slaymaker, O. (2006), Towards the identification of scaling relations in drainage basin sediment budgets, *Geomorphology*, *80*, 8–19.

Sutherland, R. A., and R. B. Bryan (1991), Sediment budgeting: a case study in Katiorin drainage basin, Kenya, *Earth Surf. Processes and Landforms*, *16*(5), 383–398.

Swanson, F. J., R. J. Janda, T. Dunne, and D. N. Swanston (Eds.) (1982), *Sediment Budgets and Routing in Forested Drainage Basins*, USDA Forest Service, General Technical Report PNW-141.

Symader, W. and N. Strunk (1993), Determining the source of suspended particulate material, in *Erosion, Debris Flows and Environment in Mountain Regions*, edited by D. E. Walling *et al*., *IAHS Publ., 209*, 177–185.

Trimble, S.W. (1999), Decreased rates of alluvial sediment storage in the Coon Creek basin, Wisconsin, 1975–93, *Science*, *285*, 1244–1246.

Trimble, S. W. (2009) Fluvial processes, morphology and sediment budgets in the Coon Creek Basin, WI, USA, 1975–1993, *Geomorphology*, *108*, 8–23.

Walling, D. E., and A. L. Collins (2008), The catchment sediment budget as a management tool, *Environmental Science and Policy*, *11*, 136–143, doi:10.1016/j.envsci.2007.10.004.

Walling, D. E., and A. J. Horowitz (2005), *Sediment Budgets 1*, Proceedings of Foz do Iguaçu Symposium April 2005, Brazil, *IAHS Publ*., *291*.

Wang, Z. -Y., Y. Li, and Y. He (2007), Sediment budget of the Yangtze River, *Water Resour. Res.*, *43*, W04401, doi:10.1029/2006WR005012.

Wasson, R. J. (2002), Sediment budgets, dynamics, and variability: new approaches and techniques, in *The Structure, Function and Management Implications of Fluvial Sedimentary Systems*, edited by F.J. Dyer et al., *IAHS Publ*., *276*, 471–478.

Wasson, R.J. (2003), A sediment budget for the Ganga–Brahmaputra catchment, *Current Science 84*(8), 1041–1047.

Wilkinson, S. N., I. P. Prosser, P. Rustomji, and A. M. Read (2009), Modelling and testing spatially distributed sediment budgets to relate erosion processes to sediment yields, *Environmental modelling & Software*, *24*, 489–501.

Xu, J. (2008), A suspended sediment budget of the Yichang-wuhan reach of the Yangtze River, China, *Geografiska Annaler: Series A, Physical Geography, 90* (2), 173–186.

CHAPTER 2 – SPATIAL PATTERNS AND VARIATION OF SUSPENDED SEDIMENT YIELD IN THE UPPER INDUS RIVER BASIN, NORTHERN PAKISTAN

Ali, K. F., and D. H. De Boer (2007), Spatial patterns and variation of suspended sediment yield in the upper Indus River basin, northern Pakistan, *J. Hydrol.*, *334*, 368–387.

2.1 Abstract

Much of the flow of the Indus River originates in the mountainous regions of the Karakoram and Himalayas, resulting in a high sediment yield which creates a number of operational and maintenance problems for downstream water use in Pakistan. Analysis of the available hydro-climatological data indicates that the upper Indus basin can be subdivided into three characteristic regions based on whether runoff production is controlled by temperature (*Region 1,* upper, glacierized sub-basins), precipitation caused by the monsoon and western disturbances (*Region 3,* lower sub-basins), or a combination of the two (*Region 2,* middle reach sub-basins). The runoff and sediment transport regimes for the Shyok, Gilgit, Hunza and Indus Rivers in *Region 1* show the role of snow- and ice-melt in generating high runoff, and 80-85% of the annual sediment load is transported in July and August. The Astore River at Doyian in *Region 2* shows an early rise of sediment yield starting in May due to the interaction of rainfall and snowmelt at lower elevations, and a comparatively lower sediment yield in August indicating a

lesser influence of glacier-melt. *Region 3* experiences two types of rainfall: summer monsoons and the western disturbances in late winter and early spring. Consequently, the Gorband River at Karora in *Region 3* exhibits two separate sediment yield peaks of equal height in April and July. The runoff and sediment transport regime along the main stem of the Indus River is dominated by the melt of snow and ice in its headwaters, and consequently is similar to the regimes of the *Region 1* sub-basins. Contrary to the conventional model, the specific sediment yield increases markedly with drainage area along the Indus River, from 355 t km^{-2} yr^{-1} at Kharmong to 1197 t km^{-2} yr^{-1} at Besham Qila, likely because of the large number of small and relatively steep catchments discharging straight into the Indus River. Analysis of the magnitude-frequency characteristics of sediment transport for the tributaries shows that the effective discharge in the basin ranges from 1.5-2.0 to 5.5-6.0 times the average discharge, and decreases downstream. The main Indus River, however, shows a consistent effective discharge of 2.5-3.0 times the average discharge.

Keywords: Indus River; Karakoram; Himalayas; suspended sediment; sediment yield; effective discharge

2.2 Introduction

Sediment yield is defined as the total sediment outflow from a basin over a specified time period, with suspended sediment as the dominant component (Knighton, 1998). Knowledge of sediment yields is required to manage reservoirs, canals, harbours, and other structures. In addition, suspended sediment concentration is a water quality parameter and a transporter of

pollutants. Estimates of sediment yield are therefore essential in water resources analyses, modelling, and engineering (Walling and Webb, 1996; Lane *et al.,* 1997). A number of interrelated geologic, hydrologic, and topographic factors cause sediment yield to vary widely from region to region (Ritter *et al*., 2002). Sediment yields are affected by both natural factors and anthropogenic factors (Meade *et al.,* 1990). These influences can be assigned to four major categories of: i) climate; ii) geology; iii) relief; and iv) land use. Relationships between sediment yield and its controlling variables have been investigated at global and regional scales through correlation and regression analysis by Milliman and Syvitski (1992), Summerfield and Hulton (1994), Ludwig and Probst (1998), and Lu and Higgitt (1999). Variables expressing basin relief characteristics and runoff magnitude are found to be most strongly associated with sediment yields. Dedkov and Moszherin (1992), Glazyrin and Tashmetov (1995) and Evans (1997) have emphasized the importance of additional factors in sediment generation in mountainous regions, including tectonics and seismic activity, recurring earthquakes, mean elevation of the basin, glaciated area, proportion of solid precipitation, and basin lithology.

The Indus River is the single most important natural resource in Pakistan, and is the source of much of the country's irrigation water and electric energy (Meadows and Meadows, 1999; Ahmad, 1993). Much of its flow originates in the mountains of the Karakoram and Himalayas, and it transports large volumes of sediment, the majority of it in suspension (MONENCO, 1984). The upper Indus River basin in northern Pakistan (Figure 2.1) has one of the highest rates of sediment transport reported in the literature (Meybeck, 1976). The sediment-laden water creates many water resources management problems such as siltation of reservoirs, damage to turbines, reduction in water quality, and transport of chemical pollutants. An understanding of the spatial

and temporal patterns of the suspended sediment yield in the upper Indus River basin is therefore essential for effective water resources development in northern Pakistan.

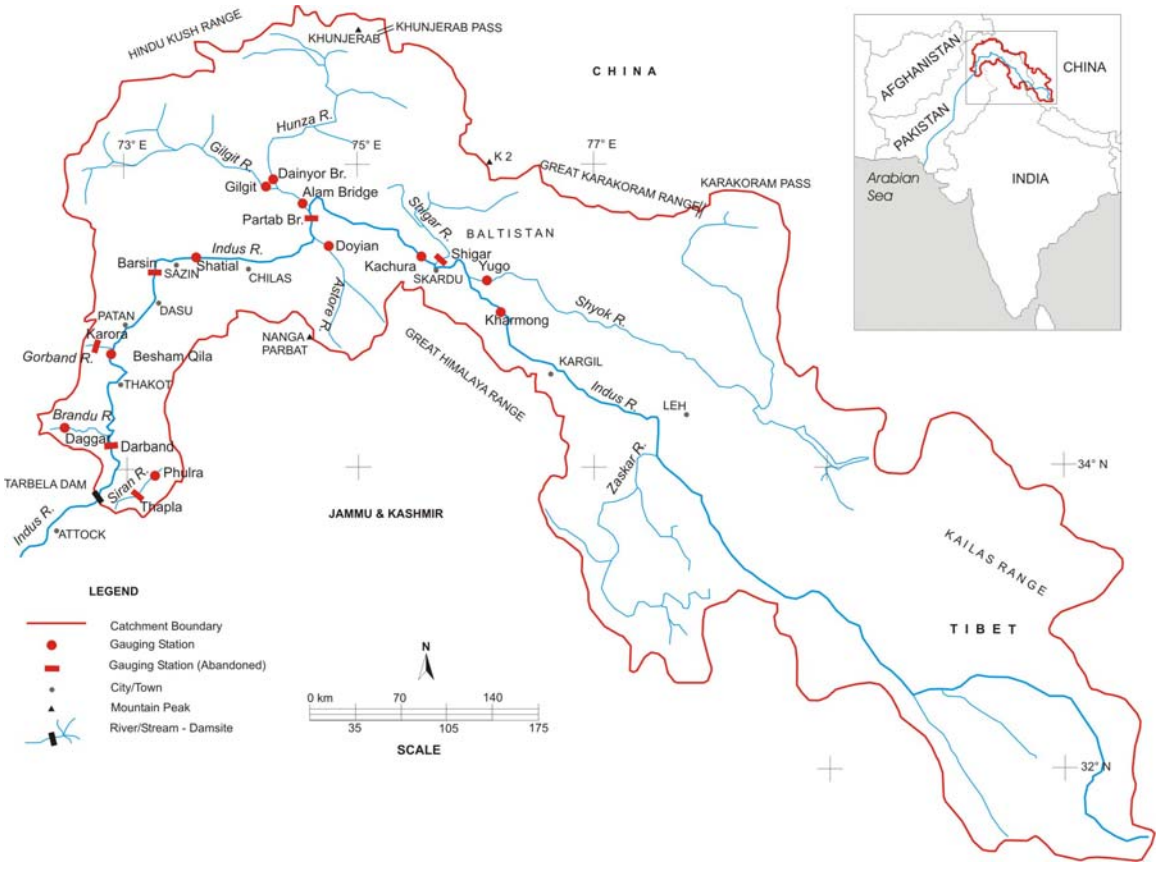

Figure 2.1 The upper Indus River basin

The Karakoram and Himalaya regions are examples of young mountain ranges that are subject to exceptionally rapid degradation by a combination of various processes (Ferguson, 1984; Searle 1991). Continuing tectonic instability and high relief, combined with runoff from glaciers in ice-covered areas, result in a potentially high sediment yield from these mountain ranges (Collins and Hasnain, 1995). Widespread mass movements and rapid weathering due to the seasonal effects of severe climatic conditions including freezing and thawing, exposure to

heavy snowfall and the action of glaciers are major factors in the high sediment yield observed in the basin. Sediment is contributed in the headwaters of the major rivers by the melt-water issuing from glaciers, by debris torrents, and by channel erosion during catastrophic outburst floods from landslide-, moraine-, and glacier-dammed lakes. The lower, southern part of the basin is subjected to heavy monsoon rainfall, and rivers in this part of the basin carry large amounts of sediment associated with flash floods. In specific areas of the basin, another important factor is human activity involving deforestation, agriculture, cattle grazing and road construction.

Although the Indus River is one of the world's largest rivers in terms of drainage area, and river discharge, little is known about its sediment yield (Milliman *et al*., 1984). Apart from some long-term discharge records for the main Indus River and some of its major tributaries, hydrological measurements are very scarce (Young and Hewitt, 1990). The primary objective of this study is to explain the variation in suspended sediment yield in the basin in terms of climatic variables, hydrologic regimes and drainage basin size. To achieve this objective, an extensive analysis of the available climatological and hydrological database has been carried out.

2.3 Study area

2.3.1 The Upper Indus River: Physiography and River System

The Indus River is one of the largest rivers in southern Asia, with a total length of 2880 km and a drainage area of 912,000 km^2 extending across portions of Pakistan, India, China and Afghanistan (Figure 2.1). The upper Indus River basin upstream of Tarbela Dam is about 1125

km long, with a drainage area of 170,000 km^2. The Indus River rises in the Tibetan Plateau at elevations above 5500 m in the Kailas Range, and follows a well-defined valley parallel to the geologic strike. It flows north and west through high mountain ranges, and enters the southeastern corner of Kashmir at an elevation of 4000 m where it is joined by the Zaskar River. Flowing over a long alluvial plain, it meets its biggest tributary, the Shyok River in Baltistan at an elevation of 2400 m, 45 km upstream of Skardu. Here its valley is wide and contains extensive glacially-deposited sediments down to Skardu, where large quantities of silt have been deposited in a large basin. Within its wide valley, the Indus has an alternating meandering and braiding river pattern. The downstream end of Skardu basin has been dammed by glacial deposits through which the present river channel has been eroded. Downstream of Skardu basin, the river valley narrows at Kachura, and the Indus flows in a northwesterly direction between steep valley walls through Kashmir. The river parallels the regional trend of the mountain ranges, including a northerly loop around the Nanga Parbat massif, south of the town of Gilgit where the Gilgit River meets the Indus River. Between the Gilgit confluence and Chilas, the river valley has a relatively wide cross section and contains extensive glacially-deposited sediments. Just downstream of Sazin, the river bends and flows in a southerly direction in a steeper and narrower section. This configuration continues to Besham Qila with occasional wider sections such as at Patan. Downstream of Besham Qila, the river valley begins to widen. Tarbela Dam, the first major structure on the Indus River, is situated downstream of Besham Qila. The Gorband, Brandu and Siran Rivers are notable Indus tributaries between Besham Qila and Tarbela. Besham Qila, located 65 km upstream of Tarbela Reservoir, has usually been taken as the station defining the Karakoram portion of the overall basin, and effectively fixes the extent of the upper Indus basin (Collins, 1994). However, Tarbela Reservoir serves as a sediment sink for the upper

Indus basin, which is helpful for constructing a sediment budget for the basin (Ali and De Boer, 2003). In this study the upper Indus basin therefore is considered to extend downstream to Tarbela Dam.

2.3.2 Geology and Tectonics

During the Cretaceous dispersal of Gondwana, the Indo-Pakistani tectonic plate moved across what is now the Arabian Ocean from its position between Antarctica and Arabia, and collided with the Eurasian Plate (Miller, 1984). This major tectonic activity, resulting in the Himalayan orogeny during the mid-Eocene era, has shaped the high relief and complex geologic structures observed in northern Pakistan today (Molnar and Tapponnier, 1975; Shroder, 1993). The series of mountain ranges of extreme ruggedness and high elevations in northwestern Pakistan, southwestern China and northern India, run approximately east to west in an arc from the Hindu Kush and Pamirs in the west and north, to the main Himalayan chain in the south and east. The latter culminates in the Nanga Parbat massif (8125 m). The great granite-gneiss massifs of Karakoram, named the "roof of the world", have five peaks higher than 8000 m and more than 36 above 7000 m including the famous K-2 (8611 m), Gasherbrum (8068 m), Masherbrum (7821 m) and Rakaposhi (7788 m).

The bedrock in the basin is composed of a wide variety of igneous and metamorphic rocks that have undergone extensive deformation due to high degree of tectonic activity (Figure 2.2). There is a large variety of surficial materials, which predominantly occur as glacial deposits, alluvial fans and recently-deposited alluvium (MONENCO, 1984). Landforms in the study area

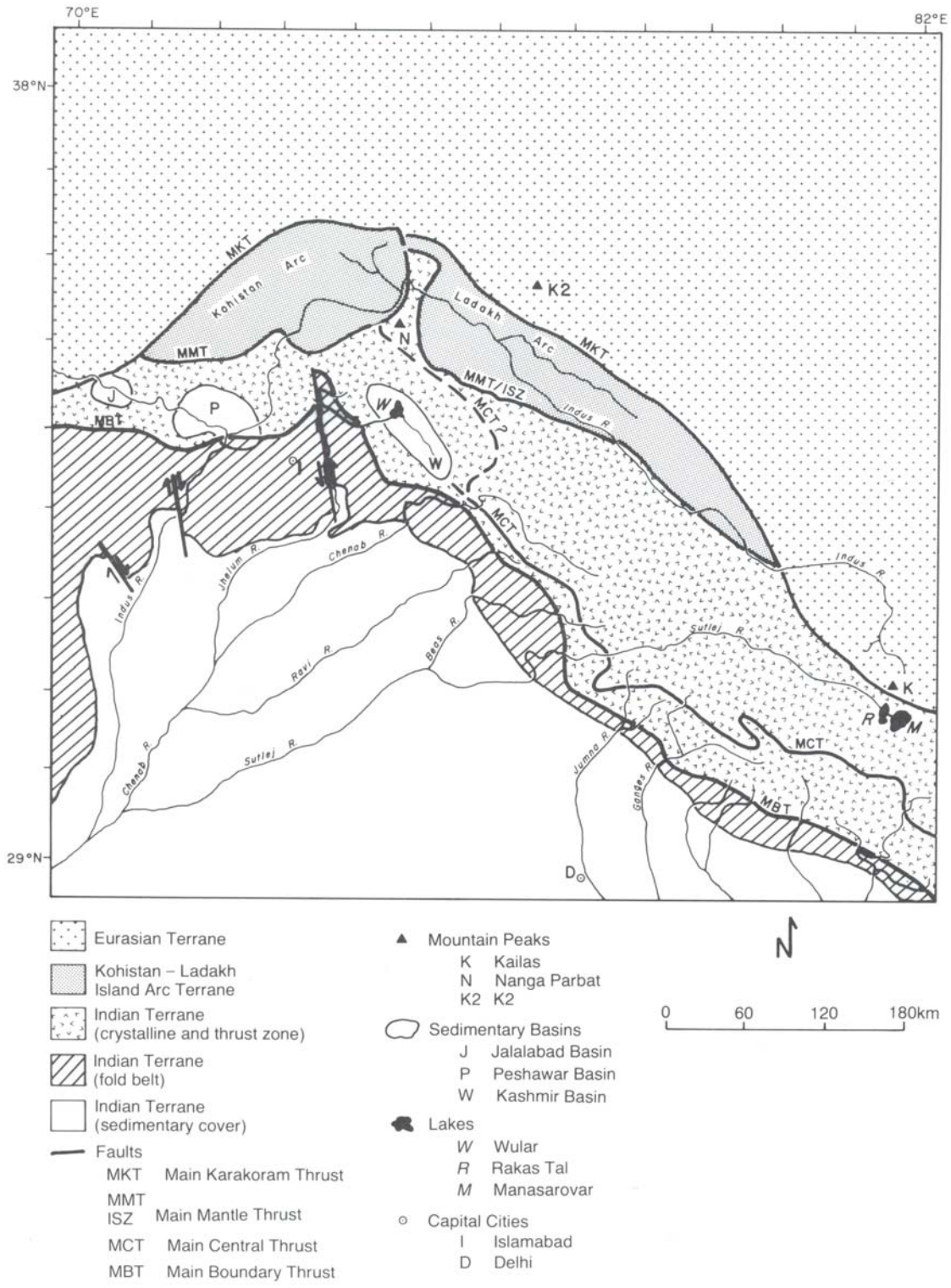

Figure 2.2 Geology of the upper Indus River basin (after Shroder, 1993)

are changing rapidly. The bedrock in the region is subjected to high weathering rates (Ferguson, 1984) and extreme variations in climate. Frequent rock slides, avalanches and other mass movements in the basin play an important role in generating large sediment fluxes (Hewitt, 1998; Shroder and Bishop, 1998). A substantial portion of the basin has been glaciated one or more times. There have been several natural dams associated with landslides which have contributed to the development of extensive deposits of reworked glacial and fluvial sediment. These comprise interbedded glaciofluvial and till deposits, with less frequent occurrence of glaciolacustrine material. Large boulders and rock slabs are commonly found in the valley talus slopes and in the riverbed.

2.3.3 Climate

The upper Indus basin is surrounded by high mountain ranges that dominate the climate of the region. The climate in the northernmost, glacierized part of the basin is semi-arid to arid. It changes from subtropical to tropical dry as the Indus descends to the Arabian Sea (Ludwig and Probst, 1998). There are two well-defined mechanisms producing precipitation, namely the summer monsoon and western disturbances in late winter and early spring. During the summer months (June to September), Pakistan is strongly affected by the monsoon system. The monsoon causes frequent short spells of heavy precipitation that result in flooding at lower elevations and snow accumulation at high altitudes. The month of August has the highest monsoon precipitation. During the winter and spring seasons, the basin is affected by large scale weather systems originating primarily in the Mediterranean or Caspian Sea regions (Singh *et al.*, 1995). From November to April, these extra-tropical cyclones known as western disturbances move at

regular intervals from west to east and are usually associated with well developed cold and warm fronts. Winter precipitation is of relatively low intensity, and generally in the form of snow at high altitudes above 2150 m and as rain at lower elevations. The snow line descends as low as 700 m as the winter progresses.

The upper Indus basin can be divided into two distinct upper and lower climatic zones. The upper zone covers over 90% of the catchment area, and is a narrow, elongated basin lying between the Karakoram and Himalaya mountain ranges, with its major axis running southeast-northwest (Figure 2.1). About one-quarter of this mountainous portion of the basin is perpetually covered with snow and ice, and melt-waters contribute a major part of the annual flow reaching Tarbela. As the flow in the upper Indus is mostly snow and glacier melt, the energy balance controls the temperature and the melting rate of snow and ice, and hence the seasonal changes in river flow. Nanga Parbat acts as a barrier to the incoming monsoon from the south (Young and Hewitt, 1990) and limits the penetration of the monsoon into the Karakoram Mountains. As a result, the upper Indus basin upstream of Dasu, where the valley changes direction from east-west to northeast-southwest, lies in a rain-shadow area and the annual total precipitation ranges from 80 to 160 mm (Collins, 1994). The lack of moisture results in an arid landscape, except where runoff from side valleys has been diverted to irrigate small terraces.

The lower climatic zone covers about 10% of the drainage area, and lies immediately upstream of Tarbela Dam where the Indus River bends around the southern mountain wall and flows generally southwards. The eastern and western boundaries of this zone are formed by hills that separate the Indus drainage basin from adjoining basins. At its lower end, this zone opens

southward toward the Indus plain and there is no barrier to the entry of monsoon storms from the south that causes the major part of the runoff from this lower region. This part of the basin has a fast response, and the monsoon rains result in short duration floods that are superimposed on the slower responding snowmelt runoff. The rainfall occurs as high intensity storms with durations of several days, and produces pronounced flood peaks in July and August. For the present study the climatological data, mainly precipitation and temperatures, have been obtained from the Pakistan Meteorological Services and the Surface Water Hydrology Project (SWHP) and the Pakistan Water and Power Development Authority (WAPDA).

2.3.4 Suspended Sediment Yield of the Indus River

Estimates of the annual sediment yield of the Indus River reported in literature vary widely, ranging from 100 to 675 Mt yr^{-1} (Table 2.1). These estimates, however, concern the actual amount of the sediment reaching the ocean, and depend on where, when, and how they were obtained (Milliman and Meade, 1983). The suspended sediment yield of the upper Indus basin was estimated for the feasibility study of Tarbela Dam by Tippetts-Abbett-McCarthy-Stratton Consultants (TAMS, 1962) as 275 Mt yr^{-1}, based on the 1868-1960 discharge records at Attock converted to the Darband gauging station. Adjustments to this figure to conform to the more recent sediment rating curve increased the yield to 360 Mt yr^{-1} (TAMS, 1962). TAMS (1984) report that the Water Resources Division of the Peshawar University analyzed the 1960-1968 record of sediment sampling at Darband, and estimated the sediment yield to be 331 Mt yr^{-1}. In 1975, WAPDA estimated the annual sediment yield of the Indus and the Siran Rivers as 320 Mt yr^{-1}, using the 1960-1973 suspended sediment record at Darband (TAMS, 1984). Since the

construction of Tarbela Dam, Darband has been flooded and the hydrological data at Besham Qila have been used for calculating the sediment inflow to Tarbela Reservoir. TAMS and HR Wallingford (1998) have estimated the sediment discharge to Tarbela Reservoir as 200 Mt yr^{-1}. Preliminary suspended sediment yields in the upper Indus basin have been reported in recent literature by Ali and De Boer (2003).

Table 2.1 Estimates of the sediment yield of the Indus River cited in different studies

Suspended sediment yield (Mt yr^{-1})	Reference
435	Strakhov (1961) (reported by Milliman *et al*., 1984)
480	Holeman (1968)
475	Meybeck (1976)
675	WAPDA (1982) (reported by Milliman *et al*., 1984)
100	Milliman and Meade (1983)
300	Kazmi (1984)
245	Milliman and Syvitski (1992)
300	Summerfield and Hulton (1994)
250	Ludwig and Probst (1998)

2.3.5 Tarbela Reservoir Sedimentation

The 148 m high Tarbela dam is one of the world's largest earth and rockfill dams. Coarse sediment tends to be deposited in the upper reaches of the reservoir, while the finer particles are transported further downstream towards the dam. During months of low discharge, the water level in the reservoir decreases and sediment deposited in the upper reaches is reworked and carried downstream within the reservoir. During months of high flows, the river channel widens and the banks collapse in the upper reaches of reservoir, resulting in a considerable increase in sediment concentration. Sediment brought into the reservoir from upstream and sediment eroded

from the upstream section of the reservoir is deposited in the main reservoir. A small portion of the finer sediment escapes the reservoir through the power and irrigation tunnels, but the bulk of the sediment accumulates as a major delta behind the dam. As a result, the reservoir has an 89% trapping efficiency, and sediment deposition has reduced the 14.3 x 10^9 m^3 gross storage capacity of the reservoir by 27.6% since 1974 (Survey and Hydrology, 2005). In the absence of sediment flushing arrangements, the residence time of sediment is quite large, and sediment remains trapped behind the dam. The situation in Tarbela reservoir is in strong contrast to, for example, the Susquehanna River basin in Pennsylvania, where approximately 80% of the 50 Mt suspended sediment stored behind the dams between 1966 and 1976 was discharged into northern Chesapeake Bay by floodwaters associated with just two hurricanes (Barros and Gordon, 2002). The growth of the delta in Tarbela Reservoir has been recorded by annual hydrographic surveys since 1979. These surveys consist of systematic soundings along approximately 73 range lines.

2.4 Data Availability, Quality and Methods

The available sediment transport data for the upper Indus basin consist of a long-term hydrological database, published annual suspended sediment yield records (SWHP, 2001) and hydrographic surveys of Tarbela reservoir. Long-term, continuous discharge and occasional suspended sediment concentration data are available for 17 active and discontinued gauging stations in the upper Indus River basin (Table 2.2 and Figure 2.1). The stations were established by the SWHP since the early 1960s, and have drainage areas ranging from 598 (Brandu River at Daggar) to 166,154 km^2 (Indus River at Darband). As a result of the collaboration between the

Table 2.2 Stream gauging stations in the upper Indus River basin

Region	Station	River	Period of record	Location		Drainage area	Elevation	Runoff	Sediment yield	
				Latitude	Longitude	(km^2)	(masl)	(mm)	($Mt\ yr^{-1}$)	($t\ km^{-2}\ yr^{-1}$)
Region 1	Kharmong	Indus	1983-1998	34º 56' 00"	76º 13' 00"	67,856	2542	227	23.9	355
	Yugo	Shyok	1973-1998	35º 11' 00"	76º 06' 00"	33,670	2469	325	31.1	924
	Shigar	Shigar	1985-1998	35º 20' 00"	75º 45' 00"	6610	2438	989	16.8	2542
	Kachura	Indus	1970-1998	35º 27' 00"	75º 25' 00"	112,665	2341	296	80.1	710
	Dainyor Bridge	Hunza	1966-1998	35º 55' 40"	74º 22' 35"	13,157	1370	804	44.4	3373
	Gilgit	Gilgit	1963-1998	35º 55' 35"	74º 18' 25"	12,095	1430	738	6.0	498
	Alam Bridge	Gilgit	1966-1998	35º 46' 03"	74º 35' 50"	26,159	1280	780	54.8	2095
	Partab Bridge	Indus	1963-1995	35º 43' 50"	74º 37' 20"	142,825	1250	391	138.3	968
Region 2	Doyian	Astore	1974-1998	35º 32' 42"	74º 42' 15"	4040	1583	1012	1.7	427
	Shatial Bridge	Indus	1983-1998	35º 31' 56"	73º 33' 52"	150,220	1040	423	118.6	789
	Barsin	Indus	1974-1979	35º 18' 00"	73º 16' 00"	157,600	NA	356	140.5	892
Region 3	Karora	Gorband	1975-1997	34º 53' 31"	72º 45' 58"	635	880	1035	0.2	250
	Besham Qila	Indus	1969-1998	34º 55' 27"	72º 52' 55"	162,393	580	469	194.4	1197
	Daggar	Brandu	1970-1998	34º 29' 45"	72º 27' 43"	598	700	299	0.3	442
	Darband	Indus	1960-1973	34º 21' 47"	72º 50' 29"	166,154	NA	465	287.6	1731
	Phulra	Siran	1970-1998	34º 18' 50"	73º 04' 42"	1057	732	630	2.4	2306
	Thapla	Siran	1960-1973	34º 08' 00"	72º 54' 00"	2799	NA	349	2.9	1024

German Agency for Technical Cooperation (GTZ) and the SWHP since the 1980s, a number of steps have been taken to improve the quality of hydrological data (GTZ, 1999). These include: i) extension of the network to ensure a minimum acceptable coverage; ii) systematic field measurements at gauging sites to derive reliable rating curves; iii) modernization of laboratory facilities and equipment; and iv) software development to improve the reliability and transparency of the data processing methods. This has resulted in electronic processing of all records and publication of yearbooks. The data reported in the yearbooks is claimed to be collected, processed and analyzed using the best methods available and accurate enough for general use (SWHP, 2004).

Records of river stage are obtained either from periodic readings of a staff gauge or wire weight gauge, or from an automatic water stage recorder. The non-recording gauges are generally read hourly from 08:00-16:00 daily during period of low flow, and more frequently during flood season. The frequency of discharge measurement varies from station to station, and depends on the stability of the channel and the importance and accessibility of the station. At most stations, discharge is measured twice a month, except during flood periods when measurements may be made as often as several times a day. Discharge is measured using Price type AA current meters following the USGS method (Rantz and others, 1982). Daily mean discharges are computed from daily mean gauge heights using the rating curves established for each site. Suspended sediment sampling is carried out following standard USGS procedures (Edwards and Glysson, 1999) in combination with discharge measurements on an occasional basis at the gauging stations so that sediment rating curves can be developed. The samples are

analyzed for total concentration by filtration, and for particle size distribution using settling tubes, pipetting, and sieving.

There is little information available on bed load transport in the Indus River basin (GTZ, 1999). Occasional bed material data, however, have been collected at a few places in the basin. Steep slopes, large boulders structured in armor layers, as well as strong currents during floods characterize the morphological conditions of mountain rivers in northern Pakistan. These conditions are not suitable for the classical box type bed load samplers such as the Dutch Arnhem or the Helley-Smith. A modified version of the Mühlhofer sampler was developed and locally manufactured by the GTZ, and has been used on smaller hill torrents on an experimental basis. NEAC Consultants (2004) suggested a value of 13.5% as the unmeasured bed load for the Indus River at Besham Qila, based on 1962-2000 interpolated data. The Water Resources Division of Peshawar University recommends a correction for unmeasured bed load of 10% or 15% of the suspended sediment load for the upper Indus River and its tributaries for flood and non-flood conditions, respectively (NEAC Consultants, 2004). These estimates are in agreement with the USBR (1987) guidelines for evaluating the unmeasured load as a bed load correction.

To establish the seasonal patterns of sediment yield and to relate them to climatic patterns and hydrological regimes, a detailed analysis of the available hydrological and climatological data has been carried out. Annual and monthly volumes of water discharges and precipitation have been determined. Suspended sediment rating curves were established for all the stream gauging stations in the basin. Sediment yields have been calculated at mean annual and mean monthly time scales. Specific discharges and specific sediment yields have also been calculated.

The analysis is based on the entire record at each of the 17 hydrologic stations. Given the year to year variability in precipitation, discharge, and sediment load, it might be argued that the analysis should be based on the same set of years from each station. The period of record for the stations, however, ranges from 6 to 36 years. Using data for the same years would drastically reduce the number of years used in the analysis, and would also exclude some of the stations altogether from the dataset. Because this analysis is based on mean values, it was decided to use all available data.

2.5 Results and Discussion

2.5.1 Hydrologic Regimes

Sediment transport in a river basin strongly depends on stream flow conditions. Archer (2003) characterized the upper Indus River by three contrasting hydrological regimes based on the mechanisms generating runoff during the summer season: i) melt of glaciers and permanent snow in high elevation drainage basins, where summer runoff is predominantly controlled by the temperature; ii) melt of seasonal snow, controlled by preceding winter and spring precipitation; and iii) winter and monsoon rainfall, controlled by precipitation in the current season. Using these hydrologic regimes, the upper Indus basin was divided into three characteristic regions for explaining the spatial patterns of sediment yield in the current study (Figure 2.1).

Region 1 comprises the high elevation, glacierized areas of the Karakoram and Himalaya located in the northernmost part of the basin. This region extends downstream to Partab Bridge on the Indus River, but does not include the areas around Nanga Parbat, which acts as a barrier to

the monsoon. Figure 2.3 and Figure 2.4 show the distribution of monthly mean precipitation and monthly mean discharges, respectively, for selected climatological and hydrological stations in the upper Indus basin. The aridity of the region is evident from the low mean annual precipitation observed at Leh (93 mm) and Gilgit (131 mm) (Figure 2.3). The runoff regime of this region is dominated by sustained melting of glacier ice from June to September. This trend is evident for the Shyok, Hunza and Gilgit sub basins (Figure 2.4), which generate a major portion of the runoff in the summer months. The quantity and timing of discharge in these rivers with snow- and ice-melt contributions therefore depends on the incidence, amount, and form of precipitation, and on the thermal regime which determines the melting pattern of the winter snowpack in spring and of the glacier ice throughout the summer (Collins, 1994). The melt contribution can be divided into two components: one from snow at relatively low elevations, and the other from glacial ice at higher elevations. The low-elevation snowmelt contribution starts in late April to May as temperatures rise. The major flow contribution, however, is derived from glacial-melt and high elevation snowmelt. This would be expected to start somewhat later in the year in June and July. It is difficult to determine the relative contributions of these two snowmelt components due to a sparse gauging network in the basin.

Region 2 extends from Partab Bridge to Besham Qila and comprises the area between the upper, glacierized portion of the basin and the lower, monsoon-affected area. The mean annual rainfall recorded in this region at Astore valley is 511 mm, and the seasonal pattern exhibits the influence of western disturbances in producing significant amounts of early spring rainfall (Figure 2.3). The highest specific discharges in the upper Indus basin are observed from the southeast flanks of Nanga Parbat, where monsoon rain and snowmelt interact and the Astore

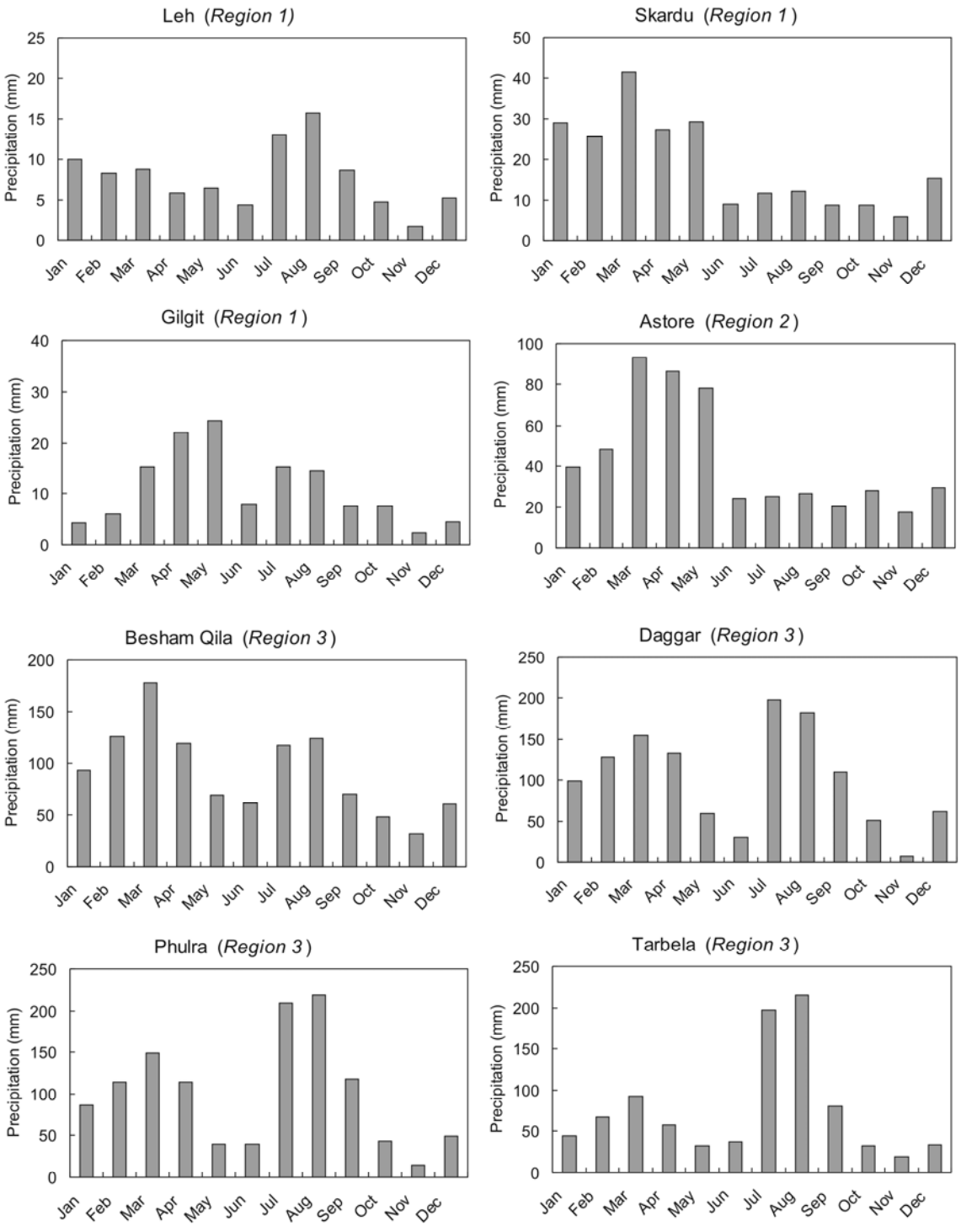

Figure 2.3 Monthly precipitation for selected climatological stations in the upper Indus River basin

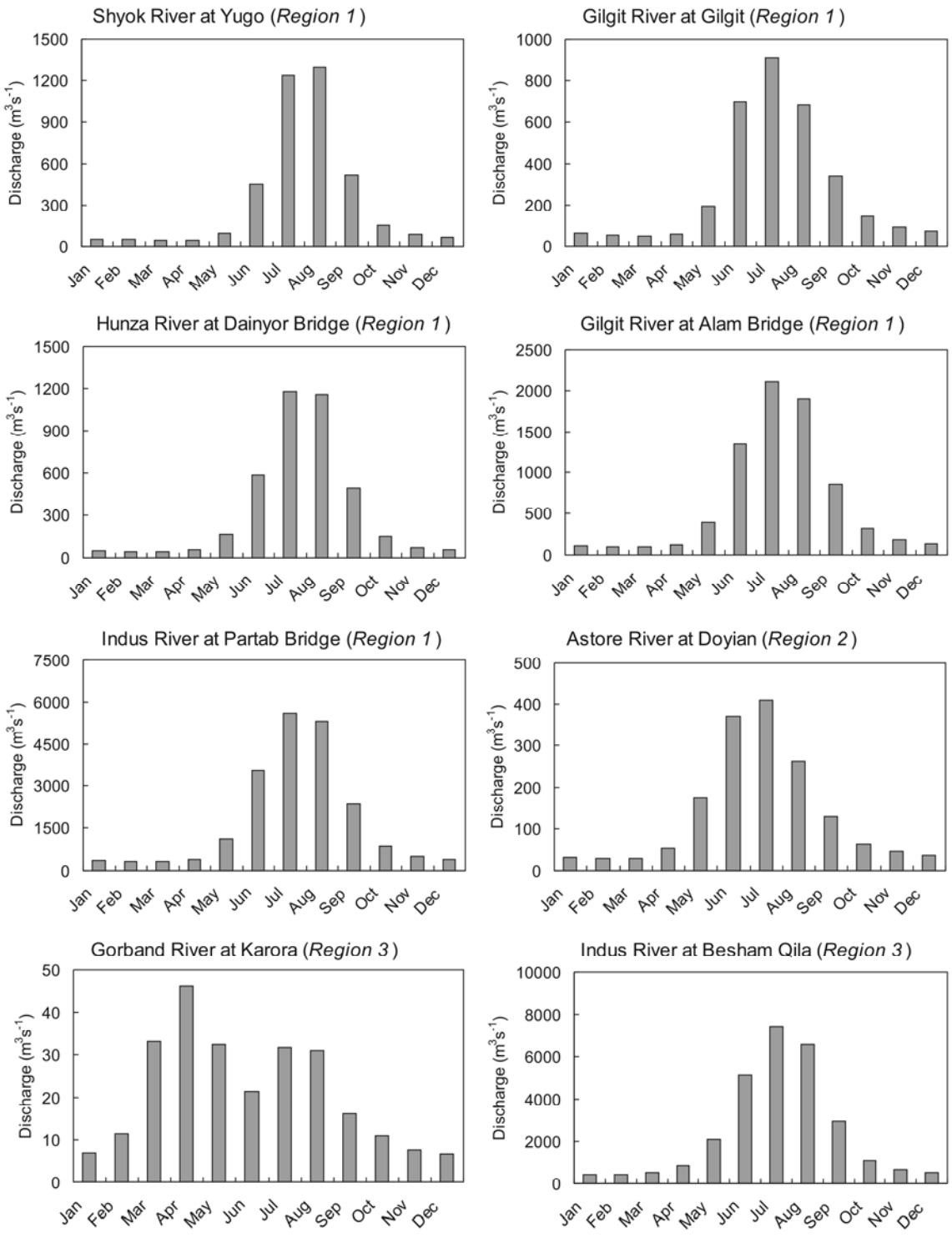

Figure 2.4 Monthly mean discharges for selected hydrological stations in the upper Indus River basin

River at Doyian exhibits one of the highest specific discharges of 1012 mm year^{-1}. The discharge pattern shows the combined effect of snowmelt and rainfall in producing the summer runoff, and compared to *Region 1*, this region shows the influence of an earlier spring snowmelt in May and June (e.g., Astore River at Doyian, Figure 2.4). It should be noted that the considerable difference between the runoff for the Astore River at Doyian (Table 2.2) and precipitation recorded in the Astore valley is explained by precipitation that occurs predominantly at high altitudes between 2500 and 5500 m in the upper Indus basin (Hormann, 1996). Because most rain gauges are located in the lower valleys (Hydrology and Research Directorate, 1997), the precipitation occurring at high altitudes is in many cases not taken into account.

Region 3 is the remaining, southernmost part of the basin, and includes the area between Besham Qila and Tarbela Dam. Three of the main tributaries in this region are the Gorband, Siran and Brandu Rivers. This part of the basin is mainly rainfed with little snow, and experiences two types of rainfall: summer monsoon rains, and late winter and early spring rainfall produced by disturbances coming from the west. This seasonal rainfall pattern is prominent with heavy rainfalls for Besham Qila (1099 mm), Daggar (1214 mm), Phulra (1196 mm) and Tarbela (910 mm) (Figure 2.3). The two distinct rainfall seasons generate two separate peaks of runoff, and the shape of the hydrograph is determined by the timing and intensity of respective rainstorm inputs (e.g., April and July for the Gorband River at Karora, Figure 2.4). Compared to the glacierized part of the basin, the monsoon-affected portion of the basin contributes a greater proportion of inflow during July to September. In general, the nature of the hydrological response in monsoon and non-monsoon drainage basins is very different. In the monsoon-affected basins the discharge can vary significantly over a few days. Conversely, the

non-monsoon basins in the glacierized area are predominantly fed by snowmelt, and therefore do not show such high variability.

2.5.1.1 Flood Generating Mechanisms

Floods in the upper Indus basin are generated by four distinct mechanisms (Archer, 2001):

(i) melting of snow and glaciers

(ii) monsoon rainfalls

(iii) dam-breaks following landslides into rivers

(iv) glacial lake outburst floods.

The relative importance of these mechanisms depends on location within the basin. High flows occur during summer months and are the results of a combination of snow and ice melt and monsoon rainfall, sometimes supplemented by the breaching of natural dams formed in the headwaters by glaciers or land slides. The snow and ice melt contribution is relatively constant from year to year. The monsoon rainfall is highly variable, and as noted earlier, the frequency and intensity of monsoon rainstorms diminishes markedly upstream along the upper Indus valley upstream of Besham Qila. The storm of 8-10 September 1992, for example, estimated to be a 100-year event, produced 230 mm rainfall at Besham Qila, but the flood rise above the prevailing glacier and snowmelt flow was only 3600 m^3s^{-1} which is approximately 23% of the total flood (NEAC Consultants, 2004). The contribution of monsoon storms is even smaller in the more northerly part of the basin. Bookhagen and Burbank (2006) noted the absence of an inner monsoon rainfall belt along the northwestern Himalaya and proposed as the explanation that the topography does not rise in a two-step pattern and the high relief appears closer to the

mountain front. It would be useful to investigate the role of extreme monsoon storms in generating large sediment pulses within the monsoon and the inter-annual variability of the monsoon (Barros et al., 2006); however, event-based monsoon storm data are not available. The regular snow and ice melt floods in the upper Indus basin are occasionally augmented by glacial lake outburst floods and dam-breaks following landslides into rivers. Intense tectonic activity in the basin results in catastrophic mass movements and landslides dams that block the river flow (Shroder and Bishop, 1998). Hewitt (1998, 2002) has documented the major catastrophic landslides and their effects on the upper Indus streams. He noted that at least 73 of the 115 historic landslide-rock avalanche events in the Himalayan region formerly dammed the main Indus River or its tributaries.

2.5.2 Sediment Rating Curves

Suspended sediment rating curves have been developed for all the stream gauging sites in the upper Indus basin (Figure 2.5). Considerable scatter indicates that there are other variables beside stream discharge influencing sediment concentrations in the river. These factors include episodic mass movements, bank collapses and inflows from local, rainfed catchments. Irregular sampling of suspended sediment concentrations is also a cause of somewhat weak relationships. The commonly used equation for a sediment rating curve is the power function

$$C = a Q^b \tag{2.1}$$

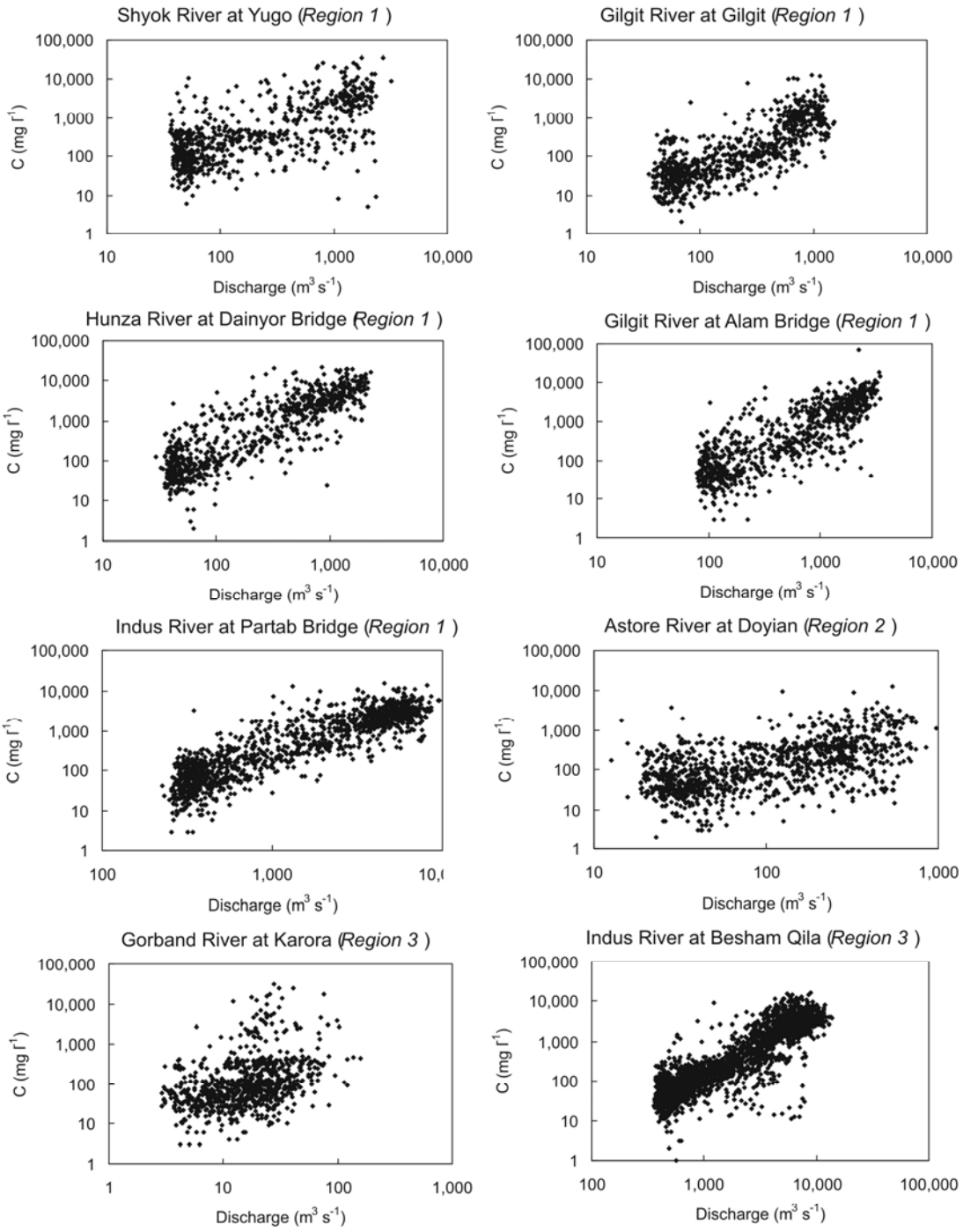

Figure 2.5 Suspended sediment rating scatter plots for selected stations in the upper Indus River basin

in which C is the suspended sediment concentration (mg l^{-1}), Q is the discharge (m^3 s^{-1}), and a and b are the regression coefficients. Ferguson (1986) argues that the river load is likely to be underestimated by discharge-sediment concentration rating curves and suggests a correction factor based on statistical considerations for removing bias when rating plots are linear with normal scatter. The regression coefficient b increases downstream along the main Indus River (Table 2.3). This contrasts with the findings of Asselman (2000) who reported that the steepness of the rating curves decreased downstream along the Rhine River. For the Indus River, the downstream increase of the coefficient b is consistent with the spatial pattern of sediment supply in the basin, with high values of b resulting from low suspended sediment concentrations at low discharges, as indicated by the lower values of the coefficient a.

The regression coefficients a and b are known to be inversely correlated (Asselman, 2000; Syvitski *et al*., 2000) and this trend is also found in the upper Indus River basin (Figure 2.6). The coefficients obtained for locations along the main Indus plot as a single lower line, whereas the coefficients obtained for the tributaries plot above this line. The upper line indicates the sample locations along the Siran River (monsoon area in *Region 3*). In between these two lines, a third line can be drawn for the stations along the Gilgit River and other tributaries. For the main Indus River, the relationship between the coefficients a and b is given by:

$$b = 0.9042 - 0.2676 \log a \qquad (r^2 = 0.9955) \qquad (2.2)$$

Relationships like this may be used further for relating the rating curve coefficients to the basin characteristics like drainage area, basin relief and mean runoff for estimating sediment yields in the ungauged sub-basins.

Table 2.3 Regression coefficients of rating curves fitted for gauging stations in the upper Indus River basin

Region	Station name	River	$C = a\,Q^b$		
			a	b	r^2
Region 1	Kharmong	Indus	1.3906	0.8355	0.2775
	Yugo	Shyok	4.5095	0.8895	0.4425
	Shigar	Shigar	30.9650	0.6674	0.3356
	Kachura	Indus	6.8986	0.7116	0.3881
	Dainyor Bridge	Hunza	0.6092	1.2439	0.7317
	Gilgit	Gilgit	0.2254	1.1852	0.6288
	Alam Bridge	Gilgit	0.1088	1.3285	0.6935
	Partab Bridge	Indus	0.0203	1.3782	0.7935
Region 2	Doyian	Astore	5.6371	0.6973	0.2793
	Shatial Bridge	Indus	0.0548	1.2288	0.7577
	Barsin	Indus	0.0051	1.5173	0.7294
Region 3	Karora	Gorband	13.9400	0.7265	0.1495
	Besham Qila	Indus	0.0047	1.4936	0.7987
	Daggar	Brandu	29.5340	1.0052	0.3165
	Darband	Indus	0.0004	1.8365	0.9263
	Phulra	Siran	1.2554	1.7198	0.6465
	Thapla	Siran	0.3356	1.8957	0.6186

2.5.3 Spatial Patterns of Seasonal Sediment Yield

Monthly mean sediment yields for selected stations are presented in Figure 2.7, which exhibit a strong variability in terms of the minimum and maximum values. Alternatively, this variation can also be shown by plotting error bars amounting to ±2 times the standard deviations (Ashmore and Day, 1988a). The sediment transport regimes for the Shyok, Gilgit, Hunza and Indus Rivers in *Region 1* clearly show the role of melting snow and ice in generating high runoff in the summer months, and a major portion (80-85%) of the annual sediment load is transported in July and August.

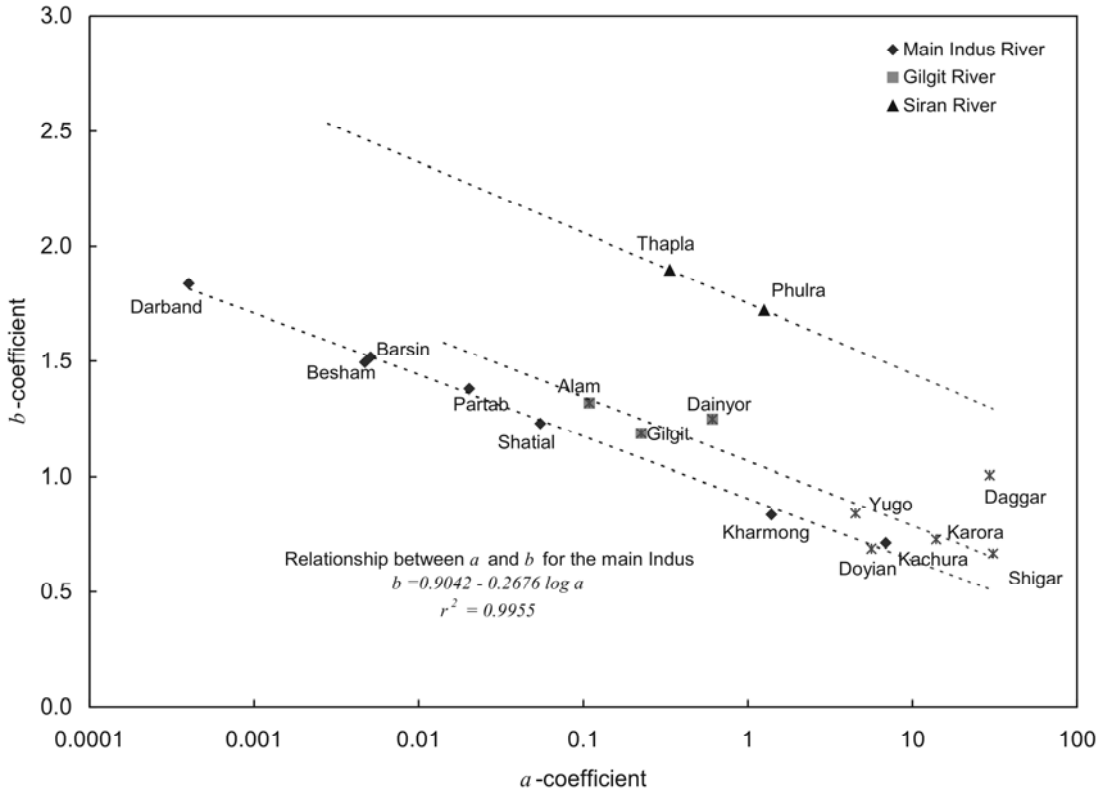

Figure 2.6 Correlation between the coefficients of the sediment rating curves in the upper Indus River basin (after Asselman, 2000)

In terms of sediment transport regime, *Region 2* appears to be similar to *Region 1*. In *Region 2*, the sediment transport regime is controlled by the interaction of rainfall and lower-elevation snowmelt as shown for the Astore River at Doyian which has an early rise of sediment yield in May, followed by a considerable increase in June (Figure 2.7). The somewhat smaller sediment yield in August as compared to *Region 1* likely reflects the decreasing contribution of glacier-melt in generating runoff and sediment.

In *Region 3*, the late winter to early spring rainfall and the summer monsoon rainfall result in two separate, similarly-sized peaks of sediment yield in April and July as shown for the Gorband

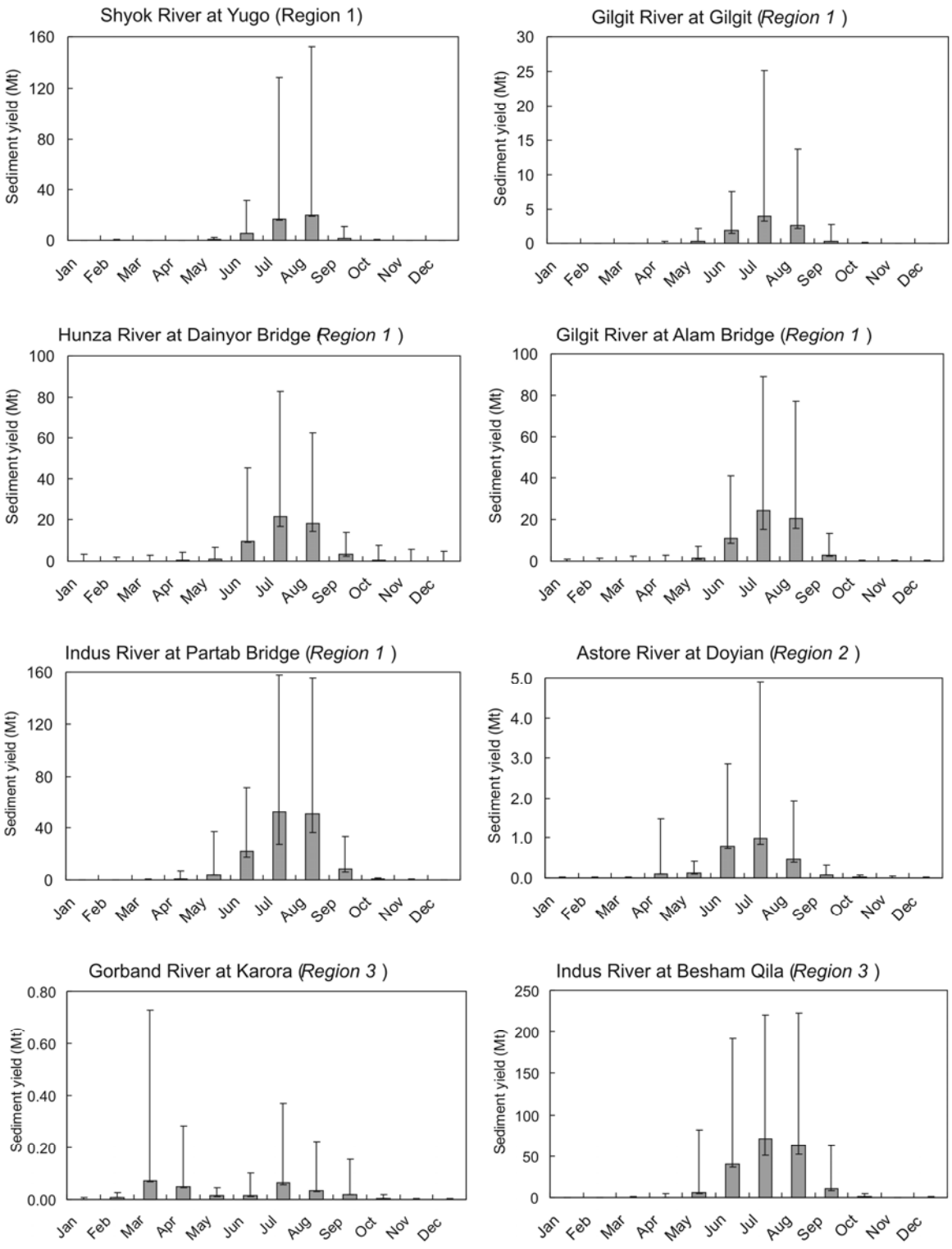

Figure 2.7 Monthly mean sediment yield for selected stations in the upper Indus River basin

River at Karora (Figure 2.7). In this region, sediment concentrations show an immediate and large response to monsoon rainstorms. Although Besham Qila is located in *Region 3*, a significant portion of its basin extends upstream into the glacierized part. The sediment transport regime therefore reflects the discharge regime of the Indus River, and does not exhibit a significant effect of spring rainfall.

2.5.4 Spatial Variation of Mean Annual Sediment Yield

A schematic representation of the spatial distribution of the mean annual sediment yield (Mt yr^{-1}) in the upper Indus River basin shows a general pattern of increasing sediment yield in the downstream direction along the main Indus River and in each of the three regions (Figure 2.8). Notable features of this diagram are a substantial sediment contribution from the Hunza River, a decrease in sediment yield between Partab Bridge and Shatial Bridge, and a major sediment yield increase between Partab Bridge and Besham Qila. A comparative plot of the sediment yield and drainage area of a few major Indus sub-basins reveals that the Hunza River contributes a greater proportion of sediment (22.8%) than its drainage area (8.1%) would indicate (Figure 2.9). This is largely caused by the very high suspended sediment concentrations in summer melt-water discharges of the Hunza River (Ferguson, 1984). The decrease in sediment yield between Partab Bridge and Shatial is likely an artifact caused by the low frequency of sampling and site specific, uneven distribution of sediments concentration near one bank of the river. The section of the basin between Partab Bridge and Besham Qila provides a major contribution to the sediment yield measured at Besham Qila. This sediment is derived from the large number of small,

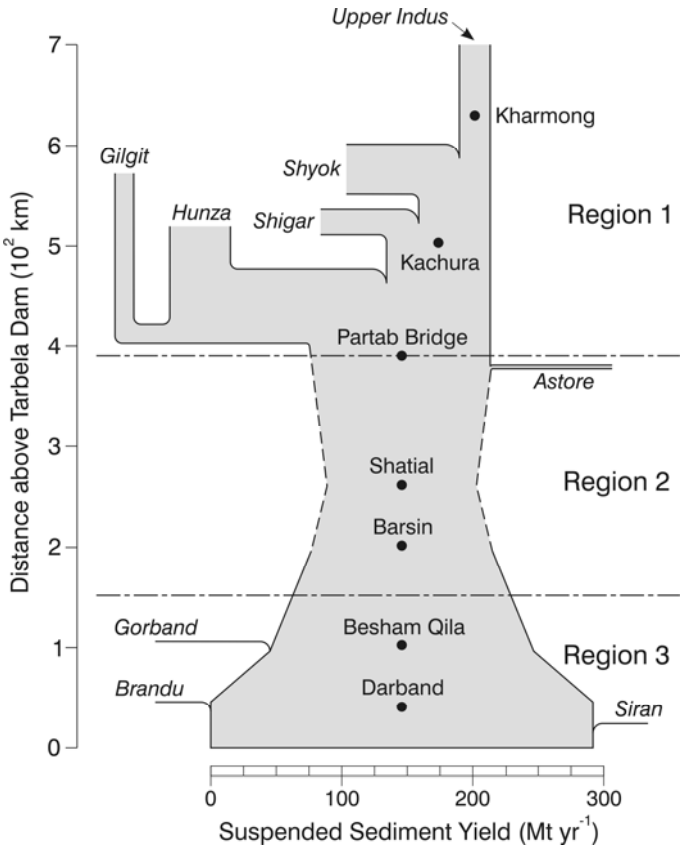

Figure 2.8 Spatial distribution of long-term mean annual sediment yield in the upper Indus River basin, northern Pakistan (Mt yr^{-1})

relatively steep catchments that discharge straight into the Indus River so that there is little opportunity for sediment storage in the steep, narrow valleys.

Sediment from the upper Indus basin is deposited in the Tarbela Reservoir. The drainage areas of the Tarbela Reservoir and the next upstream gauging station of Besham Qila are nearly the same, enabling a comparison of the cumulative sediment accumulation in Tarbela Reservoir, obtained by processing the annual hydrographic surveys of the reservoir, and the sediment yield calculated for Besham Qila. The World Commission on Dams (2000) reports an 89% trapping efficiency for Tarbela Reservoir which is attributed to the portion of sediment leaving the

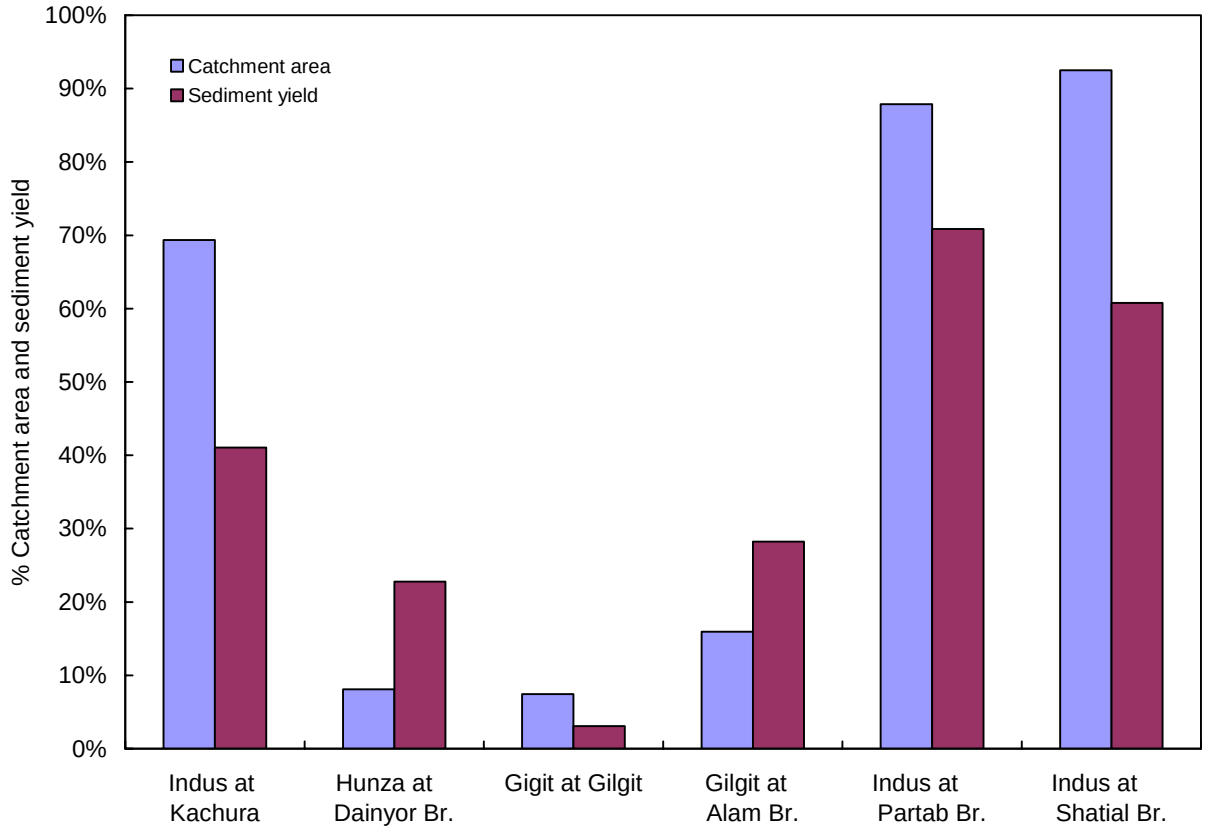

Figure 2.9 Comparison of % (Besham Qila) drainage areas and sediment yields for selected upper Indus sub-basins

reservoir through the powerhouse turbines and the spillways. However, the trapping efficiency was not considered in the comparison in Figure 2.10 which generally does not show higher values of the sediment yield at Besham Qila compared to the reservoir accumulation. A possible explanation of the similarity between the sediment yield at Besham Qila and in Tarbela Reservoir is the bed load component of the total load, which is not measured at Besham Qila but is included in the reservoir accumulation determined from reservoir hydrographic surveys, thus masking the effect of trapping efficiency in the comparison.

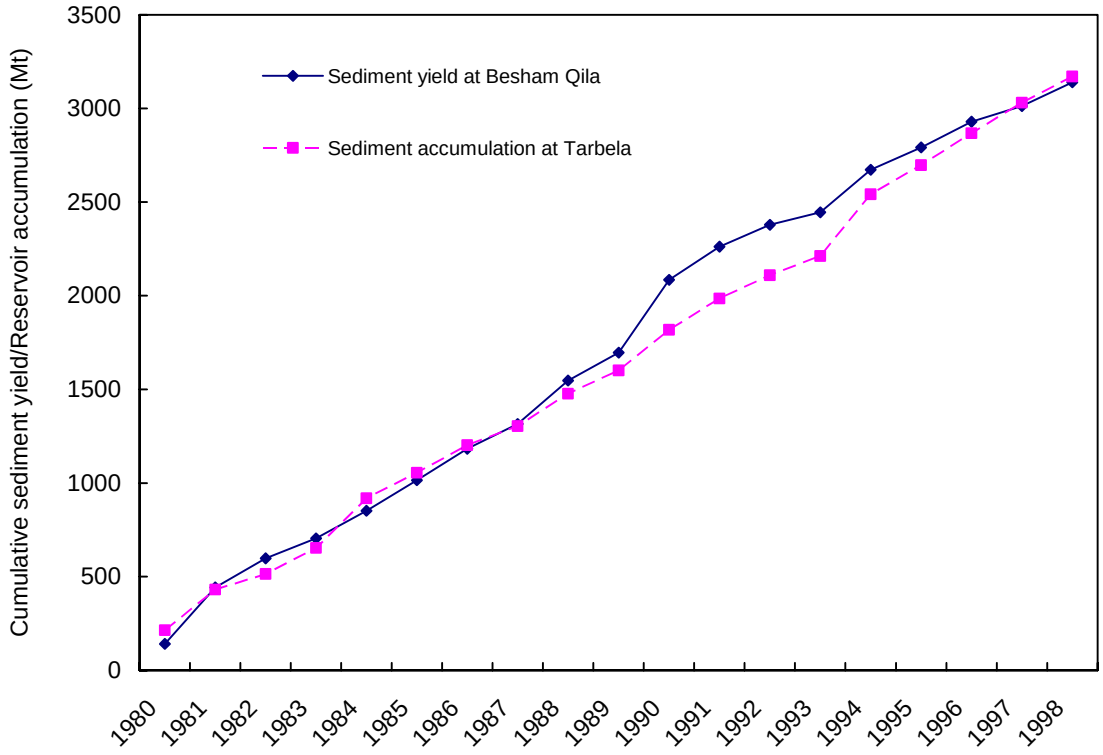

Figure 2.10 Comparison of cumulative sediment accumulation in Tarbela Reservoir and the sediment yield of the upper Indus River at Besham Qila

2.5.5 Specific Sediment Yield in the Upper Indus Basin

Different morphological and climatological characteristics within the upper Indus basin cause the specific sediment yield (t km^{-2} yr^{-1}) to vary from one sub-basin to another (Table 2.2). At Kharmong, the first gauging station on the Indus after it enters Pakistan, the specific sediment yield is 355 t km^{-2} yr^{-1}. The next station downstream on the upper Indus is near Kachura, where the specific sediment yield increases to 710 t km^{-2} yr^{-1}. In this high altitude reach of the upper Indus, two main tributaries, the Shyok and Shigar Rivers, contribute considerable amounts of

suspended sediment at rates of 924 and 2542 t km^{-2} yr^{-1}, respectively. The Gilgit River is the next major tributary, and contributes 2095 t km^{-2} yr^{-1} to the Indus River at Alam Bridge. The major portion of the sediment in the Gilgit River comes from the Hunza River basin, which shows the highest sediment yield of 3373 t km^{-2} yr^{-1}. The Hunza basin has the highest glacierized area (28%) in the Indus River basin (Collins, 1994). At Partab Bridge on the Indus River, below its confluence with the Gilgit River, the specific sediment yield is 968 t km^{-2} yr^{-1}. The record of the Astore River at Doyian indicates a specific sediment yield of 427 t km^{-2} yr^{-1}, which is relatively low. The specific sediment yield of the Indus River decreases to 789 t km^{-2} yr^{-1} at Shatial, which likely reflects deposition within the valley in this reach. The specific sediment yield then gradually increases downstream, from 892 t km^{-2} yr^{-1} at Barsin to 1197 t km^{-2} yr^{-1} at Besham Qila. Between Besham Qila and the basin outlet at Tarbela Dam, three tributaries that are under the influence of the monsoon join the Indus River. The Gorband River at Karora has a specific sediment yield of 250 t km^{-2} yr^{-1}. The specific sediment yield of the Siran River is 2306 t km^{-2} yr^{-1}at Phulra and 1024 t km^{-2} yr^{-1}at Thapla, whereas the specific sediment yield of the Brandu River is relatively small at 442 t km^{-2} yr^{-1}.

Drainage area is one of the most commonly used factors to analyze specific sediment yield. The conventional model of specific sediment yield shows an inverse relationship between drainage area and specific sediment yield (Walling, 1983). This can be attributed to the fact that larger areas have lower overall slopes, smaller percentages of erodible rock formations, and more opportunities for sediment eroded from the steeper slopes upstream to be deposited on downstream floodplains. With a specific sediment yield of approximately 1197 t km^{-2} yr^{-1}, the

upper Indus falls in the upper ranges for large mountainous drainage basins of the world (Dedkov and Moszherin, 1992).

The relationship of drainage area and specific sediment yield for various upper Indus sub-basins does not show an obvious general trend (Figure 2.11). The scatter is greatly reduced, however, when the stations are divided into two sets, i.e, the Indus River and its tributaries. No relationship is found between the drainage area and specific sediment yields for the tributaries (Figure 2.11), possibly because of the variability in the characteristics of the tributary basins, the low density of stream gauging stations, and anomalously high sediment concentrations associated with the failure of dams formed by landslides. The main Indus River, however, displays a trend of increasing specific sediment yield with drainage area, from 355 t km^{-2} yr^{-1} at Kharmong to 1197 t km^{-2} yr^{-1} at Besham Qila. This follows the same pattern observed by Church and Slaymaker (1989) in British Columbia, De Boer and Crosby (1996) in the southeastern Prairie region of Saskatchewan, Lu and Higgitt (1999) in the upper Yangtze, China and Schiefer *et al*. (2001) in the Canadian Cordillera. Church *et al*. (1989) attribute the increasing specific sediment yields to the dominance of secondary remobilization of Quaternary sediments from stream banks and valley bottom areas over primary denudation of the land surface. The sharp increase in specific sediment yield with drainage area in the upper Indus River is shown in Figure 2.12 along with the two contemporary specific sediment yield models, i.e., the conventional sediment yield model and the Church-Slaymaker model. The Indus River shows a clear deviation from the conventional model and falls above the upper limits of the Church-Slaymaker model. If the Indus River curve is extended by including data points from the downstream Indus plains, it is possible that a trend similar to the Church-Slaymaker model of decreasing sediment yields with increasing basin areas beyond 200,000 km^2 will be found.

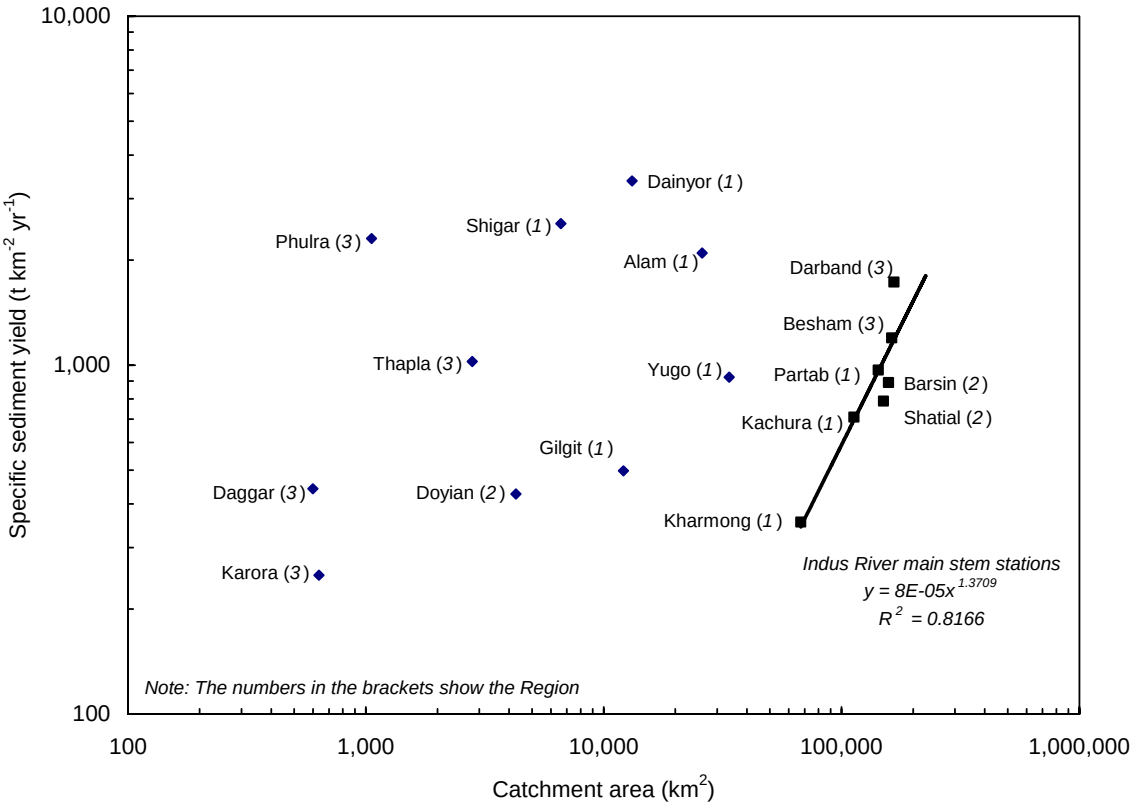

Figure 2.11 Relationship between specific sediment yield and drainage area in the upper Indus River basin

2.5.6 Magnitude-Frequency Characteristics

An analysis of the magnitude-frequency characteristics of sediment transport in the upper Indus River basin (Table 2.4) shows that $Q_{s,avg}$, the percentage of the total annual sediment load transported at discharges below the annual average discharge (Q_{avg}) ranges from 1 to 6% for the main Indus River and its tributaries (Shyok, Hunza and Gilgit) in the northern, glacierized *Region 1*. However, $Q_{s,10\%}$, the percentage of the total annual sediment load transported at discharges exceeded 10% of the time ($Q_{10\%}$), i.e., about 36 days per year, constitutes the major portion of the transported sediment, ranging from 49 to 69%. Further downstream in the basin,

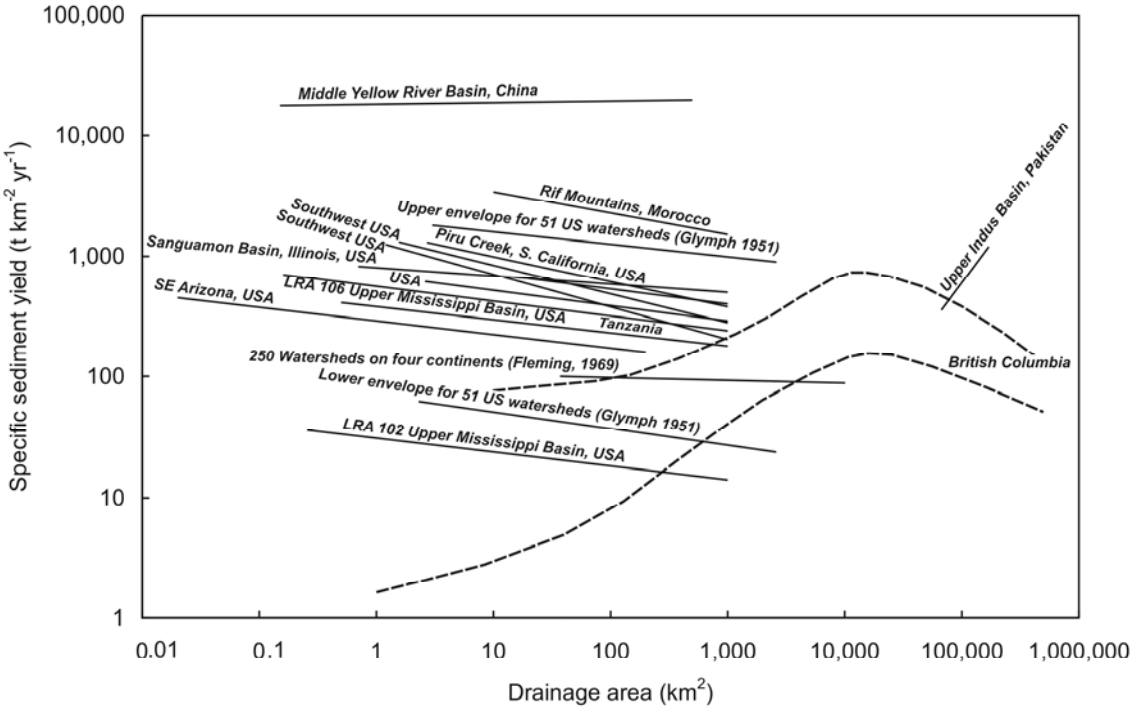

Figure 2.12 Comparison between contemporary specific sediment yield models and the upper Indus River basin (after results in Walling, 1983; Church *et al*., 1989 and Schiefer *et al*., 2001)

$Q_{s,avg}$ gradually increases to 8.4% for the Astore River at Doyian in *Region 2*, and to 12.4% for the Gorband River at Karora in the monsoon-affected *Region 3*, whereas $Q_{s,10\%}$ decreases to 38-49% in the lower *Regions 2* and *3*. Although the steepness of the sediment rating curves increases downstream along the Indus River, no significant differences in the sediment transport regime are observed. This is in agreement with Asselman's (2000) finding that differences in the steepness of rating curves do not necessarily indicate differences in sediment transport regimes. The only considerable increase of sediment transported at higher discharges from Kachura to Partab Bridge along the main Indus River, as depicted by the respective rating curves, is explained in terms of the major sediment input from the Gilgit River upstream of Partab Bridge.

Table 2.4 Magnitude-frequency characteristics of sediment transport along the upper Indus River and its main tributaries (after Asselman, 2000)

Station	River	Q_{avg} (m^3s^{-1})[a]	$Q_{avg\%}$ (% time)[b]	$Q_{s,avg}$ (% Q_s)[c]	$Q_{10\%}$ (m^3s^{-1})[d]	$Q_{s,10\%}$ (%Q_s)[e]
Yugo	Shyok	341.6	69.9	2.9	1177.8	66.1
Dainyor Bridge	Hunza	337.2	67.6	1.4	1079.0	68.5
Gilgit	Gilgit	281.1	66.1	2.6	789.1	54.9
Alam Bridge	Gilgit	639.4	66.8	1.8	1914.0	58.9
Doyian	Astore	136.1	66.7	8.4	354.4	48.5
Karora	Gorband	20.7	55.6	12.4	44.0	37.8
Kachura	Indus	1060.0	66.5	6.1	3105.1	49.1
Partab Bridge	Indus	1759.1	66.9	1.8	5263.6	57.9
Shatial Bridge	Indus	2018.3	65.3	2.4	5832.1	52.3
Besham Qila	Indus	2393.7	66.2	2.1	6819.8	57.5
Darband	Indus	2448.6	66.9	1.1	6901.3	57.1

[a] Q_{avg}, annual average discharge
[b] $Q_{avg\%}$, percentage of time during which discharges are lower than Q_{avg}
[c] $Q_{s,avg}$, percentage of the total annual sediment load transported at discharges below Q_{avg}
[d] $Q_{10\%}$, discharge that is exceeded 10% of the time, i.e. about 36 days per year
[e] $Q_{s,10\%}$, percentage of the total annual sediment load transported at discharges higher than $Q_{10\%}$

The importance of extreme events for sediment transport in the Indus River basin contrasts with Wolman and Miller's (1960) conclusion that a large proportion of the work done by rivers occurs during events of modest magnitude and high frequency. Nevertheless, Petts and Foster (1985) note that extreme events may be much more significant in high relief areas with semi-arid climates as found in the upper Indus River basin. Sichingabula (1999) observed the same trend for the mountainous Fraser River Basin in British Columbia, where 50% of the sediment load was transported by 12 to 22% of the total discharge.

The effective discharge refers to the discharge class that transports a greater portion of suspended sediment load than any other discharge class (Pickup, 1976). Sediment discharge

histograms for selected stations in the upper Indus River basin (Figure 2.13) reveal a wide range of effective discharges (Figure 2.13). The effective discharges for all stations are larger than the average discharge, and range from 1.5-2.0 to 5.5-6.0 times the average discharge. There is a trend of a downstream decrease in the effective discharge. For example, the stations located in the headwaters of the basin in glacierized *Region 1* (Shyok River at Yugo and Hunza River at Dainyor) have the highest effective discharges, ranging from 5.0-5.5 to 5.5-6.0 times the average discharge. The effective discharge decreases to a value of 2.5-3.0 (Astore River at Doyian) in *Region 2*, and to 1.5-2.0 times the average discharge (Gorband River at Karora) in *Region 3*. The main Indus River, however, shows a consistent effective discharge of 2.5-3.0 times the average discharge.

The shape of the various histograms varies considerably in different regions of the basin (Figure 2.13). The first group of histograms consists of stations for which the effective discharge occurs at relatively high discharges and extreme events transport sediment loads comparable to the effective discharge. This results in a histogram with at least one secondary peak at the extreme end of the discharge range (e.g., the Shyok River at Yugo and Hunza River at Dainyor in the upper glacierized *Region 1*). In the second group of stations, an effective discharge can be recognized, but the histograms have erratic forms, with discharges of widely varying magnitudes transporting nearly similar sediment loads (e.g., the Astore River at Doyian in *Region 2*). The third group of histograms consists of stations that fit the classical model, with a well defined single mode and an effective discharge that is relatively frequent (e.g., the Gorband River at Karora in *Region 3*). The stations along the main Indus River like Shatial Bridge and Darband constitute the fourth group with a clear unimodal shape. For this group, most of the sediment is

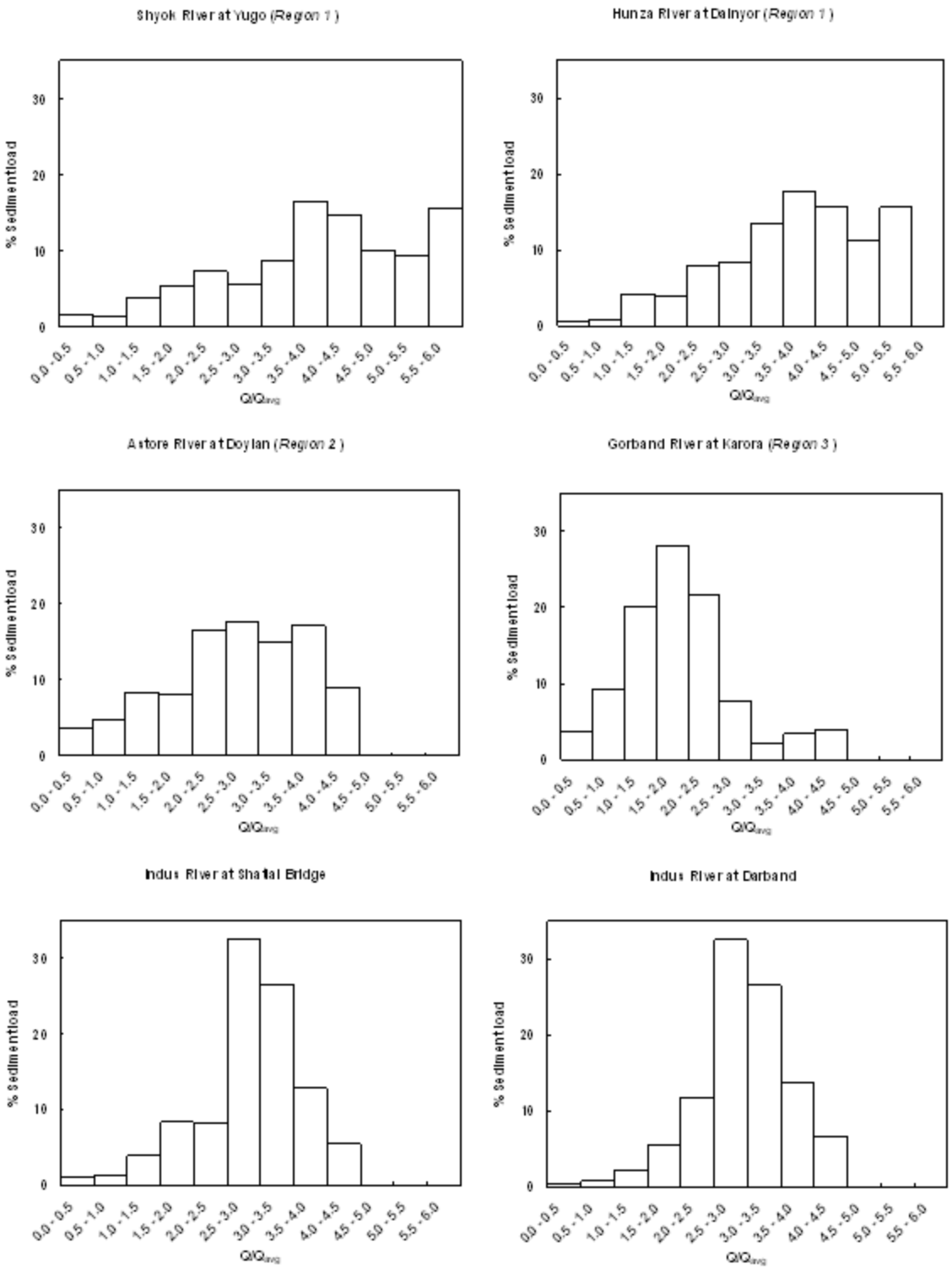

Figure 2.13 Forms of sediment discharge histograms in the upper Indus River basin

moved at very high discharges. A similar variety in histogram shapes was also noticed by Ashmore and Day (1988b) for the Saskatchewan River basin and by Sichingabula (1999) for the Fraser River in British Columbia.

2.6 Conclusions

The suspended sediment transport characteristics in the upper Indus basin show considerable variation due to differences in physiography, climate, hydrologic regime, and drainage area. Following the hydrologic regimes observed by Archer (2003), the basin was subdivided into three characteristic regions based on whether runoff production is controlled by temperature (*Region 1*, upper, glacierized sub-basins), precipitation (*Region 3*, lower sub-basins), or a combination of the two (*Region 2*, middle reaches). The nature of the hydrological response is very different in the monsoon-affected southern part of the basin and non-monsoon, glacierized northern part of the basin. In the monsoon basins, the discharge can vary significantly over a few days, with an immediate and large response in the sediment concentration. Conversely, the non-monsoon basins are predominantly fed by snowmelt, and therefore do not show such high variability.

Analysis of the regression coefficients of the sediment rating curves ($C = aQ^b$) shows that the coefficient b increases downstream along the main Indus River, and in each of the three regions. This suggests that the sediment transport capacity of the rivers at high discharges increases in the downstream direction. However, no significant differences in the magnitude-frequency characteristics of sediment transport are observed for the upper Indus River. The

coefficients obtained for locations along the main Indus plot as a single lower line, whereas the coefficients obtained for the tributaries plot above this line. The upper line indicates the sample locations in monsoon-affected area along the Siran River. In between these two lines, a third line can also be drawn for the stations along the Gilgit River and other tributaries.

The seasonal sediment transport regimes for the Shyok, Gilgit, Hunza and Indus Rivers in the glacierized northern *Region 1* show the effect of melting snow and ice on generating high runoff in summer months. In *Region 1*, 80 to 85% of the annual sediment load is transported in July and August. The seasonal distribution in *Region 2* is influenced by the interaction of snowmelt and rainfall. In this region, the Astore River at Doyian shows an early ascend of sediment yield starting in May due to snowmelt at lower elevations, and a comparatively lower sediment yield in August due to a decreased importance of ice-melt. *Region 3* is mainly rainfed and experiences two types of rainfall: summer monsoon rains, and late winter to early spring rainfall produced by western disturbances. Consequently, two separate peaks of sediment discharge are observed for the Gorband River at Karora in April and July. The seasonal pattern also shows that the sediment yield is spread equally over two seasons.

The mean annual sediment yield increases downstream along the Indus River. The Hunza River contributes a greater proportion of sediment than its drainage area would indicate. The sediment yield decreases between Partab Bridge and Shatial Bridge, possibly reflecting deposition in the valley. The section between Partab Bridge and Besham Qila provides a major contribution to the sediment load at Besham Qila. This can be attributed to the presence of a

large number of small, relatively steep catchments that discharge straight in to the Indus River without much opportunity for sediment storage in the narrow valleys.

The specific sediment yield of the main Indus River increases with drainage area, from 355 t km^{-2} yr^{-1} at Kharmong to 1197 t km^{-2} yr^{-1} at Besham Qila. This is contrary to the conventional sediment yield model which holds that specific sediment yield generally decreases with drainage area due to the increased opportunity for sediment storage as drainage area increases. The increase in specific sediment yield along the Indus River can be explained by the predominance of channel erosion as compared to slope (sheet, gully) erosion, and the steep straight channels discharging directly into the Indus River. No relationship is found between drainage area and specific sediment yields for the tributaries. Overall, the upper Indus basin exhibits distinct patterns of suspended sediment yield along the main Indus River and in each of the three regions that reflect the hydrologic regimes of the basin.

An analysis of the magnitude-frequency characteristics of sediment transport in the basin reveals a trend of transporting most sediment during extreme events. The percentage of sediment transported at high discharges decreases downstream. The sediment discharge histograms reveal a variety of forms and a wide range of effective discharges. The effective discharges for tributaries range from 1.5-2.0 to 5.5-6.0 times the average discharge, and decrease downstream. The main Indus River, however, shows a consistent effective discharge in the range of 2.5-3.0 times the average discharge.

The magnitude and frequency of sediment transport depend not only on the hydraulics of the river system, but also on the complex pattern of sediment availability from the sources in the basin. A true picture of sediment dynamics therefore can be presented by constructing a sediment budget since it provides a comprehensive accounting of the sources and disposition of sediments in the drainage basin (Walling and Horowitz, 2005). Construction of a sediment budget for the upper Indus basin; however, demands a better understanding of the link between the source areas and delivery process. The upper Indus exists in natural basin conditions without significant human impacts. Since a number of high dams are planned for future development of the area and the already sparse gauging network in this large basin is rapidly decreasing in density, the upper Indus represents a good case study for investigating sediment dynamics of a large mountainous data-sparse river basin as a contribution to the Prediction in Ungauged Basins (PUB) program.

2.7 References

Ahmad, N. (1993) Water Resources of Pakistan and their Utilization. Shahid Nazir, Lahore.

Ali, K.F., De Boer, D.H. (2003) Construction of sediment budgets in large scale drainage basins: the case of the upper Indus River. Proc. Sapporo Symp., July 2003, IAHS Publ. 279, pp. 206-215.

Archer, D. (2001) The climate and hydrology of northern Pakistan with respect to assessment of flood risk to hydropower schemes. Unpublished report, GTZ/WAPDA/VSO, Lahore.

Archer, D. (2003) Contrasting hydrological regimes in the upper Indus basin. *J. Hydrol*. *274*, 198-210. DOI: 10.1016/S0022-1694(02)00414-6

Ashmore P.E., Day T.J. (1988a) Spatial and temporal patterns of suspended-sediment yield in the Saskatchewan River basin. *Canadian Journal of Earth Sciences 25*(9), 1450-1463.

Ashmore, P. E., Day, T. J. (1988b) Effective discharge for suspended sediment transport in streams of the Saskatchewan River basin. *Water Resour. Res*., *24*(6), 864–870.

Asselman, N.E.M. (2000) Fitting and interpretation of sediment rating curves. *J. Hydrol*. *234*, 228-248.

Barros, A.P., Gordon, S.J. (2002) Assessing the linkages among climate variability, land-use change, and the sedimentary regime of the Upper Chesapeake Bay. Proc. Coastal Environment 2002, WIT Press, pp. 183-192.

Barros, A.P., Chiao, S., Lang, T.J., Burbank, D., Putkonen, J. (2006) From weather to climate - Seasonal and interannual variability of storms and implications for erosion processes in the Himalayas. In: Willet, S.D., Hovius, N., Brandon, M.T., Fisher, D.M. (Eds.), Tectonics,

Climate and Landscape Evolution, Geological Society of America A Special Paper 398, pp. 17-38. DOI:10.1130/2006.2398(02).

Bookhagen, B., Burbamk, D.W. (2006) Topography, relief, and TRMM-derived rainfall variations along the Himalaya. *Geophysical Research Letters 33*, L08405. DOI: 10.1029/2006GL026037, 2006.

Church, M., Slaymaker, O. (1989) Disequilibrium of Holocene sediment yield in glaciated British Columbia. *Nature 337*, 452-454.

Church, M., Kellerhals, R., Day, T.J. (1989) Regional clastic sediment yield in British Columbia. *Can. J. Earth Sci*. *26*, 31-45.

Collins, D.N. (1994) Hydrology of Glacierized Basins in the Karakoram: Snow and Ice Hydrology Project Pakistan. Alpine Glacier Project, University of Manchester.

Collins, D.N., Hasnain, S.I. (1995) Runoff and sediment transport from glacierized basins at the Himalayan scale. Proc. Boulder Symp., July 1995, IAHS Publ. 226, pp. 17-25.

De Boer, D.H., Crosby, G. (1996) Suspended sediment yield and drainage basin scale. Proc. Exeter Symp., July 1996, IAHS Publ. 236, pp. 333-338.

Dedkov, A.P., Moszherin, V.I. (1992) Erosion and sediment yield in mountain regions of the world. Proc. Chengdu Symp., July 1992, IAHS Publ. 209, pp. 29-36.

Edwards, T.K., Glysson, G.D. (1999) Field Methods for Measurement of Fluvial Sediment. U.S. Geological Survey, TWI 3-C2.

Evans, M. (1997) Temporal and spatial representativeness of alpine sediment yields: Cascade Mountains, British Columbia. *Earth Surf. Process. Landforms 22*, 287-295.

Ferguson, R.I. (1984) Sediment load of the Hunza River. In: Miller K.J. (Ed.), The International Karakoram Project. Cambridge University Press, Cambridge, pp. 580-598.

Ferguson, R.I. (1986) River loads underestimated by rating curves. *Wat. Resour. Res. 22*(1), 74-76.

Fleming, G. (1969) Design curves for suspended load estimation. Proc. Institution of Civil Engineers, 43, 1-9.

Glazyrin, G.E., Tashmetov, H.K. (1995) Sediment yield alteration of mountain rivers and climate change in central Asia. Proc. Boulder Symp., July, 1995, IAHS Publ. 226, pp. 187-190.

Glymph, L.M. (1951) Relation of sedimentation to accelerated erosion in the Missouri River basin. U.S. Department of Agriculture, Soil Conservation Service Technical Paper 102.

GTZ (German Agency for Technical Cooperation) (1999) Preliminary Report on Hydrological Activities in Northern Pakistan: Main Report. Programme for National Hydropower Development, Government of Pakistan, Ministry of Water and Power in collaboration with GTZ, Lahore.

Hewitt, K. (1998) Catastrophic landslides and their effects on the upper Indus streams, Karakoram Himalaya, northern Pakistan. *Geomorphology 26*, 47-80.

Hewitt, K. (2002) Postglacial landform and sediment associations in a landslide-fragmented river system: the Trans Himalayan Indus streams, central Asia. In: Hewitt K, Byrne M-L, English M, Young G (Eds.), Landscapes of Transition: Landform Assemblages and Transformations in Cold Regions, Kluwer Academic Publishers, Dordrecht, pp. 61-91.

Holeman, J.N. (1968) The sediment yield of major rivers of the world. *Wat. Resour. Res*. *4*, 737-747.

Hormann, K. (1996) Precipitation Distribution in Space and Time in Northern Pakistan High-Mountain Area. Pakistan-German Technical Cooperation, WAPDA/GTZ, Kiel.

Hydrology and Research Directorate (1997) Pakistan Snow and Ice Hydrology Project (Phase II). Hydrology and Research Directorate, WAPDA, Lahore.

Kazmi, A.H. (1984) Geology of the Indus Delta. In: Haq, B.U., Milliman, J.D. (Eds.), Marine Geology and Oceanography of Arabian Sea and Coastal Pakistan. Van Nostrand Reinhold, New York, pp. 71-84.

Knighton, D. (1998) Fluvial Forms and Processes: A New Perspective. Arnold, London.

Lane, L.J., Hernandez, M., Nichols, M. (1997) Processes controlling sediment yield from watersheds as functions of spatial scale. *Environmental Modelling and Software 12*, 355-369.

Lu, X.X., Higgitt, D.L. (1999) Sediment yield variability in the Upper Yangtze, China. *Earth Surf. Process. Landforms 24*, 1077-1093.

Ludwig, W., Probst, J.L. (1998) River sediment discharge to the oceans: Present-day controls and global budgets. *Am. J. Sci*. *298*, 265-295.

Meade, R.H., Yuzyk, T.R., Day, T.J. (1990) Movement and storage of sediment in rivers of the United States and Canada. In: Wolman, M.G., Riggs, H.C. (Eds.), Surface Water Hydrology. Geological Society of America, Boulder, pp. 255-280.

Meadows, A., Meadows, P.S. (Eds) (1999) The Indus River: Biodiversity, Resources, Humankind. Oxford University Press, Karachi.

Meybeck, M. (1976) Total mineral dissolved transport by world major rivers. *Hydrol. Sci. Bull*. *21*, 265-284.

Miller, K.J. (Ed) (1984) The International Karakoram Project. Cambridge University Press, Cambridge.

Milliman, J.D., Meade, R.H. (1983) World-wide delivery of river sediment to the oceans. *J. Geol*. *91*, 1-21.

Milliman, J.D., Quraishee, G.S., Beg, M.A.A. (1984) Sediment discharge from the Indus River to the ocean: past, present and future. In: Haq, B.U., Milliman, J.D. (Eds.), Marine Geology and Oceanography of Arabian Sea and Coastal Pakistan. Van Nostrand Reinhold, New York, 65-70.

Milliman, J.D., Syvitski, J.P.M. (1992) Geomorphic/tectonic control of sediment discharge to the ocean: the importance of small mountainous rivers. *J. Geol*. *100*, 525-544.

Molnar, P., Tapponnier, P. (1975) Cenozoic tectonics of Asia: Effects of a continental collision. *Science 189*, 419-426.

MONENCO (Montreal Engineering Company) (1984) Hydroelectric Inventory Ranking and Feasibility Studies for Pakistan. CIDA Project 714/00603. WAPDA, Lahore.

NEAC Consultants (2004) Feasibility study of the Basha Diamer Dam Hydropower Project. WAPDA, Lahore.

Petts, G., Foster, I. (1985) Rivers and Landscapes. Edward Arnold, London, UK.

Pickup, P.G. (1976) Adjustment of stream-channel shape to hydrologic regimes. *J Hydrol*. *30*, 365-373.

Rantz, S.E. and others (1982) Measurement and Computation of Streamflow - Volume 1. Measurement of Stage and Discharge: U. S. Geological Survey Water-Supply Paper. 2175.

Ritter, D.F., Kochel, R.C., Miller, J.R. (2002) Process Geomorphology. McGraw-Hill, New York.

Schiefer, E., Slaymaker, O., Klinkenberg, B. (2001) Physiographically controlled allometry of specific sediment yield in the Canadian Cordillera: A lake sediment based approach. *Geografiska Annaler 83A*(1-2), 55-65.

Searle, M.P. (1991) Geology and Tectonics of the Karakoram Mountains. John Wiley & Sons, New York.

Shroder, J.F. (Ed) (1993) Himalaya to the Sea: Geology, Geomorphology and the Quaternary. Routledge, Chichester.

Shroder, J.F., Bishop, M.P. (1998) Mass movement in the Himalaya: new insights and research directions. *Geomorphology 26*, 13-35.

Sichingabula, H.M. (1999) Magnitude-frequency characteristics of effective discharge for suspended sediment transport, Fraser River, British Columbia, Canada. *Hydrol. Processes*, *13*, 1361-1380.

Singh, P., Ramasastri, K.S., Kumar, N. (1995) Topographical influence on precipitation distribution in different ranges of Western Himalayas. *Nordic Hydrology 26*, 259-284.

Summerfield, M.A., Hulton, N.J. (1994) Natural controls of fluvial denudation rates in major world drainage basins. *J. Geophys. Res*. *99*(B7), 13,871-13,884.

Survey and Hydrology (2005) Tarbela Reservoir Sedimentation Report 2004. Tarbela Dam Project, Tarbela.

SWHP (Surface Water Hydrology Project) (2001) Sediment Appraisal of Pakistan Rivers 1960-1998. SWHP, WAPDA, Lahore.

SWHP (Surface Water Hydrology Project) (2004) Annual Report of River Discharge, Sediment and Quality Data for the Year 2002: Vol-1. SWHP Publication No. 62, Surface Water Hydrology Project, WAPDA, Lahore.

Syvitski, J.P., Morehead, M.D., Bahr, D.B., Mulder, T. (2000) Estimating fluvial sediment transport: the rating parameters. *Wat. Resour. Res*. *36*(9), 2747-2760.

TAMS (1962) Tarbela Dam Project: Project Planning Report. West Pakistan Water and Power Development Authority, Lahore.

TAMS (1984) Tarbela Dam Project: Completion Report on Design and Construction. WAPDA, Lahore.

TAMS and HR Wallingford (1998) Tarbela Dam Sediment Management Study. WAPDA, Lahore.

USBR (U.S. Bureau of Reclamation) (1987) Design of Small Dams. U.S. Bureau of Reclamation, Water Resources Technical Publication, Denver, Colorado.

Walling D.E. (1983) The sediment delivery problem. *J. Hydrol*. *65*, 209-237.

Walling, D.E., Webb, B.W. (Eds) (1996) Erosion and Sediment Yield: Global and Regional Perspectives. Proc. Exeter Symp., July 1996, IAHS Publ. 236.

Walling, D.E., Horowitz, A.J. (Eds) (2005) Sediment Budgets 1. Proc. Foz do Iguaçu Symp., April 2005, IAHS Publ. 291.

Wolman, M.G., Miller, J.P. (1960) Magnitude and frequency of forces in geomorphic processes. *J. Geol*. *68*, 54-74.

World Commission on Dams (2000) Tarbela Dam and the Related Aspects of the Indus River Basin Pakistan. World Commission on Dams (WCD), Cape Town.

Young, G.J., Hewitt, K. (1990) Hydrology research in the upper Indus basin. Proc. Štrbské Pleso Symp., June 1988, IAHS Publ. 190, pp. 139-152.

CHAPTER 3 – FACTORS CONTROLLING SPECIFIC SEDIMENT YIELD IN THE UPPER INDUS RIVER BASIN, NORTHERN PAKISTAN

Ali, K. F., and D. H. De Boer (2008), Factors controlling specific sediment yield in the upper Indus River basin, northern Pakistan, *Hydrol. Processes*, *22*, 3102–3114, doi: 10.1002/hyp.6896.

3.1 Abstract

Estimates of sediment yield are essential in water resources analysis, modeling and engineering, in investigations of continental denudation rates, and in studies of drainage basin response to changes in climate and land use. The availability of high resolution, global environmental datasets offers an opportunity to examine the relationships between specific sediment yield (SY_{sp}) and drainage basin attributes in a GIS environment. This study examines SY_{sp} at 14 long-term gauging stations within the upper Indus River basin. Twenty-nine environmental variables were derived from global datasets, the majority with a 1 x 1 km resolution. The SY_{sp} ranges from 194 to 1302 t km^{-2} yr^{-1} for sub-basins ranging from 567 to 212,447 km^2. The high degree of scatter in SY_{sp} is greatly reduced when the stations are divided into three groups: upper, glacierized sub-basins; lower, monsoon sub-basins; and the main Indus River. Percent snow/ice cover (LC_s) emerges as the single major land cover control for SY_{sp} in

the high mountainous upper Indus River basin. A regression model with percent snow/ice cover (LC_s) as the single independent variable explains 73.4% of the variance in SY_{sp} for the whole Indus basin. A combination of percent snow/ice cover (LC_s), relief and climate variables explains 98.5% of the variance for the upper, glacierized sub-basins. For the lower monsoon region, a regression model with only mean annual precipitation (P) explains 99.4% of the variance. Along the main Indus River, a regression model including just basin relief (R) explains 92.4% of the variance in SY_{sp}. Based on the R^2_{adj} and *p-value* statistics, the variables used explain the majority of variance in the upper Indus River basin.

Keywords: Indus River, Himalayas, sediment yield, sediment transport, snow and ice, GIS

3.2 Introduction

Sediment yield is defined as the total sediment output from a basin over a specified time period, with suspended sediment as the dominant component. Estimates of sediment yield are essential in water resources analysis, modeling and engineering (*e.g.,* Walling and Webb, 1996; Lane *et al*., 1997), in investigations of continental denudation rates (*e.g.,* Summerfield and Hulton, 1994), in studies of drainage basin response to changes in climate (*e.g.,* Glazyrin and Tashmetov, 1995; Tucker and Slingerland, 1997) and land use (*e.g.,* Walling, 1999; Van Rompaey *et al*., 2002), and for understanding the evolution of Earth's surface (*e.g.,* Church and Slaymaker, 1989). The factors that determine sediment yields fall into four major categories (Meade *et al.,* 1990): i) climate; ii) geology; iii) relief; and iv) land use. A number of studies have addressed the relationships between sediment yield and its controlling factors through

correlation and regression analysis at the global and regional scales. Variables expressing basin relief characteristics and runoff magnitude tend to be most strongly associated with sediment yields at global scale (Jansen and Painter,1974; Pinet and Souriau, 1988; Milliman and Syvitski, 1992; Summerfield and Hulton, 1994; Ludwig and Probst, 1998; Hovius, 1998; and Syvitski and Milliman, 2007) (see Table 3.1). Human actions are persistently changing the trends in the suspended load of the world's rivers by simultaneously increasing the river transport of sediment through soil erosion activities and decreasing this flux to the coastal zone through sediment retention in reservoirs (Meybeck 2003; Walling and Fang 2003; Syvitski *et al*., 2005). Dedkov and Moszherin (1993), Glazyrin and Tashmetov (1995) and Evans (1997) have emphasized the importance of additional factors in sediment generation in mountainous regions, including tectonics and seismic activity, glacierized area, proportion of solid precipitation and basin lithology.

A number of researchers have investigated sediment dynamics at the regional scale, such as in the basin of the Amazon (Meade 1985, 1994; Richey *et al*., 1986), Colorado (Gellis *et al*., 1991; Webb *et al*., 2000, 2001), Fraser (McLean *et al*., 1999; Sichingabula, 1998, 1999), Ganges-Brahmaputra (Goodbred and Kuehl, 2000, Islam *et al*., 1999, 2001; Wasson 2003), Mississippi (Parker, 1988), Rhine (Van Dijk and Kawaad, 1998; Asselman, 1999), St. Lawrence (Rondeau *et al*., 2000), South Saskatchewan (Ashmore and Day, 1988a, 1988b), and Yellow River (Binwen and Yoqian, 1988; Yang *et al*., 1996; Xu, 2002; Xu and Cheng, 2002; Xu and Yunxia, 2005). The efforts to establish the relative importance of major controls on sediment yield in the previous regional studies, however, have been hampered by the scarcity of high resolution, spatially distributed data at the required scales. Recent increases in the availability of

Table 3.1 Overview of large scale studies on factors controlling sediment yield

	Variables	Global					Regional		
		Milliman & Syvitski (1992)	Summerfield & Hulton (1994)	Hovius (1998)	Ludwig & Probst (1998)	Syvitski & Milliman (2007)	Lu & Higgitt (1999)	Restrepo et al. (2006)	Ali & De Boer (this study)
		280 basins	35 basins	97 basins	60 basins	488 rivers	62 stations	40 station	17 stations
Hydrologic	Specific sediment yield	●		●	●		●	●	●
	Sediment yield	●		●		●		●	●
	Mechanical denudation rate		●	●				●	●
	Dissolved sediment load			●					
	Mean discharge			●				●	●
	Maximum discharge			●				●	●
	Discharge peakedness			●				●	●
	Specific runoff	●	●	●	●	●	●	●	●
	Runoff variability		●						
	Runoff coefficient			●					
Topographic	Drainage area	●	●	●		●		●	●
	Basin length			●				●	●
	Channel length			●				●	●
	Minimum elevation							●	●
	Maximum elevation	●		●	●			●	●
	Mean elevation		●	●	●		●	●	●
	Basin Relief		●		●	●	●		●
	Relief peakedness			●				●	●
	Relief ratio		●	●				●	●
	Hypsometric integral		●					●	●
	Mean surface slope				●		●	●	●
	Channel gradient		●	●					●
	% Depositional area			●					
Climatic	Mean annual temperature		●	●	●	●		●	●
	Temperature range			●				●	●
	Mean annual precipitation		●	●	●		●	●	●
	Maximum monthly precip			●				●	●
	Precipitation peakedness			●				●	●
	Seasonal precip. variability				●				
	Aridity index				●				
Human	Mean population density				●		●		●
	Percent of cultivated area				●				
Land cover	glacier/snow cover					●			●
	Percent forest cover				●				
Litho-logical	Chemical erodibility index				●	●			
	Mechanical erodibility index				●				
Soil	Average soil depth				●				
	Average soil texture				●				
Biological	Biomass density				●				
	Netto primary production				●				
	Organic C content in soils				●				

Note: Shaded cells represent major controls on sediment yield for each specific study

global environmental datasets provide an opportunity to examine systematically the relationships between sediment yield and controlling drainage basin variables using GIS. Lu and Higgitt (1999) made an early attempt and applied GIS techniques to the 1,005,501 km^2 Yangtze River. They extracted three topographical parameters from the GTOPO30 dataset. The coarse resolution of the corresponding spatial climate data available at that time, however, restricted their analysis to only one climatic variable, the mean annual precipitation. Lu and Higgitt (1999) found that sediment yield was correlated with specific runoff and mean elevation. Restrepo *et al*. (2006) examined the factors controlling sediment yield in the 257,438 km^2 Magdalena River basin in Colombia using a database of more than 70 stream gauging stations together with readily available geospatial topographic and climatological data at a resolution of 120 arc-seconds, and found that specific runoff and peak discharge explained 58% of the variance in sediment yields. An overview of selected global and regional studies is presented in Table 3.1.

Ali and De Boer (2007) evaluated the spatial and temporal patterns of sediment yield in the upper Indus River basin. The spatial patterns described in the study suggest that a number of environmental variables such as topography, hydro-climatology, lithology, land use and soil erodibility affect sediment yield. The objectives of this study are to examine the major factors controlling specific sediment yield in the upper Indus basin using high resolution, geospatial data extracted from various public domain global datasets in a GIS environment, and to develop regression models for estimating specific sediment yield in the basin. Due to its remote location, the upper Indus River basin has received little attention in the past, and no attempt has been made to examine systematically the relationship between specific sediment yield and its controlling variables in this region.

3.3 Study Area - The Upper Indus River Basin

The Indus River is one of the largest rivers in southern Asia, with a total length of 2880 km and a drainage area of 912,000 km^2 extending across portions of Pakistan, India, China and Afghanistan (Figure 3.1). The upper Indus River basin upstream of Tarbela Dam is reported to be about 1125 km long, with a drainage area of 181,500 km^2. The Indus River rises in the Tibetan Plateau at elevations above 5500 m in the Kailas Range, follows a well-defined valley parallel to the geologic strike, and descends down to the Arabian Sea. Much of its flow originates in the mountains of the Karakoram and Himalayas. The major Indus tributaries include the Shyok, Shigar, and Gilgit in the upper, glacierized portion; the Astore in the middle reaches; and the Gorband, Brandu, and Siran in the lower, monsoon-affected portion.

Major tectonic activity, culminating in the Himalayan orogeny during the mid-Eocene, has shaped the high relief and complex geologic structures observed in the upper Indus basin today (Molnar and Tapponnier, 1975; Miller, 1984). These young mountain ranges of extreme ruggedness and high elevations are subject to exceptionally rapid degradation by a combination of processes (Searle, 1991; Shroder, 1993, Collins and Hasnain, 1995). Widespread mass movements generated by tectonic instability, rapid weathering due to the severe climatic conditions, heavy snowfall resulting in a spring snowmelt, the action of glaciers, and catastrophic outburst floods from landslide-, moraine-, and glacier-dammed lakes are major factors in the high sediment yield observed in the basin (Ferguson, 1984; Hewitt, 1998; Shroder and Bishop, 1998). The lower, southern part of the basin experiences heavy monsoon rainfall, and rivers in

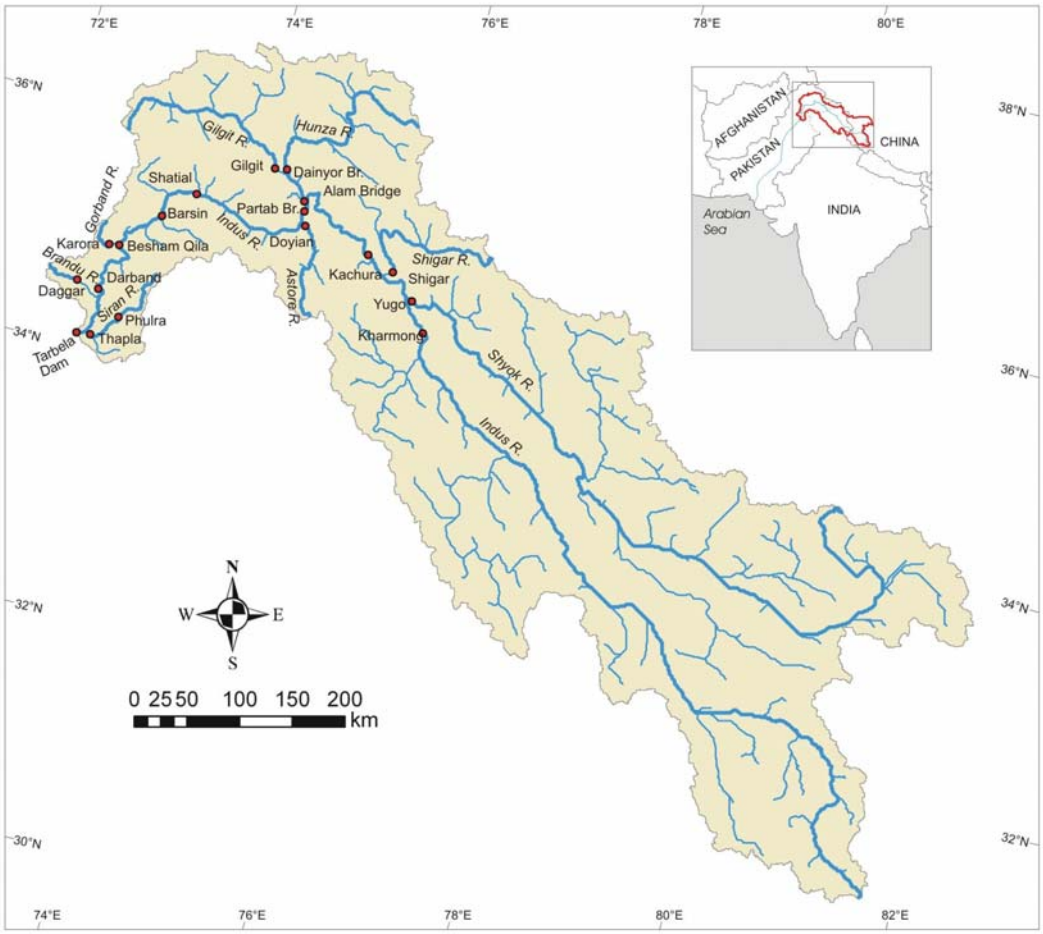

Figure 3.1 The upper Indus River basin

this part of the basin carry large amounts of sediment associated with flash floods. Ali and De Boer (2007) provide a detailed account of the physiography, geology and tectonics, and climate of the basin.

3.4 Data Sources and Methods

This study utilizes a number of environmental datasets for investigating major factors controlling specific sediment yield in the upper Indus basin. In addition to 7 sediment and runoff

variables, a total of 22 other characteristics were derived from geospatial, public domain datasets providing information on topography, climate, population and land cover. The investigated variables, their definitions, data sources, and resolutions are summarized in Table 3.2.

3.4.1 Sediment Yield and Runoff Data

Apart from some long-term discharge records for the Indus and some of its major tributaries, hydrological data for the upper Indus River basin are very scarce (Young and Hewitt, 1990). Long-term, continuous discharge and occasional suspended sediment concentration data are available for only 17 active and discontinued gauging stations in the basin (Figure 3.1). These stations were established by the Pakistan Water and Power Development Authority (WAPDA) from the early 1960s to 1980s, and their drainage areas range from 598 (Brandu River at Daggar) to 166,154 km^2 (Indus River at Darband). Suspended sediment samples in combination with discharge measurements are obtained following standard USGS procedures (Rantz and others, 1982; Edwards and Glysson, 1999) on an occasional basis at the gauging stations so that sediment rating curves can be developed. During low flow periods, when sediment concentrations are small, measurements are taken once a month. During average flows, the measurement frequency is increased to twice a month, and during the snowmelt and monsoon seasons, when extreme peaks might occur, samples are taken several times a day (SWHP, 2000). Since bed load sampling presents a challenge in large mountain rivers, field measurements have been carried out only for some smaller hill torrents like Allai Khwar and Duber near Besham area. NEAC Consultants (2004) suggested a value of 13.5% as the unmeasured bed load for the Indus River at Besham Qila, based on 1962-2000 interpolated data. The Water Resources

Table 3.2 Potential variables, definitions, resolutions and data sources

	Variable	Definition	Source and Resolution
		Hydrological Variables	
SY_{sp}	Specific sediment yield (t km^{-2} yr^{-1})	Mean annual sediment yield averaged over the drainage area	Pakistan WAPDA
SY	Mean annual sediment yield (Mt yr^{-1})	Sediment transported in suspension by the river annually at a stream gauging station	SWHP (2000)
D	Mechanical denudation rate (mm ka^{-1})	Average mechanical denudation per unit time of the land surface (calculated from SY_{sp})	Ali and De Boer (2007)
Q	Mean annual discharge (m^3 s^{-1})	Long term average discharge at the sub-basin outlet	
Q_{max}	Long term annual maximum discharge (m^3 s^{-1})	Long term average annual maximum discharge in the time series	
Q_{pk}	Discharge peakedness	Ratio of mean discharge over maximum discharge	
RO	Specific runoff (mm yr^{-1})	Height of the water column on a unit surface area which leaves the basin annually as surface runoff	
		Topographic variables	
A	Drainage area (km^2)	Sum of the areas of all the cells contributing to the flow at the basin outlet	GTOPO30 DEM USGS (2006a) (30 arc-second)
L_b	Basin length (km)	Straight-line distance from the most remote point on the water divide to the basin mouth	
L_c	Channel length (km)	Length of the main channel of the drainage basin from its headwater to the outlet	
EL_{min}	Minimum elevation (m)	Elevation of the lowest cell in the basin	
E_{max}	Maximum elevation (m)	Elevation of the highest cell in the basin	
EL_{ch}	Upstream channel elevation (m)	Upstream elevation of the channel at headwaters	
EL	Mean elevation (m)	Arithmetic mean of the elevations of all cells in the sub-basin	
R	Basin relief (m)	Difference between the maximum and the minimum cell values in the basin	
R_{pk}	Relief peakedness	Ratio of the mean elevation and the maximum elevation of the basin	
R_r	Relief ratio	Ratio of the basin relief and the basin length	
HI	Hypsometric integral	Given by: $(EL-EL_{min})/(EL_{max}-EL_{min})$	
G_m	Mean surface slope (%)	Mean of the slopes of all the cells in the basin	
G_c	Channel gradient (m km^{-1})	Average slope of the main river channel	
G_1	Slope 1 (m km^{-1})	Ratio of the mean elevation of the basin and the square root of the basin area	
		Climatic variables	
T	Mean annual temperature (°C)	Long term mean annual temperature in the drainage basin	WORLDCLIM (2006) Hijmans *et al.* (2005) (1 km)
T_r	Temperature range (°C)	Difference between the mean monthly temperatures for the hottest and coldest months	
P	Mean annual precip. (mm yr^{-1})	Mean annual precipitation in the drainage basin	
P_{max}	Maximum monthly precip. (mm month^{-1})	Long term mean monthly precipitation for the wettest month of the year	
P_{pk}	Precipitation peakedness	Ratio of the mean annual precipitation and the maximum monthly precipitation of the basin	
		Anthropogenic variables	
PD	Mean population density (humans km^{-2})	Mean population density in the drainage basin	APD (2006) (2.5 minutes)
		Land use and land cover	
LC_s	Percent snow/ice cover (%)	Percentage of snow and ice covered area in the basin	USGS (2006b) (1 km)

Division of Peshawar University recommends a correction for unmeasured bed load of 10% or 15% of the suspended sediment load for the upper Indus River and its tributaries for flood and non-flood conditions, respectively (NEAC Consultants, 2004). These estimates are in agreement with the USBR (1987) guidelines for evaluating the unmeasured load as a bed load correction and comparable to an 18% observed bed load for the mountainous Fraser River Basin in British Columbia (McLean *et al*., 1999).

The periods of record for the 17 available hydrological stations range from 6 to 36 years (Figure 3.2). Given the year-to-year variability in precipitation, discharge, and sediment load, three discontinued stations (Indus River at Barsin and Darband, and the Siran River at Thapla) were excluded from the dataset, and the analysis is based on the overlapping eleven years (1985-1995) for the remaining 14 stations. The decision to use the hydrological data from the same years for all stations is consistent with the observation of Meybeck *et al*. (2003) that basins influenced by glacier and snowmelt, like the upper Indus basin, are characterized by high temporal variability of suspended sediment fluxes. All hydrological variables were derived from the sediment and runoff data (Table 3.3). The derived discharge variables include mean annual discharge (Q), maximum annual discharge (Q_{max}), discharge peakedness (Q_{pk}) and specific runoff (RO). Suspended sediment rating curves were established for all stations, and mean annual sediment yield (SY), specific sediment yield (SY_{sp}) and mechanical denudation rate (D) were calculated. As an example, the suspended sediment rating curve for the Indus River at Besham Qila is presented in Figure 3.3. Ali and De Boer (2007) investigated the correlation between suspended sediment rating curve coefficients (after Asselman, 2000; Syvitski *et al*., 2000) in the upper Indus basin and describe the methods for calculating sediment yields in the basin.

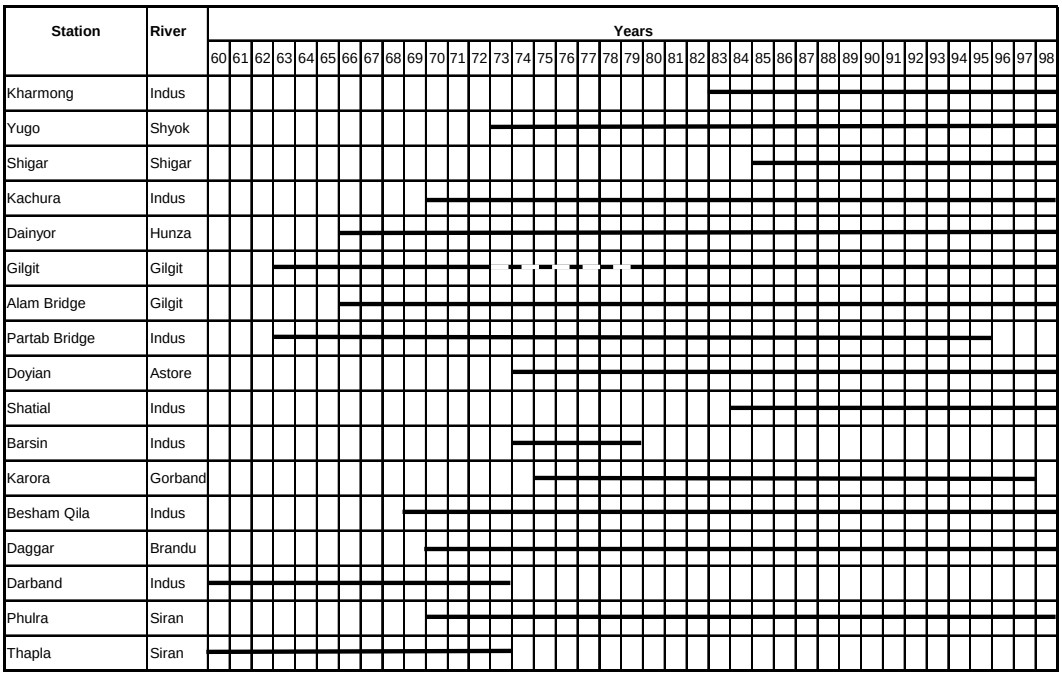

Figure 3.2 Overview of available records for stream gauging stations in the upper Indus River basin

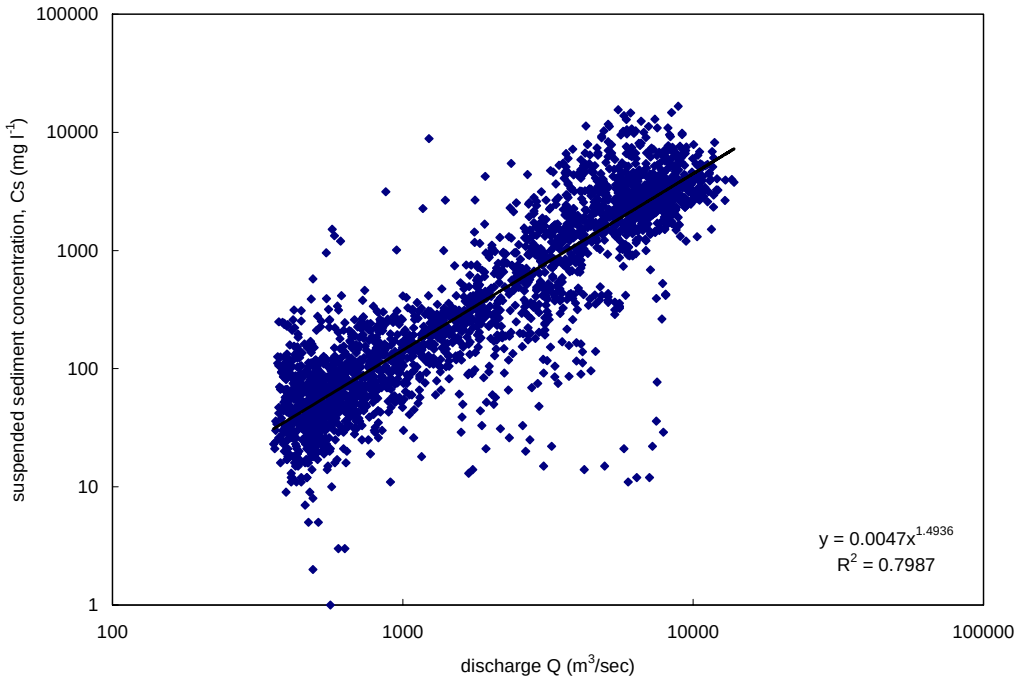

Figure 3.3 Suspended sediment rating curve for the Indus River at Besham Qila

3.4.2 Extraction of Sub-Basin Variables from Geospatial Datasets

The topographic parameters were derived from the 30 arc-second resolution GTOPO30 dataset (USGS, 2006a). The raw data was preprocessed to fill sinks and to delineate the basin. The channel network and the longest flow paths obtained from further processing are shown in Figure 3.1. Using the extracted DEM window and the gauging stations coverage, sub-basin segmentation and parameterization were carried out. A total of 14 variables, including sub-basin area, length, elevation, relief and slope parameters were derived for each of the 14 sub-basins (Table 3.3). The mean, maximum and minimum values of the topographic and other environmental variables for each sub-basin were obtained from a statistical file obtained after clipping the respective database using the delineated sub-basin boundaries from the DEM. Based on these extracted parameters, a number of maps portraying the variability of the major variables were developed (Figure 3.4). The relief map (Figure 3.4a) shows large areas of high elevation in the Tibet Plateau and Kailas Range, along with deep and narrow valleys draining the Kashmir and Kohistan part of the basin. The exceptionally high relief of the basin is evident in a mean elevation > 4000 m for 11 sub-basins in the upper glacierized part (Table 3.3). The surface slope map (Figure 3.4b) shows the contrast between the high plateaus in the uppermost part of the basin in the Tibet and Kailas Range and the very high surface slopes in the northwestern Gilgit and Hunza River basins. A gradual decrease in relief is also apparent in the lower, monsoon part of the basin from Besham Qila to Tarbela Dam.

Table 3.3 Hydrologic, morphometric, climatic, anthropogenic and land cover parameters of the 17 sub-basins in the upper Indus River basin

Station	River	SY_{sp} (t km^{-2} yr^{-1})	SY (Mt yr^{-1})	D (mm ka^{-1})	Q (m^3 s^{-1})	Q_{max} (m^3 s^{-1})	Q_{pk} (-)	RO (mm yr^{-1})	A (km^2)	L_b (km)	L_c (km)	EL_{min} (m)	EL_{max} (m)	EL_{ch} (m)	EL (m)	R (m)	R_{pk} (-)	R_r (-)	HI (-)	G_m (%)	G_c (m km^{-1})	G_l (m km^{-1})	T (°C)	T_r (°C)	P (mm)	P_{max} (mm)	P_{pk} (-)	PD (h km^{-2})	LC_s (%)
Kharmong	Indus	194	13.9	144.3	473	2009	0.236	208	71685	674	862	2718	6774	5518	4799	4056	0.71	6.0	0.51	15.0	3.2	17.9	-3.2	36.5	208.0	39.7	5.2	11.8	5.3
Yugo	Shyok	288	22.9	214.0	333	1904	0.175	132	79586	447	819	2718	7607	6315	5083	4889	0.67	10.9	0.48	16.2	4.4	18.0	-5.3	40.0	79.3	21.1	3.8	4.1	9.6
Shigar	Shigar	3888	26.8	2888.6	199	1173	0.170	910	6891	94	190	2371	8239	7103	4611	5867	0.56	62.1	0.38	32.3	24.9	55.5	-4.2	39.3	115.6	17.3	6.7	8.0	41.8
Kachura	Indus	464	75.1	345.0	1125	4797	0.235	219	161651	765	969	2371	8239	5518	4912	5867	0.60	7.7	0.43	16.5	3.2	12.2	-4.2	38.5	139.7	28.8	4.9	7.7	9.0
Dainyor	Hunza	1302	17.7	967.1	294	1557	0.189	684	13576	131	239	1464	7595	5474	4535	6131	0.60	46.9	0.50	34.4	16.8	38.9	-4.0	38.5	132.1	22.0	6.0	8.8	43.3
Gilgit	Gilgit	531	6.6	394.6	285	1350	0.211	726	12379	144	213	1550	6560	4985	4076	5010	0.62	34.7	0.50	30.4	16.1	36.6	-0.8	35.8	308.8	49.0	6.3	10.7	12.5
Alam	Gilgit	1298	36.3	964.2	625	3013	0.207	705	27953	180	278	1401	7595	4985	4257	6194	0.56	34.5	0.46	32.4	12.9	25.5	-2.1	37.2	217.4	33.7	6.5	9.8	26.7
Partab	Indus	701	135.2	521.1	1827	7749	0.236	299	192701	838	1099	1401	8239	5518	4798	6837	0.58	8.2	0.50	19.2	3.7	10.9	-3.8	38.2	152.0	26.9	5.7	8.1	11.6
Doyian	Astore	549	2.1	407.8	153	776	0.197	1241	3891	87	114	1625	7861	4163	4004	6236	0.51	71.5	0.38	27.5	22.3	64.2	-1.0	36.0	343.5	49.1	7.0	4.5	7.5
Shatial	Indus	543	110.5	403.4	2022	8924	0.227	313	203430	913	1232	1401	8239	5518	4726	6837	0.57	7.5	0.49	19.7	3.3	10.5	-3.4	38.0	163.5	27.5	5.9	8.5	11.1
Karora	Gorband	429	0.2	318.4	21	362	0.059	1193	567	23	38	1096	4193	3880	2263	3097	0.54	132.4	0.38	23.3	72.5	95.0	11.8	30.4	945.5	132.8	7.1	266.6	0.7
Besham	Indus	830	176.3	616.5	2505	11379	0.220	372	212447	935	1346	671	8239	5518	4665	7567	0.57	8.1	0.53	20.1	3.6	10.1	-3.1	37.8	183.0	29.4	6.2	13.3	10.8
Daggar	Brandu	468	0.3	348.0	6	121	0.051	310	634	31	38	802	2600	1789	1156	1798	0.44	57.1	0.20	16.0	26.2	45.9	18.2	33.8	972.8	156.3	6.2	500.7	0.0
Phulra	Siran	3047	3.2	2263.6	24	401	0.059	726	1035	56	73	791	4069	4069	1632	3278	0.40	59.0	0.26	14.0	44.7	50.7	15.1	30.6	1224.7	228.2	5.4	590.1	0.0

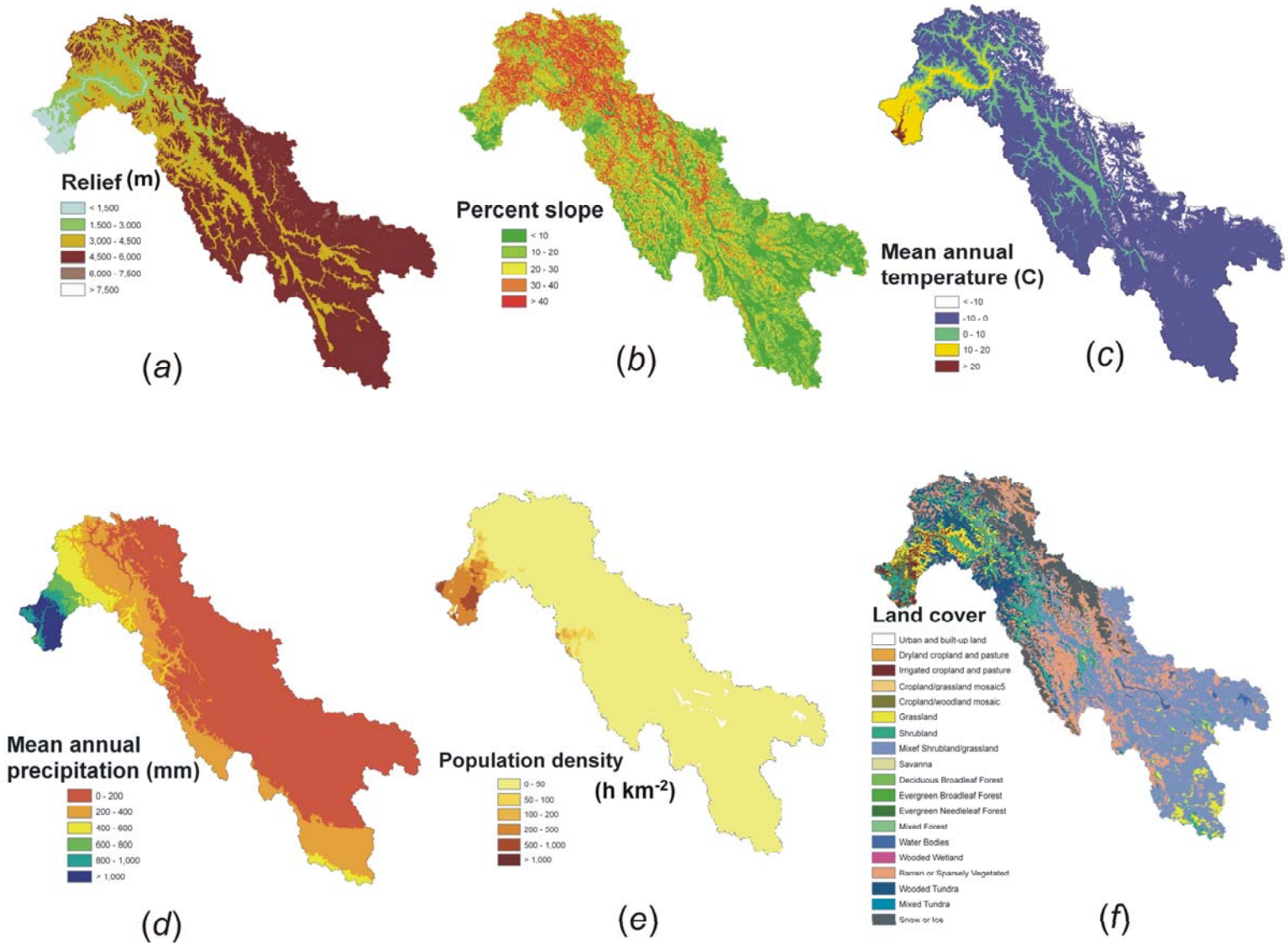

Figure 3.4 Maps of geospatial data portraying the variability of major controls of specific sediment yield

Spatially distributed precipitation and temperature data were derived from WORLDCLIM (2006). This is a set of global climate layers generated through the interpolation of average monthly climate data from weather stations on a 30 arc-second resolution (Hijmans *et al*., 2005). The five variables obtained from this database were mean annual precipitation (P), mean annual temperature (T), maximum monthly precipitation (P_{max}), precipitation peakedness (P_{pk}), and temperature range (T_r) (Table 3.3). The derived temperature map (Figure 3.4c) portrays a clear temperature increase with decreasing elevation from the upstream to the downstream portion of the basin. The precipitation map (Figure 3.4d) shows the contrast between the upper, arid, glacierized sub-basins with a low mean annual precipitation (< 200 mm yr^{-1}), and the lower monsoon region where precipitation exceeds 1000 mm yr^{-1}.

The population density (PD) for the delineated sub-basins was determined from the 2.5 minute resolution Asian Population Database (APD, 2006). The population density map (Figure 3.4e) shows a very low population density (< 50 people km^{-2}) in the upper glacierized region which has a total estimated population of about 1.5 million. In the lower monsoon region, the population density shows an inverse relationship with elevation, and increases gradually in a downstream direction.

Percent snow/ice cover (LC_s) was derived from the USGS global land cover database which uses 24 characteristic classes at a 1-km nominal spatial resolution (USGS, 2006b). The derived land cover map of the basin (Figure 3.4f) shows a wide variety of cover types. A high percent snow/ice cover, ranging up to 40%, is evident in the Shyok, Shigar, Hunza and Gilgit

river basins (Table 3.3). This is in contrast to the lower, monsoon basins, which receive very little solid precipitation.

3.5 Results and Discussion

3.5.1 Correlation between Specific Sediment Yield and Sub-Basin Variables

To evaluate the correlation between sub-basin variables, Pearson correlation coefficients (r) were determined (Table 3.4). The analysis using all fourteen stations in the basin shows that the only potential controlling variable significantly correlated to specific sediment yield is percent snow/ice cover (LC_s) (r = 0.50). This shows a considerable variability of specific sediment yield in the basin and its complex dependence on different controlling variables. The importance of ice as an agent of erosion is well established and is suggested to be more significant during and just after major glaciations (Syvitski and Milliman, 2007). Hallet *et al*. (1996) found that sediment yields increase with the extent of glacial ice cover, in particular at high elevations in the heavily-glacierized basins of southern Alaska, where sediment yields exceed by about one order of magnitude the yields of other European, Asian, and North American basins. Glacier area has been used successfully as a parameter in glacial erosion indices (e.g., Gurnell, 1995; Zemp *et al*., 2005). The absence of significant correlation between specific suspended sediment yield and glacier area for 90 glacierized basins by Gurnell *et al*. (1996) was attributed primarily to the variability in the length of record.

Table 3.4 Pearson correlation coefficients between specific sediment yield and potential controlling variables for different groups of stations

Variables	Whole Indus basin	Main Indus River	Upper glacierized sub-basins	Lower monsoon sub-basins
# of Stations	14	5	11	3
Q	-0.24	**0.94**	-0.24	0.59
Q_{max}	-0.22	**0.93**	-0.22	0.60
Q_{pk}	-0.27	-0.63	-0.58	0.50
RO	0.35	**0.89**	0.47	-0.05
A	-0.33	**0.91**	-0.37	**0.99**
L_b	-0.38	**0.87**	-0.45	**0.97**
L_r	-0.37	**0.87**	-0.43	**1.00**
EL_{min}	-0.06	**-0.94**	0.06	-0.54
EL_{max}	-0.01	0.81	0.32	0.43
EL_{ch}	0.27	-	**0.61**	0.55
EL	-0.16	-0.53	-0.11	-0.09
R	0.01	**0.96**	0.15	0.58
R_{pk}	-0.43	-0.88	-0.37	-0.75
R_r	0.24	**0.93**	**0.57**	-0.49
HI	-0.35	0.24	-0.52	-0.20
G_m	0.30	**0.91**	**0.60**	-0.67
G_c	0.28	0.81	**0.65**	-0.13
G_1	0.27	-0.89	0.51	-0.43
T	0.11	0.03	-0.19	0.04
T_r	-0.06	0.62	0.37	-0.44
P	0.18	-0.38	-0.28	**1.00**
P_{max}	0.23	-0.78	-0.49	**0.97**
P_{pk}	0.19	0.70	0.46	-0.87
PD	0.26	0.08	0.00	0.72
LC_s	**0.50**	0.88	***0.80***	-0.51

Note: Numbers in shaded rectangles indicate a significant correlation at 95% level

Subdividing the stations into groups based on basin characteristics has proved to be an effective tool for reducing scatter in previous regional studies like Lu and Higgitt (1999) and Restrepo *et al.* (2006) who grouped basins on the basis of tributary location, basin area, and maximum elevation. For the upper Indus basin, the following three groups of stations were distinguished: i) upper, glacierized sub-basins; ii) lower, monsoon sub-basins; and iii) the main Indus River. Pearson correlation coefficients were calculated for specific sediment yield and potential controlling variables for each group (Table 3.4). Subdividing the stations into the three groups results in considerably improved relationships between specific sediment yield and potential controlling variables. For example, more than 10 variables become significant in the main Indus River group compared to only one in the whole basin. Furthermore, the values of the correlation coefficients are substantially increased. The correlation coefficient for LC_s, for example, increases from 0.50 for the whole basin to 0.80 for the upper, glacierized sub-basins (Table 3.4).

Sediment transport dynamics in the upper, glacierized sub-basins differ in many ways from those in the lower, monsoon sub-basins. High rates of mass movement, supraglacial transport, and subglacial erosion supply large quantities of loose sediment to the valleys where it is stored in alluvial cones and fans, moraines, and outwash trains (Ferguson, 1984). The sediment is mainly transported by meltwater from snow and ice which drains along a variety of routes to the river channel. Collins (1996) estimated that 60% of the annual sediment yield of the glacierized Hunza River basin at Dainyor (LC_s of 43.3%) was glacier-derived. Collins (1996) also concluded that more than 40% load of the upper Indus River leaving the Karakoram at Besham Qila was glacier-derived. Debris transport in the supraglacial zone of these Himalayan

glacierized regions is found to be an important contributor to contemporary glacial sediment production, yielding large volumes of coarse angular rock debris, in addition to the coarse sediment from basal traction zone (Owen *et al*., 2003).

3.5.2 Modeling Specific Sediment Yield Variability

The statistical software package MINITAB (MINITAB Inc., 2006) was used to develop multiple regression models for estimating specific sediment yield in different regions of the upper Indus basin by using the stepwise regression procedure. This procedure involves building the regression equations one variable at a time by adding at each step the variable that explains the largest amount of the remaining unexplained variation (Haan, 2002). After each step, all the variables in the equation are examined for significance and discarded if they are no longer explaining a significant amount of variation. The procedure is continued until all of the variables not in the equation are found to be insignificant and all the variables in the equation are significant. Model assessment to determine if the data can adequately be described by the regression model was carried out by comparing R^2, R^2_{adj}, F-ratio and p-value statistics.

Table 3.5 displays the regression models along with model assessment and validation parameters. For the whole basin, the model incorporating the percent snow/ice cover (LC_s), maximum monthly precipitation (P_{max}), hypsometric integral (HI), upstream channel elevation (EL_{ch}), and relief peakedness (R_{pk}) explains 93.7% of the variance in observed specific sediment yield (Table 3.5). The diversity of variables in the model indicates considerable variability and complexity of the major controls on specific sediment yield in the basin. A regression model

Table 3.5 Regression models predicting specific sediment yield in the upper Indus River basin along with assessment and validation parameters

Regression Models	Model Assessment				Model Validation			
					Paired *t*-test			
	R^2	R^2_{adj}	*F-ratio*	*p-value*	*t*	t_{cr}	*p-value*	*ME*
Whole basin								
$SY_{sp} = 654 + 38.4\ LC_s + 10.2\ P_{max} - 3787\ HI + 0.815\ EL_{ch} - 5711\ R_{pk}$	0.937	0.898	23.9	0.000	-0.043	2.15	0.096	0.937
$SY_{sp} = 319 + 25.4\ LC_s$	0.734	0.707	27.5	0.000	-0.360	2.18	0.723	0.681
Main Indus River								
$SY_{sp} = - 522 + 0.172\ R$	0.924	0.898	36.4	0.009	-0.118	2.57	0.912	0.924
Upper, glacierized sub-basins								
$SY_{sp} = - 5445 + 21.3\ LC_s + 0.915\ EL_{ch} - 4916\ HI + 568\ P_{pk}$	0.985	0.974	95.9	0.000	-0.047	2.20	0.936	0.985
Lower, monsoon sub-basins								
$SYsp = - 8867 + 9.72\ P$	0.994	0.989	175.4	0.048	-0.024	3.18	0.983	0.994

with LC_s as a single independent variable explains 25% variance. However, after excluding two outliers from the dataset the explained variance increases to 73.4%. The outliers are the Shigar River at Shigar in the upper, glacierized region and the Siran River at Phulra in the lower, monsoon region. Both exhibit excessively high specific sediment yields owing to high specific runoff (RO) and mean annual precipitation (P), respectively. Although the model with LC_s as the only independent variable explains less of the variance, it is very useful for a first-hand estimate of specific sediment yield at the basin scale.

The subdivision of the stations into smaller groups increases R^2 from 0.937 for the whole basin to 0.985 and 0.994 for the upper, glacierized sub-basins and lower, monsoon sub-basins, respectively (Table 3.5). The model for the upper, glacierized basins includes percent snow/ice cover (LC_s), upstream channel elevation (EL_{ch}), hypsometric integral (HI), and precipitation peakedness (P_{max}). The percent snow/ice cover (LC_s) emerges as the single most important variable influencing specific sediment yields in the upper Indus River basin. The percent snow/and ice cover (LC_s) is also correlated to other variables such as relief, slope, and climatic parameters. The lower, monsoon region shows somewhat different behaviour, and 99.4% of the variance is explained by mean annual precipitation (P) as the single independent variable in the model (Table 3.5). This part of the basin has less relief but is subjected to heavy monsoon rainfall which becomes the dominant factor in mobilizing and transporting the sediment. The intensity of the monsoon acts as a first-order control of the erosion rate in this part of the basin (Galy and Frances-Lanord, 2001). Bookhagen and Burbank (2006) also note that the summer monsoon controls erosive processes and rates along the Himalayan topographic front. The model for the main Indus River only includes basin relief (R) as an independent variable, and explains

92.4% of the variance. Relief has an exponential relationship with sediment yields (Meade *et al.,* 1990) and is a major factor in producing abnormally high sediment yields in mountain areas (Ahnert, 1970). Some of the locations with the greatest relief on Earth, such the Nanga Parbat Massif, are found in the upper Indus Basin. The high relief results in denudation rates ranging up to 6 mm yr^{-1} (Cornwell *et al*., 2003). Data presented by Vance *et al*. (2003) demonstrate a log-linear relationship between relief and erosion rate over three orders of magnitude in erosion rate for very different climatic and tectonic regimes in the Himalayas.

3.5.3 Model Validation

Model assessment investigates the adequacy of the model for describing the data. Model validation, on the other hand, determines the intended functional capability of the model by comparing the observed and predicted specific sediment yields (Montgomery and Peck, 1992). The regression models in this study were validated by applying a paired *t*-test and by calculating the model efficiency (*ME*) (Table 3.5). The paired *t*-test (Hammond and McCullagh, 1978) evaluates whether the mean difference between the observed and predicted specific sediment yield ($\mu_{difference}$) is significantly different from zero, i.e., test $H_0 : \mu_{difference} = 0$, versus the alternative hypothesis $H_1 : \mu_{difference} \neq 0$. Model efficiency (*ME*) as defined by Nash and Sutcliffe (1970) is given by:

$$ME = 1 - \frac{\sum_{i=1}^{n}(O_i - P_i)^2}{\sum_{i=1}^{n}(O_i - O_{mean})^2} \qquad (3.1)$$

where n is the number of observations, O_i is the observed value, O_{mean} is the mean observed value, and P_i is the predicted value. *ME* can range from -∞ to 1, and represents the proportion of the initial variance accounted for by the model. The closer the value of *ME* to 1, the more efficient the model. All the models pass the paired *t*-test with calculated *t* values considerably smaller than the critical values t_{cr} (Table 3.5). The *p-value* statistics approaching 1.0 indicate that the null hypothesis should be rejected. This means that the difference between observed and predicted specific sediment yields is not significantly different from zero. Moreover, *ME* values are close to 1 (0.985, 0.994, and 0.924 for upper, glacierized sub-basins, lower, monsoon sub-basins and the main Indus River, respectively). A comparison of the observed and predicted specific sediment yields (Figure 3.5) indicates that the models developed in this study present valuable tools for the prediction of specific sediment yield in different regions of the upper Indus basins.

3.6. Conclusions

The availability of high resolution, global datasets provides an opportunity for examining major controls of specific sediment yield by using modern GIS techniques at a regional scale in large, data-sparse drainage basins. The hydrologic, topographic, climatic, and land use variables extracted from these datasets provide the detailed spatial patterns of the various environmental characteristics in the upper Indus River basin. These extracted variables were used to develop multiple regression models for estimating specific sediment yield in different regions of the basin. For the whole basin, a model incorporating percent snow/ice cover (LC_s), maximum monthly precipitation (P_{max}), hypsometric integral (*HI*), upstream channel elevation (EL_{ch}), and

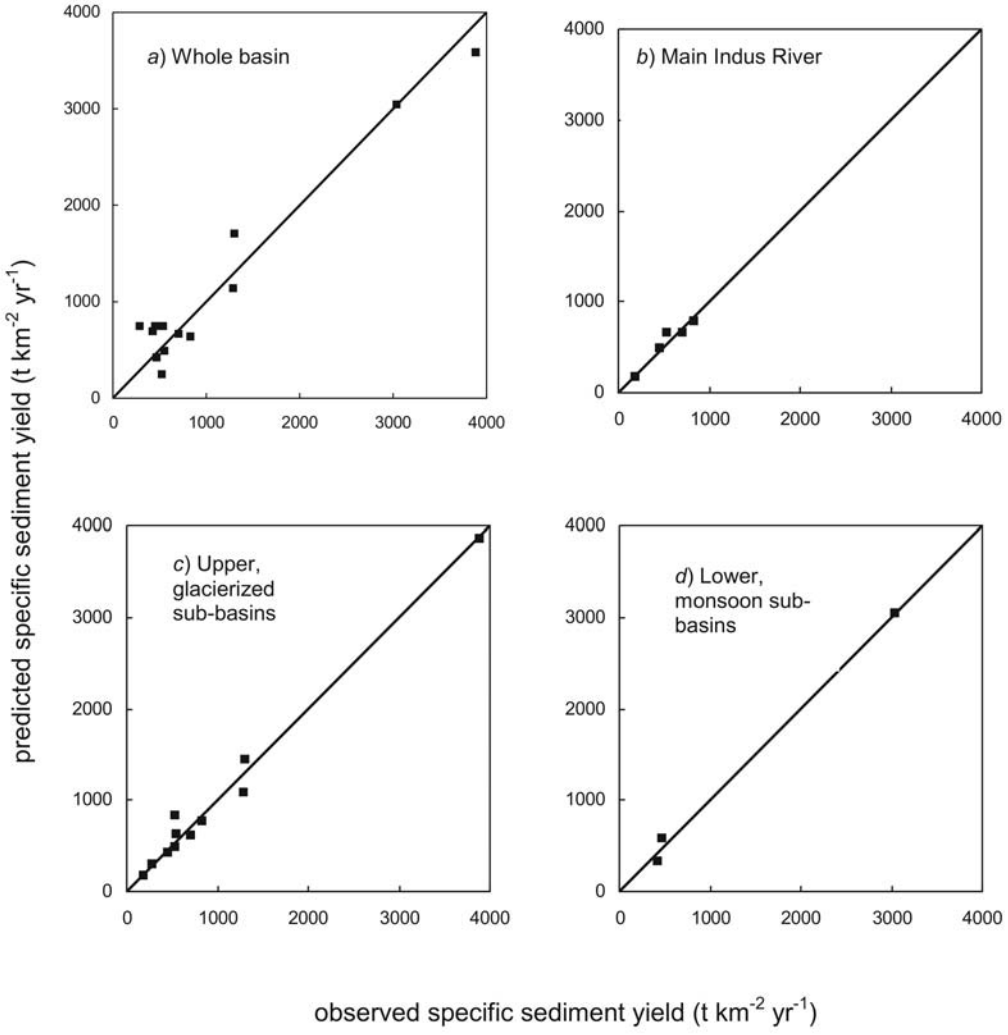

Figure 3.5 Comparison of observed and predicted specific sediment yields for different groups of stations

relief peakedness (R_{pk}) explains 93.7% of the variance in observed specific sediment yield (Table 3.5). The diversity of variables in the model indicates considerable variability and complexity of the controls of suspended specific sediment yield in the basin. A regression model with LC_s as a single independent variable, however, explains 73.4 % of the variance, after excluding two

outliers from the dataset (Table 3.5). Thus, the percent snow/ice cover (LC_s) emerges as the major control of specific sediment yield in the basin.

Subdivision of the stations into smaller groups improves the prediction of specific sediment yield in terms of variance explained by the multiple regression models (98.5% in the upper, glacierized sub-basins, 99.4% in the lower, monsoon basins, and 92.4% along the main Indus River) (Table 3.5). The variables used in the models reflect the different processes of sediment load generation in the various regions. The major role of percent snow/ice cover (LC_s) in predicting specific sediment yield in the upper, glacierized basins reflects the importance of glacial and glaciofluvial processes for generating the sediment load. The emergence of percent snow/ice cover (LC_s) as the most important control of specific sediment yield in the upper Indus River basin is a significant finding for predicting specific sediment yield in mountainous areas. Even though the glacierized areas in the basin are located at high elevations with high rates of precipitation and mechanical weathering, elevation is not significantly correlated with specific sediment yield (Table 3.4), leaving percent snow/ice cover (LC_s) rather than elevation as the main factor controlling specific sediment yield in the glacierized portion of the basin.

Mean annual rainfall (P) is the main controlling variable for the lower, monsoon part of the basin. This part of the basin has less relief but is subjected to heavy monsoon rainfall which becomes the dominant factor in controlling erosional processes and in transporting the sediment along the Himalayan topographic front. The importance of relief is well established in producing abnormally high sediment yields in mountain areas and basin relief (R) is also the dominant control along the main Indus River. The validation parameters, in terms of positive paired t-test

results and model efficiency (*ME*) values close to 1.0, show that the models present useful tools for predicting specific sediment yield in the upper Indus River basin (Table 3.5).

The models of specific sediment yield presented in this paper link hydrological variables and environmental characteristics on a regional scale, and allow the prediction of specific sediment yield at ungauged sites within the basin. The models, however, do not explain all the observed variation in specific sediment yield in the basin, which emphasizes the importance of and need for physically-based, spatially distributed models. Given the current level of understanding of the major controls of specific sediment yield in the basin, the next step in this study would be to use this information to develop a physically-based, spatially distributed model for estimating specific sediment yield in different parts of the basin, and subsequently to construct a detailed sediment budget for comprehensive accounting of the sources and disposition of sediments in the basins (Ali and De Boer, 2003).

3.7 References

Ahnert F. (1970) Functional relationships between denudation, relief and uplift in large mid-latitude drainage basins. *American Journal of Science 268*, 243-263.

Ali K.F., De Boer D.H. (2003) Construction of sediment budgets in large scale drainage basins: the case of the upper Indus River. In *Erosion Prediction of Ungauged Basins (PUBs): Integrating Methods and Techniques*, De Boer D.H., Froehlich W., Mizuyama T., Pietroniro A. (Eds.). IAHS Publication No 279. IAHS Press, Wallingford, 206-215.

Ali K.F., De Boer D.H. (2007) Spatial patterns and variation of suspended sediment yield in the upper Indus River basin, northern Pakistan. *Journal of Hydrology 334*, 368-387.

APD (2006) Asian Population Database (APD), http://www.grida.no/cgiar/asia/intro.htm

Ashmore P.E., Day T.J. (1988a) Effective discharge for suspended sediment transport in streams of the Saskatchewan River basin. *Water Resources Research 24*(6), 864–870.

Ashmore P.E., Day T.J. (1988b) Spatial and temporal patterns of suspended-sediment yield in the Saskatchewan River basin. *Canadian Journal of Earth Sciences 25*(9), 1450-1463.

Asselman N.E.M. (1999) Suspended sediment dynamics in a large drainage basin: the River Rhine. *Hydrological Processes 13*, 1437-1450.

Asselman N.E.M. (2000) Fitting and interpretation of sediment rating curves. *Journal of Hydrology 234*, 228-248.

Binwen L., Yoqian L. (1988) A study of total load transport by Yellow River. In *Sediment Budgets,* Bordas M.P., Walling D.E. (Eds.). IAHS Publication No. 174. IAHS Press, Wallingford, 483-496.

Bookhagen B., Burbank D.W. (2006) Topography, relief, and TRMM-derived rainfall variations along the Himalaya. *Geophysical Research Letters 33*, L08405. DOI: 10.1029/2006GL026037, 2006.

Church M., Slaymaker O. (1989) Disequilibrium of Holocene sediment yield in glaciated British Columbia. *Nature 337*, 452-454.

Collins D.N. (1996) Sediment transport from glacierized basins in the Karakoram mountains. In *Erosion and Sediment Yield: Global and Regional Perspective*, Walling D.E., Webb B.W. (Eds.). IAHS Publication No. 236. IAHS Press, Wallingford, 85-96.

Collins D.N., Hasnain S.I. (1995) Runoff and sediment transport from glacierized basins at the Himalayan scale. In *Effects of Scale on Interpretation and Management of Sediment and Water Quality,* Osterkamp W.R. (Ed.). IAHS Publication No. 226. IAHS Press, Wallingford, 17-25.

Cornwell K., Norsby D., Marston R. (2003) Drainage, sediment transport, and denudation rates on the Nanga Parbat Himalaya, Pakistan. *Geomorphology 55*, 25–43

Dedkov A.P., Moszherin V.I. (1993) Erosion and sediment yield in mountain regions of the world. In *Erosion, Debris Flows and Environment in Mountain Regions*, Walling D.E. (Ed.). IAHS Publication No. 209. IAHS Press, Wallingford, 29-36.

Edwards T.K., Glysson G.D. (1999) *Field Methods for Measurement of Fluvial Sediment*. U.S. Geological Survey, TWI 3-C2.

Evans M. (1997) Temporal and spatial representativeness of alpine sediment yields: Cascade Mountains, British Columbia. *Earth Surface Processes and Landforms 22*, 287-295.

Ferguson R.I. (1984) Sediment load of the Hunza River. In *The International Karakoram Project*, Miller K.J. (Ed.) Cambridge University Press, Cambridge, 580-598.

Galy A., France-Lanord C. (2001) Higher erosion rates in the Himalaya: Geochemical constraints on riverine fluxes. *Geology 29*(1), 23–26.

Gellis A., Hereford R., Schumm S.A., Hayes B.R. (1991) Channel evolution and hydrologic variations in the Colorado River Basin: Factors influencing sediment and salt loads. *Journal of Hydrology 124*, 317-344.

Glazyrin G.E., Tashmetov H.K. (1995) Sediment yield alteration of mountain rivers and climate change in central Asia. In *Effects of Scale on Interpretation and Management of Sediment and Water Quality*, Osterkamp W.R. (Ed.) IAHS Publication No. 226. IAHS Press, Wallingford, 187-190.

Goodbred S.L., Kuehl S.A. (2000) Enormous Ganges-Brahmaputra sediment discharge during strengthened early Holocene monsoon. *Geology 28*, 1083-1086.

Gurnell A.M. (1995) Sediment yield from alpine glacier basins. In *Sediment and Water Quality in River Catchments*, Foster I., Gurnell A., Webb B. (Eds.) Wiley, Chichester, 407-435.

Gurnell A., Hannah D., Lawler D. (1996) Suspended sediment yield from glacier basins. In *Erosion and Sediment Yield: Global and Regional Perspective*, Walling D.E., Webb B.W. (Eds.) IAHS Publication No. 236. IAHS Press, Wallingford, 97-104.

Haan C.T. (2002) *Statistical Methods in Hydrology.* Iowa State Press, Ames, Iowa, 496.

Hallet B., Hunter L., Bogen J. (1996) Rates of erosion and sediment evacuation by glaciers: A review of field data and their implications. *Global and Planetary Change 12*, 213-235.

Hammond R., McCullagh P.S. (1978) *Quantitative Techniques in Geography: An Introduction*. Oxford University Press, London, 384.

Hewitt K. (1998) Catastrophic landslides and their effects on the upper Indus streams, Karakoram Himalaya, northern Pakistan. *Geomorphology 26*, 47-80.

Hijmans R.J., Cameron S.E., Parra J.L., Jones P.G., Jarvis A. (2005) Very high resolution interpolated climate surfaces for global land areas. *International Journal of Climatolology 25*, 1965-1978.

Hovius N. (1998) Controls on sediment supply by large rivers. In *Relative Role of Eustasy, Climate and Tectonism in Continental Rocks*, Shanley K.W., McCabe S.J. (Eds.) SEPM (Society for Sedimentary Geology) Special Publication No. 59, Tulsa, OK, 3-16.

Islam M.R., Begum S.F., Yamaguchi Y., Ogawa K. (1999) The Ganges and Brahmaputra Rivers in Bangladesh: basin denudation and sedimentation. *Hydrological Processes 13*, 2907-2923.

Islam M.R., Yamaguchi Y., Ogawa K. (2001) Suspended sediment in the Ganges and Brahmaputra Rivers in Bangladesh: observation from TM and AVHRR data. *Hydrological Processes 15*, 493-509.

Jansen J.M.L., Painter R.B. (1974) Predicting sediment yield from climate and topography. *Journal of Hydrology 21*, 371-380.

Lane L.J., Hernandez M., Nichols N. (1997) Processes controlling sediment yield from watersheds as functions of spatial scale. *Environmental Modeling and Software 12*, 355-369.

Lu X.X., Higgitt D.L. (1999) Sediment yield variability in the Upper Yangtze, China. *Earth Surface Processes and Landforms 24*, 1077-1093.

Ludwig W., Probst J.L. (1998) River sediment discharge to the oceans: Present-day controls and global budgets. *American Journal of Science 298*, 265-295.

McLean D.G., Church M., Tassone B. (1999) Sediment transport along lower Fraser River 1. Measurements and hydraulic computations. *Water Resources Research 35*(8), 2533-2548.

Meade R.H. (1985) *Suspended Sediment in the Amazon River and its Tributaries in Brazil During 1982-84*. U.S. Geological Survey. Open-File Report 85-492, Denver, Colorado.

Meade R.H. (1994) Suspended sediment of the modern Amazon and Orinoco Rivers. *Quat. Internat. 21*, 29-39.

Meade R.H., Yuzyk T.R., Day T.J. (1990) Movement and storage of sediment in rivers of the United States and Canada. In *Surface Water Hydrology*, Wolman M.G., Riggs H.C. (Eds.) Geological Society of America, Boulder, CO, 255-280.

Meybeck M. (2003) Global analysis of river systems: from earth system controls to Anthropocene controls. *Phil. Trans. Royal Acad. London B 358*, 1935-1955.

Meybeck M., Laroche L., Dürr H.H., Syvitski J.P. (2003) Global variability of daily total suspended solids and their fluxes. *Global Planetary Changes 39*, 65-93.

Miller K.J. (Ed.) (1984) The International Karakoram Project. Cambridge University Press, Cambridge.

Milliman J.D., Syvitski J.M.P. (1992) Geomorphic/tectonic control of sediment discharge to the ocean: the importance of small mountainous rivers. *Journal of Geology 100*, 525-544.

MINITAB Inc. (2006) MINITAB® Release 14: Statistical Software for Windows. http://www.minitab.com/products/minitab/14/default.aspx

Molnar P., Tapponnier P. (1975) Cenozoic tectonics of Asia: Effects of a continental collision. *Science 189*, 419-426.

Montgomery D.C., Peck E.A. (1992) *Introduction to Linear Regression Analysis.* Wiley, New York.

Nash J.E., Sutcliffe J.V. (1970) River flow forecasting through conceptual models: Part I, A discussion of principles. *Journal of Hydrology 10*, 282-290.

NEAC Consultants (2004) Feasibility study of the Basha Diamer Dam Hydropower Project. WAPDA, Lahore.

Owen L.A., Derbyshire E., Scott C.H. (2003) Contemporary sediment production and transfer in high-altitude glaciers. *Sedimentary Geology 155*, 13-36.

Parker R.S. (1988) Uncertainties in defining the suspended sediment budget for large drainage basins. In: *Sediment Budgets,* Bordas M.P., Walling D.E. (Eds.) IAHS Publication No. 174. IASH Press, Wallingford, 523-532.

Pinet P., Souriau M. (1988) Continental erosion and large-scale relief. *Tectonics 7*(3), 563-582.

Rantz S.E. and others (1982) *Measurement and Computation of Streamflow - Volume 1. Measurement of Stage and Discharge*. U. S. Geological Survey Water-Supply Paper. 2175.

Restrepo J.D., Kjerfve B., Hermelin M., Restrepo J.C. (2006) Factors controlling sediment yield in a major South American drainage basin: the Magdalena River, Colombia. *Journal of Hydrology 316*, 213-232. DOI:10.1016/j.jhydrol.2005.05.002

Richey J.E., Meade R.H., Salati E., Devol A.H., Nordin-Jr C.F., Santos U.D. (1986) Water discharge and suspended sediment concentrations in the Amazon River: 1982-1984. *Water Resources Research 22*(5), 756-764.

Rondeau B., Cossa D., Gagnon P., Bilodeau L. (2000) Budget and source of suspended sediment transport in St. Lawrence River in Canada. *Hydrological Processes 14*(1), 21-36.

Searle M.P. (1991) *Geology and Tectonics of the Karakoram Mountains.* Wiley, New York.

Shroder J.F. (Ed.) (1993) *Himalaya to the Sea: Geology, Geomorphology and the Quaternary.* Routledge, Chichester.

Shroder J.F., Bishop M.P. (1998) Mass movement in the Himalaya: new insights and research directions. *Geomorphology 26*, 13-35.

Sichingabula H.M. (1998) Factors controlling variations in suspended sediment concentration for single-valued sediment rating curves, Fraser River, British Columbia, Canada. *Hydrological Processes 12*, 1869-1894.

Sichingabula H.M. (1999) Magnitude-frequency characteristics of effective discharge for suspended sediment transport, Fraser River, British Columbia, Canada. *Hydrological Processes 13*, 1361-1380.

Summerfield M.A., Hulton N.J. (1994) Natural controls of fluvial denudation rates in major world drainage basins. *Journal of Geophysical Research 99*(B7), 13,871-13,884.

SWHP (Surface Water Hydrology Project) (2000) A*nnual Report of River and Climatological Data of Pakistan: Vol-1: River Discharge, Sediment and Quality Data.* Surface Water Hydrology Project, WAPDA, Lahore (Pakistan).

Syvitski J.P.M., Milliman J.D. (2007) Geology, geography and humans battle for dominance over the delivery of sediment to the coastal ocean. *J. Geology 115*, 1-19.

Syvitski J.P., Morehead M.D., Bahr D.B., Mulder T. (2000) Estimating fluvial sediment transport: the rating parameters. *Water Resources Research 36*(9), 2747-2760.

Syvitski JPM, Vörösmarty C, Kettner AJ, Green P. 2005. Impact of humans on the flux of terrestrial sediment to the global coastal ocean. *Science 308*, 376-380.

Tucker G.E., Slingerland R. (1997) Drainage basin responses to climate change. *Water Resources Research 33*, 2031-2047.

USBR (U.S. Bureau of Reclamation) (1987) Design of Small Dams. U.S. Bureau of Reclamation, Water Resources Technical Publication, Denver, Colorado.

USGS (2006a) EROS Data Centre: Elevation Products. http://edc.usgs.gov/products/elevation.html

USGS (2006b) EROS Data Centre: Global land cover characterization. http://edcsns17.cr.usgs.gov/glcc/

Van Dijk P.M., Kwaad F.J.P.M. (1998) Modelling suspended sediment supply to the River Rhine drainage network: A methodological study. In: *Modelling Soil Erosion, Sediment Transport and Closely Related Hydrological Processes,* Summer W., Klaghofer E., Zhang W. (Eds.) IAHS Publication No. 249. IAHS Press, Wallingford, 165-176.

Van Rompaey A.J.J., Govers G., Puttemans C. (2002) Modelling land use changes and their impact on soil erosion and sediment supply to rivers. *Earth Surface Processes and Landforms 27*, 481-494.

Vance D., Bickle M., Ivy-Ochs S., Kubik P.W. (2003) Erosion and exhumation in the Himalaya from cosmogenic isotope inventories of river sediments. *Earth and Planetary Science Letters 206*, 273-288.

Walling D.E. (1999) Linking land use, erosion and sediment yields in river basins. *Hydrobiologia 410*, 223-240.

Walling D.E., Webb B.W. (Eds.) (1996) *Erosion and Sediment Yield: Global and Regional Perspective.* IAHS Publication No. 236, IAHS Press, Wallingford.

Walling D.E., Fang D. (2003) Recent trends in the suspended sediment loads of the world's rivers. *Global and Planetary Change 39*, 111-126

Wasson R.J. (2003) A sediment budget for the Ganga–Brahmaputra catchment. *Current Science 84*(8), 1041-1047.

Webb R.H., Griffiths P.G., Melis T.S., Hartley D.R. (2000) Sediment delivery by ungaged tributaries of the Colorado River in Grand Canyon, Arizona, U.S. Geological Survey Water-Resources Investigations Report 00-4055.

Webb R.H., Griffiths P.G., Hartley D.R. (2001) Techniques for estimating sediment yield of ungaged tributaries on the Colorado Plateau, Proceedings of the Seventh Federal Interagency Sedimentation Conference, March 25-29, 2001, Reno, Nevada. I-24 – I-31.

WORLDCLIM (2006) WORLDCLIM: Version 1.4. http://biogeo.berkeley.edu/worldclim/worldclim.htm

Xu J. (2002) Implication of relationships among suspended sediment size, water discharge and suspended sediment concentration: the Yellow River basin, China. *Catena 49*, 289–307.

Xu J., Cheng D. (2002) Relation between the erosion and sedimentation zones in the Yellow River, China. *Geomorphology 48*, 365–382.

Xu J., Yunxia Y. (2005) Scale effects on specific sediment yield in the Yellow River basin and geomorphological explanations. *Journal of Hydrology 307*(1-4), 219-232

Yang C.T., Molinas A., Wu B. (1996) Sediment transport in Yellow River. *Journal of Hydraulic Engineering, ASCE 122*(5), 237-244.

Young G.J., Hewitt K. (1990) Hydrology research in the upper Indus basin. In *Hydrology of Mountain Area*, Molnar L. (Ed.) IAHS Publication No. 190. IAHS Press, Wallingford, 139-152.

Zemp M., Kääb A., Hoelzle M., Haeberli W. (2005) GIS-based modelling of glacial sediment balance. *Z. Geomorph. 138*, 113-129.

CHAPTER 4 – SPATIALLY DISTRIBUTED EROSION AND SEDIMENT YIELD MODELING IN THE UPPER INDUS RIVER BASIN

4.1 Abstract

Spatially distributed erosion rates and sediment yields are predicted in the mountainous upper Indus River basin with coupled models of erosion and sediment delivery. Potential erosion rates are calculated with the Thornes model in combination with a surface runoff model. Sediment delivery ratios (SDR) are hypothesized to be a function of travel time of surface runoff from catchment cells to the nearest downstream channel. Modeled monthly erosion rates for the upper Indus River basin indicate that 87% of the annual gross erosion takes place in the three summer months. The erosion risk map suggests that the areas with the greatest erosion potential are concentrated in sub-basins with high relief and a substantial proportion of glacierized area. Lower erosion rates can be explained by the arid climate and low relief on the Tibetan Plateau, and by the dense vegetation and lower relief in the lower monsoon sub-region. 33.6% of the basin experiences slight to moderate erosion (0–1.0 mm a^{-1}) and 66.4% high erosion (>1.0 mm a^{-1}). The model predicts an average annual erosion rate of 3.2 mm a^{-1} or 868 Mt a^{-1}, which is approximately 4.5 times the long-term observed annual sediment yield of the basin. The Indus sub-basins generally show an increase of sediment delivery ratio with basin area. The predicted annual basin sediment yield is 244 Mt a^{-1} which compares reasonably well to the measured value

of 195.1 Mt a^{-1}. The overall sediment delivery ratio in the basin is calculated as 0.28. Model results indicate that higher delivery ratios (SDR>0.6) are found in 18% of the basin area, mostly located in the high-relief sub-basins. The sediment delivery ratio is lower than 0.2 in 70% of the basin area. Model evaluation based on accuracy statistics suggest "very good" to "satisfactory" performance ratings for predicted sediment yields. The presented modeling framework requires relatively few data, all of which can be derived from global datasets. It therefore can be used to predict erosion and sediment yield in other ungaged or poorly gaged drainage basins.

Index terms: 1815 Erosion; 1819 Geographic Information Systems; 1847 Modeling; 1862 Sediment transport; 1874 Ungaged basins

Keywords: Indus River; Himalayas; Erosion modeling; Sediment delivery ratio (SDR); Sediment yield modeling

4.2 Introduction

Problems associated with high erosion rates are particularly evident in high mountainous regions, given a combination of high relief, extreme weather conditions, climate change and resource development (Jain *et al*., 2001; Yang *et al*., 2003; Marston, 2008). The large quantity of sediment eroded and transported downstream creates a number of major water resources management problems such as siltation of reservoirs, damage to turbines, reduction in quality of water supplies, and transport of chemical pollutants. As a result, there is a continuing need for a

better quantitative estimation of erosional processes, rates, patterns, and their response to environmental change (Walling and Webb, 1996).

Even though erosion is recognized as a major issue arising from natural causes and human activity, the extent of the problem is hard to quantify, especially at larger scales as measurements of erosion are usually carried out at restricted temporal and spatial scales because of limitations in funding and time. Physically-based models can provide a quantitative approach to estimating rates of erosion, transport and deposition of sediment. However, a scarcity of fine resolution data in most drainage basins have hampered their application. Jetten *et al*. (2003) have noted that the predictive quality of physically-based erosion models is generally not very good and that simpler lumped models seem to perform equally well. Emerging GIS techniques and the availability of global environmental datasets in combination with models with a low demand for data make estimating erosion rates and their spatial distribution feasible for large areas at a reasonable cost and accuracy without time-consuming and costly field surveys (Nearing *et al*., 2000).

Delivery of eroded sediment to river channels and subsequent fluvial transport is a key off-site consequence of erosion. Reliable estimates of sediment delivered to river channels and their subsequent export from the drainage basin are essential in water resources analyses, modeling, and engineering (Lane *et al*., 1997). Assuming that reasonable estimates of gross erosion, E (M L^{-2} T^{-1}) in the basin can be made, the next step is to multiply those estimates by a sediment delivery ratio (SDR) in order to obtain the sediment yield, SY (M L^{-2} T^{-1}):

$$SY = SDR \times E \tag{4.1}$$

The sediment delivery ratio is the fraction of gross erosion that is delivered to the drainage basin outlet. Although likely to be less than 1, the sediment delivery ratio is highly variable and is influenced by a wide range of geomorphological and environmental factors such as precipitation, land cover, topography and soil properties resulting in highly variable sediment delivery ratios from basin to basin (Walling, 1983). Some shortcomings in the SDR model have been reported in literature (Parsons *et al*. 2006; Wainwright *et al*., 2001) and alternate approaches based on the entrainment and travel distance of individual particles have also been presented by *Parsons et al*. (2004) and Wainwright *et al*. (2008). The sediment delivery ratio generally varies systematically within a basin from the headwaters to the downstream regions (Golosov, 2002; Ritter *et al*., 2002; Smith, 2008). Sediment delivery ratios >90% are possible for the upland watersheds (Trimble, 1977), but they may be as low as 4% for the coastal plains (Phillips, 1991). Saavedra (2005) found higher delivery ratios (SDR>0.6) in 25% of the Laka-Laka reservoir catchment in the Bolivian Andes, whereas the sediment delivery ratios were lower than 0.2 in more than 50% of the catchment. Lu *et al*. (2006) have found sediment delivery ratios varying from 0 on the floodplains to 0.7 in the eastern uplands of the Murray Darling basin in Australia.

The classical sediment delivery ratio for a drainage basin provides a lumped approach to sediment transport in that basin. Nevertheless, sediment is generated from different source areas in the basin that each have distinct sediment delivery characteristics. It therefore may be more appropriate to model sediment delivery at a basin scale using a spatially distributed approach that takes into account local factors such as sediment detachment, transport, and travel time. Model

SedNet follows a similar approach in investigating spatial variation of erosion sources, sediment transport and deposition, providing information on the sources of sediment yield (Prosser *et al*., 2001; Wilkinson *et al*., 2004; 2006). Saavedra (2005) reviewed the performance of four distributed sediment delivery ratio models in the 59.8 km^2 Laka-Laka reservoir catchment in Bolivian Andes and concluded that the sediment delivery distributed model of Ferro and Porto (2000) provides reliable results and is suitable for predicting distributed sediment delivery ratios in situations where detailed basin data are scarce. The spatially distributed approach for modeling sediment delivery ratios is based on the travel time required for detached sediment to arrive at the basin outlet. A few studies have used this approach, such as Jain and Kothyari (2000) and Kothyari *et al*. (2002) in three small catchments (16–92 km^2) in Bihar, India; Ferro *et al*. (2003) in six Sicilian catchments (20–70 km^2); and Stefano *et al*. (2005) in a 0.014 km^2 catchment in Italy. This modeling concept has not been applied in large, mountainous drainage basins. Ali and De Boer (2008) investigated the factors affecting specific sediment yield in the upper Indus basin and have presented multiple regression models for predicting specific sediment yield in the basin. The results of that study point to the need for a distributed modeling approach for gaining a better understanding of sediment dynamics at drainage basin scale. The first objective of this study is to explore the implementation of the Thornes erosion model in the upper Indus River basin and to evaluate its ability to predict potential erosion rates in a large mountainous drainage basin setting. The second objective of this study is to evaluate the suitability of a distributed modeling approach to determine sediment delivery to the stream network, and to predict spatially distributed sediment yields within the basin by coupling distributed models of erosion and sediment delivery.

4.3 Study Area: The Upper Indus River Basin

The Indus River is one of the longest rivers in southern Asia (Ahmad, 1993; Meadows and Meadows, 1999), with a total length of 2880 km and a drainage area of 912,000 km^2 extending across portions of Pakistan, India, China and Afghanistan (Figure 4.1). The upper Indus basin upstream of Tarbela Dam is 1125 km long, with a drainage area of 219,830 km^2. The Indus River rises in the Tibetan Plateau at an elevation of 5486 m on Mount Kailash (Jain *et al*., 2007), follows a well-defined valley parallel to the geologic strike, and descends down to the Arabian Sea. Much of its flow originates in the mountains of the Karakoram and Himalayas. The major Indus tributaries include the Shyok, Shigar, and Gilgit in the upper, glacierized portion; the Astore in the middle reaches; and the Gorband, Brandu, and Siran in the lower, monsoon-affected portion. Major tectonic activity, culminating in the Himalayan orogeny during the mid-Eocene, has shaped the high relief and complex geologic structures observed in the upper Indus basin today (Molnar and Tapponnier, 1975; Miller, 1984). These young mountain ranges of extreme ruggedness and high elevations are subject to exceptionally rapid degradation by a combination of processes (Searle, 1991; Shroder, 1993, Collins and Hasnain, 1995). The lower, southern part of the basin experiences heavy monsoon rainfall, and rivers in this part of the basin carry large amounts of sediment associated with flash floods. Ali and De Boer (2007) provide a detailed account of the physiography, geology and tectonics, and climate of the basin.

4.4 Distributed Modeling of Erosion Processes

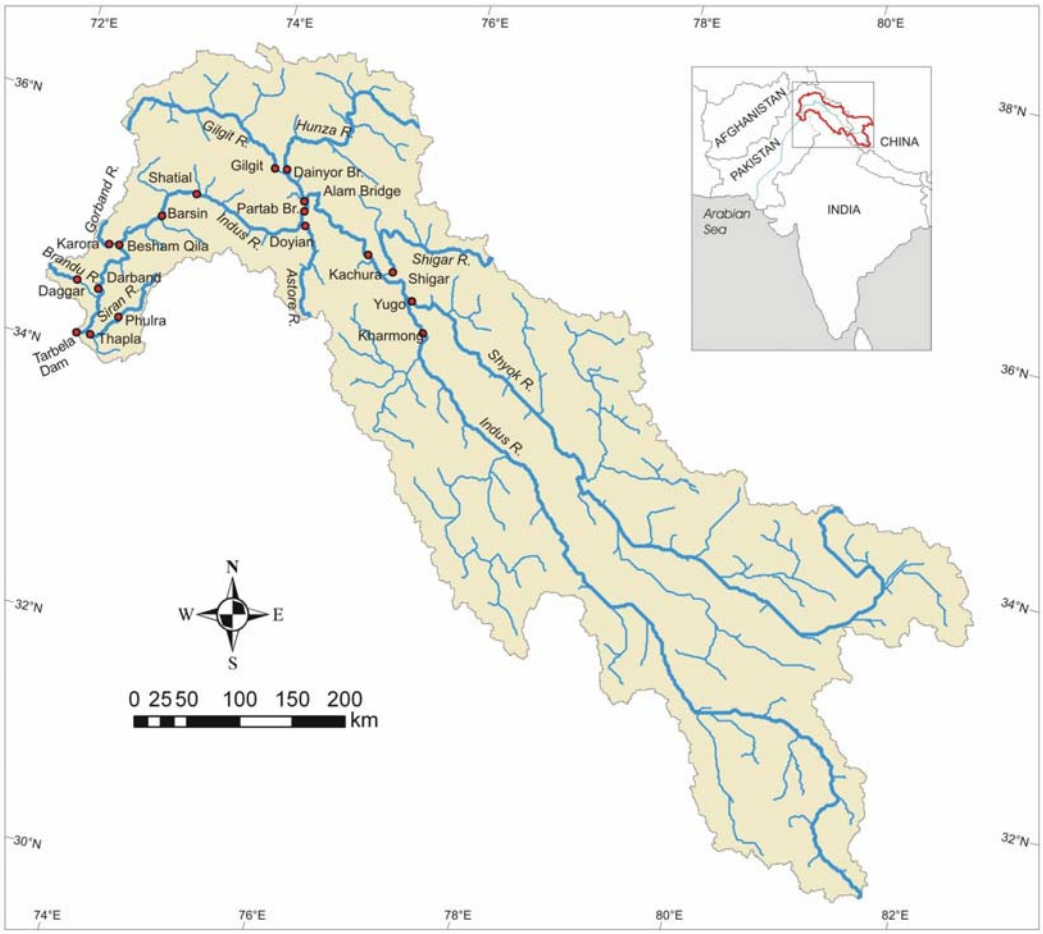

Figure 4.1 The upper Indus River basin

Erosion is calculated as a function of the indicators of driving forces (e.g., runoff rate and gradient) and resistance to erosion (e.g., soil properties and vegetation cover). Thornes (1985; 1990) developed a conceptual erosion model that contains a hydrological component based on a runoff storage type analogy, a sediment transport component and a vegetation cover component. The Thornes erosion model requires estimates of the rate of surface runoff production, and a hydrological sub-model derived by Zhang *et al*. (2002) was adopted for the present study. The Thornes model is based on square grid cells, and starts with the assumption that daily precipitation can be approximated by an exponential frequency distribution within a specified

time period, and that the soil water-storage capacity is affected by initial soil moisture. The model equation for each grid cell is:

$$RO_i = P_i \, e^{-(rc - S_i)/(P_i / D_i)} \tag{4.2}$$

where RO_i is the surface runoff (mm), P_i is the total precipitation (mm), rc is the potential water storage capacity (mm), S_i is the total initial soil moisture (mm), D_i is the number of precipitation days, and i is the time period (from 1 to 12 for months). The Thornes erosion equation for each cell reads:

$$E_i = k \, RO_i^2 \; s^{1.67} \, e^{-0.07 c_i} \tag{4.3}$$

where E_i is the erosion rate (mm month^{-1}), k is the soil erodibility coefficient, s is the slope (m m^{-1}), and c_i is the fraction of vegetation cover (%).

The Thornes erosion model is selected for this study because: i) it has low data requirements compared to other models; ii) the required data is easier to obtain; and iii) it has the flexibility of model application on multi-temporal and spatial scales. This modeling approach has been used at various hydrological scales in several geographical settings. Zhang *et al*. (2002) used the Thornes model for predicting global erosion rates. Symeonakis *et al*. (2007) predicted erosion rates for two small catchments (302 km^2) in the Xaló River basin in southeastern mediterranean Spain. Saavedra (2005) used 5 conceptual models for regional scale erosion modeling in the Bolivian Andes (54,100 km^2). Based on a semi-quantitative comparison with a pre-existing

erosion features map, the Thornes model showed improved erosion estimates and spatial distribution patterns, the input data requirements were lower than those of the other models, and the data were easier to obtain (Saavedra and Mannaerts, 2005). Moreover, the structure of the Thornes model is such that it is suitable for predicting potential erosion rates at daily, monthly and annual time scales. The Thornes model was therefore selected for this study to estimate spatially distributed potential erosion rates in the data sparse, upper Indus River basin.

4.5 Spatially Distributed Sediment Delivery Modeling

The sediment delivery ratio (SDR) for a catchment grid cell, as originally proposed by Ferro and Minacapilli (1995), is given by:

$$SDR = \exp(-\beta t) \tag{4.4}$$

where t is travel time of surface runoff from the catchment cell to the nearest channel (hrs). β is a catchment specific parameter and is considered constant for the catchment. Ferro and Minacapilli (1995) assume that the travel time t varies directly with the length of the flow path l_p and inversely with the square root of the slope of the flow path s_p. If the flow path from the cell to the nearest channel traverses m cells, then t from that cell is calculated by adding the travel times from each cell to the next along the flow path:

$$SDR = \exp\left[-\beta \sum_{p=1}^{m} \frac{l_p}{\sqrt{s_p}}\right] \tag{4.5}$$

If E_i is the erosion rate for a cell for the time period i (mm month^{-1}), the sediment yield SY_i for the cell is given by:

$$SY_i = SDR \times E_i \tag{4.6}$$

The sediment yield for the basin SY_T for the time period i is subsequently obtained by adding the sediment yields for all cells in the basin. The model is based on the assumption that the eroded sediment enters the channel network and leaves the basin during the same time period, which is reasonable as the model runs on a monthly time step.

4.6 Data Sources and Methods

4.6.1 Hydrology

Apart from some long-term discharge records for the Indus and some of its major tributaries, hydrological data for the upper Indus River basin are very scarce. Long-term, continuous discharge and occasional suspended sediment concentration data are available for only 17 active and discontinued gauging stations in the basin (Figure 4.1). Suspended sediment samples in combination with discharge measurements are obtained following standard USGS procedures (Rantz and others, 1982; Edwards and Glysson, 1999) on an occasional basis at the gauging stations so that sediment rating curves can be developed.

4.6.2 Geospatial Data and Derivation of Model Parameters

Topography controls flow paths and determines the effect of gravity on the movement of water and sediment. Topographic parameters for this study were derived from the 30 arc-second resolution GTOPO30 dataset (USGS, 2008a). The raw data were preprocessed in ArcInfo ArcGIS to fill sinks and to delineate the basin. The channel network and the longest flow paths obtained from further processing are shown in Figure 4.1. Using the extracted DEM window and the gauging stations coverage, sub-basin segmentation and parameterization were carried out. Figure 4.2 shows basin slope, an important parameter in Thornes erosion model, as derived from the GTOPO30 DEM.

Vegetation parameters account for the protection against erosion provided by the canopy and ground cover. Vegetation characteristics vary in space and time, and these changes are difficult to measure over large areas. Remote sensing techniques are therefore useful under these circumstances. The Normalized Difference Vegetation Index (NDVI) can be used for estimating temporal vegetation cover (Tucker, 1979; Purevjord *et al*., 1998). Drake *et al*. (1999) derived a regression equation for the relationship between NDVI and vegetation cover based on data reported in the literature:

$$c_i = 8.79815 + 93.07466\ NDVI_i \tag{4.7}$$

where c_i is the fraction of vegetation cover for a cell for time period i (%). For this study, 1-km NOAA-AVHRR derived 10-day composite NDVI values (USGS, 2008b) were processed to

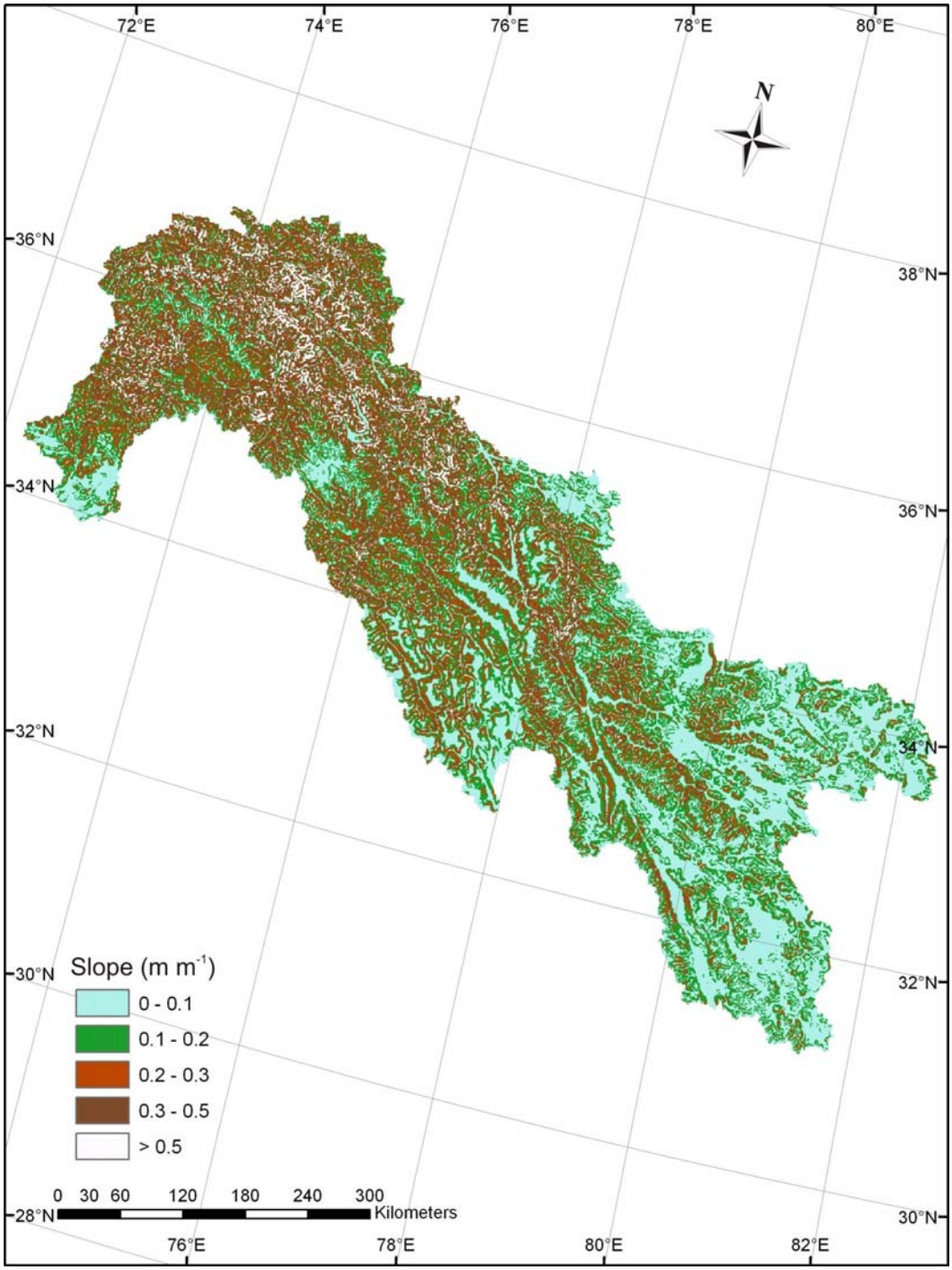

Figure 4.2 Basin slope derived from the GTOPO30 DEM (USGS, 2008a)

calculate the % vegetation cover for each month with equation (4.7). The derived vegetation cover is shown in Figure 4.3 for the months of January and August. As expected in the northern

hemisphere, the vegetation cover is denser in August than in January due to greening of deciduous vegetation in summer or burial by snow in winter.

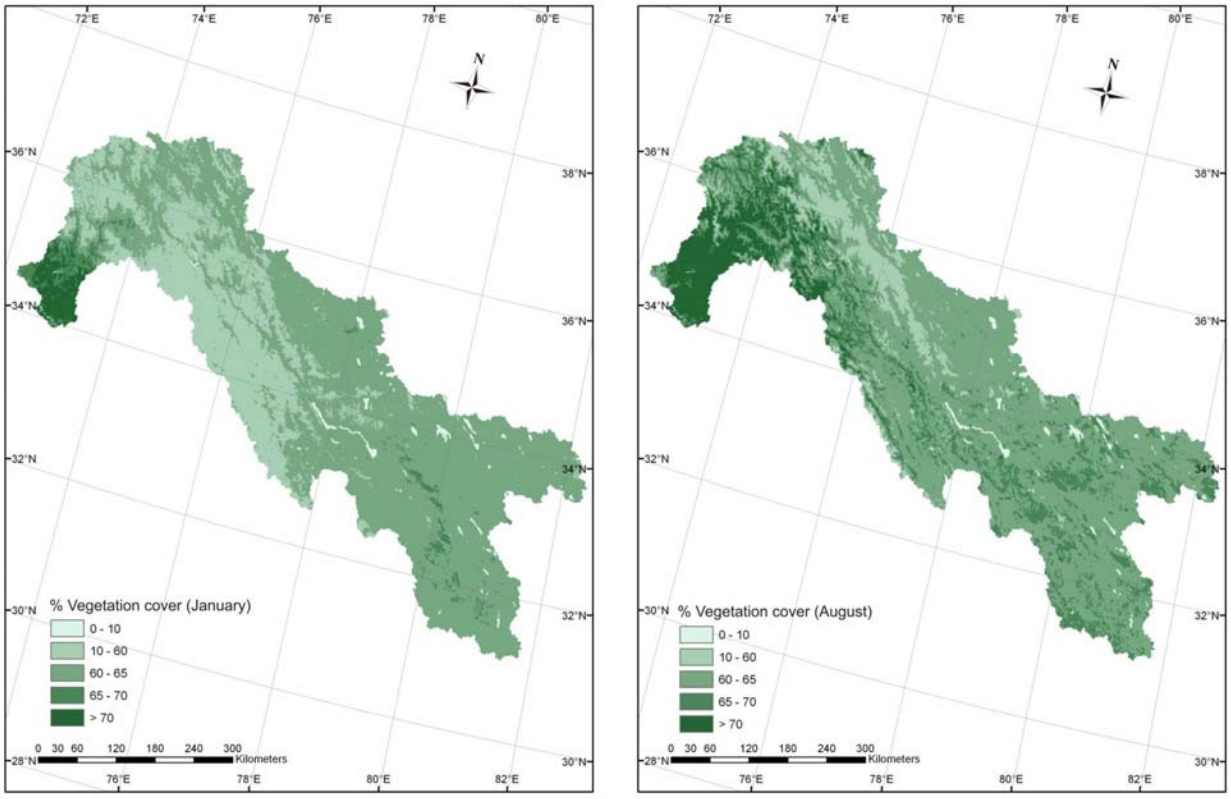

Figure 4.3 Vegetation cover for January and August derived from NDVI (USGS, 2008b)

Climatic grid data from the International Water Management Institute (IWMI) World Water and Climate Atlas (IWMI, 2008) were used for determining the average surface runoff (*RO*) for each month with equation (4.2). Application of equation (4.2) requires updating the initial soil moisture (S_i) for each month. To determine these values, the soil was assumed to be at potential water storage capacity (*rc*) at the end of monsoon period. A value of *rc* = 300 mm was found to give the best results, effectively represents a rooting zone (Zhang *et al*., 2002). The updated initial soil water for the subsequent months was calculated using equation (4.8):

$$S_i = S_{i-1} + P_{i-1} - ET_{i-1} - RO_{i-1} \quad (4.8)$$

where S_{i-1} is the total initial soil moisture for the cell for the preceding time period i–1 (mm), P_{i-1} is the total precipitation (mm), ET_{i-1} is the potential evapotranspiration (mm), and RO_{i-1} is the surface runoff (mm).

The soil erodibility k was determined from the organic matter content and soil texture following Stone and Hilborn (2000) (Table 4.1). Relevant soil properties were derived from the International Soil and Reference Information Centre (ISRIC, 2008) global soil properties database. A considerable proportion of the upper Indus River basin is characterized by bare rock and glacier ice. To account for these land classes, k values of 0 and 0.4 were adopted for bare rock and glaciers, respectively.

Table 4.1 Soil erodibility (k) factors, after Stone and Hilborn (2000)

Textural Class	Organic matter content (%)		
	Average	Less than 2 %	More than 2 %
Clay	0.22	0.24	0.21
Clay Loam	0.30	0.33	0.28
Coarse Sandy Loam	0.07	--	0.07
Fine Sand	0.08	0.09	0.06
Fine Sandy Loam	0.18	0.22	0.17
Heavy Clay	0.17	0.19	0.15
Loam	0.30	0.34	0.26
Loamy Fine Sand	0.11	0.15	0.09
Loamy Sand	0.04	0.05	0.04
Loamy Very Fine Sand	0.39	0.44	0.25
Sand	0.02	0.03	0.01
Sandy Clay Loam	0.20	--	0.20
Sandy Loam	0.13	0.14	0.12
Silt Loam	0.38	0.41	0.37
Silty Clay	0.26	0.27	0.26
Silty Clay Loam	0.32	0.35	0.30
Very Fine Sand	0.43	0.46	0.37
Very Fine Sandy Loam	0.35	0.41	0.33

After extracting the required data from the respective databases, appropriate format conversions were applied where necessary and all layers were resampled to 1 × 1 km grids and projected to a Lambert Azimuthal Equal Area projection. Individual GIS layers were built for individual model input parameters (i.e., topography, vegetation, climate, and soils) and combined using geospatial modeling procedures in ArcInfo ArcGIS to predict erosion rates using the Thornes erosion model. A raster scheme was used for identifying the hydraulic path linking each catchment cell to the nearest channel cell. The ESRI Hydro Data Model was used to define the channel system. The methodology described in Section 4.5 was utilized for predicting spatially distributed travel time, sediment delivery ratios and sediment yields. A schematic representation of data flow and processing (Figure 4.4) shows the modeling framework divided into a number of components. The erosion and SDR modeling components were coupled to predict sediment yields. Sediment yield predictions were evaluated by calculating a number of accuracy statistics using the observed sediment yields.

4.7 Results and Discussion

4.7.1 Modeled Monthly Erosion Rates

The surface runoff sub-model (equation 4.2) in combination with the Thornes erosion model (equation 4.3) was applied at a 1-km spatial scale and monthly time step for calculating potential erosion rates (mm month^{-1}) for the upper Indus River basin (Table 4.2). Basin-wide predicted potential erosion rates for the summer months of June, July and August (0.63–1.22 mm month^{-1}, average 0.90 mm month^{-1}) are substantially larger than for other months (0.01–0.21 mm month^{-}

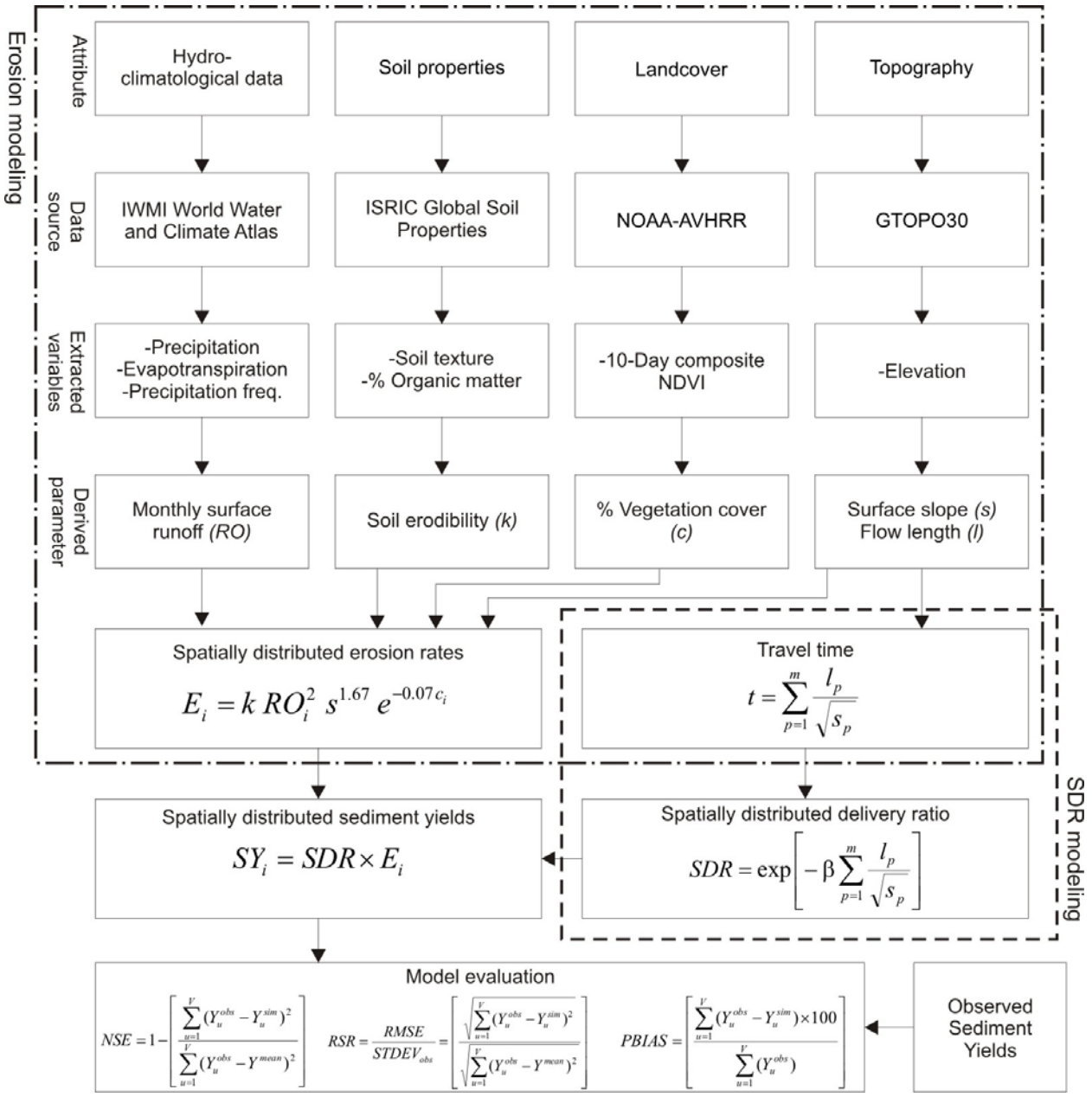

Figure 4.4 Schematic representation of data flow and processing

[1], average 0.05 mm month^{-1}), and suggest that 87% of the gross erosion takes place in these three summer months. The temporal patterns of predicted monthly erosion rates and observed sediment yields at Besham Qila by Ali and De Boer (2007) normalized to annual totals are very similar (Figure 4.5) and have a strong correlation (r^2 = 0.979). Such relationships can be applied

Table 4.2 Predicted monthly mean erosion rates for the upper Indus River basin

Month	Erosion rate (mm month^{-1})
Jan	0.01
Feb	0.01
Mar	0.01
Apr	0.04
May	0.11
Jun	0.63
Jul	1.22
Aug	0.85
Sep	0.21
Oct	0.05
Nov	0.02
Dec	0.01

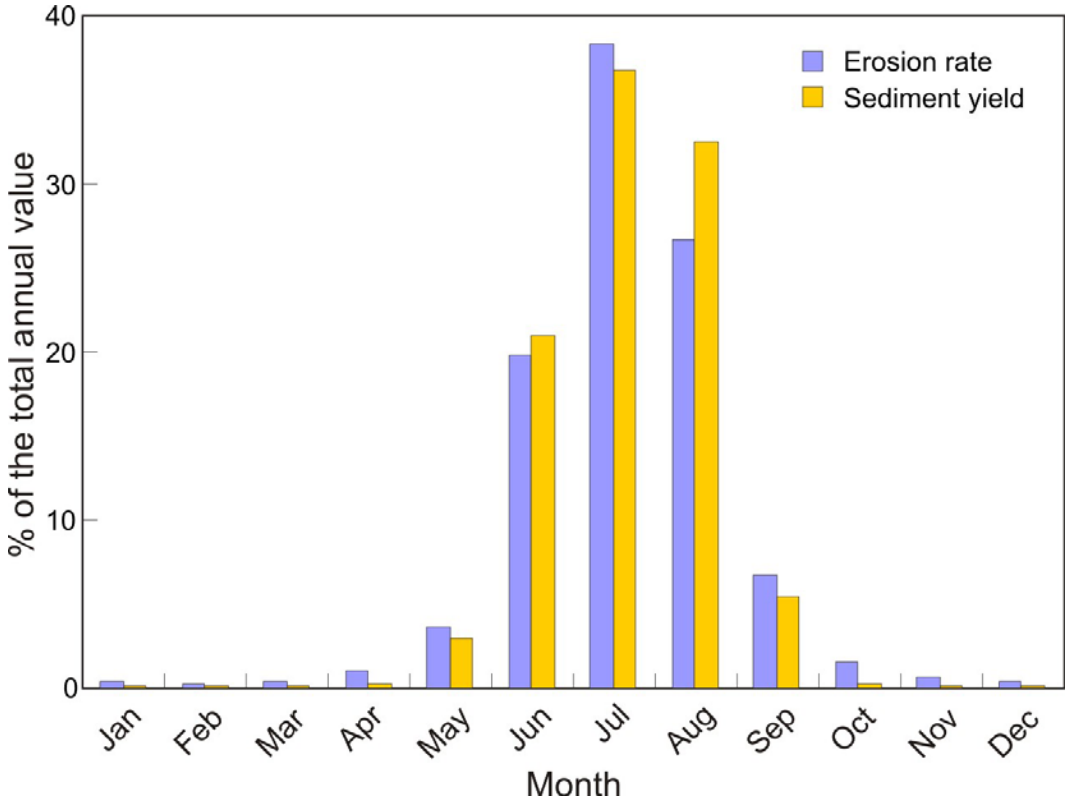

Figure 4.5 Comparison of monthly mean predicted erosion rates and measured sediment yields at Besham Qila near the mouth of the upper Indus River basin, normalized to annual totals

to get a preliminary estimate of monthly sediment yields from erosion rates in ungaged basins. The winter months seem to have relatively larger differences. Both erosion rates and sediment yields in winter are small, however, so that the discrepancies do not add up to a large difference on an annual basis. The monthly pattern found at Besham Qila is also observed at the other stations, especially in upper glacierized region 1 (Ali and De Boer, 2008). This indicates that the temporal pattern of sediment delivery to the channel and transport within the channel network are controlled by the season, i.e., the availability of water in the landscape. This is of course not necessarily the case over the long term as long-term sediment yields and gross erosion may not show a simple relationship (Trimble, 1999; Pistocchi, 2008).

4.7.2 Modeled Annual Erosion Rates

Monthly potential erosion rates were summed to obtain annual erosion rates and these were grouped into five classes (Table 4.3) following the guidelines established by Wall *et al*. (1997).

Table 4.3 Area (%) of predicted mean annual erosion rates classes for the upper Indus River basin

No.	Erosion rate (mm a^{-1})	Erosion risk class	Area	
			(km^2)	(%)
1	0 – 0.2	Low	23,779	10.8
2	0.2 – 1.0	Medium	50,189	22.8
3	1.0 – 5.0	High	93,180	42.4
4	5.0 – 10	Very high	31,441	14.3
5	> 10	Extreme	21,241	9.7

According to the classification scheme, 33.6 % of the basin experiences slight to moderate erosion (0–1.0 mm a^{-1}) and 66.4% high to severe intensity of erosion (>1.0 mm a^{-1}). High

erosion rates are concentrated in the sub-basins having a high relief and a substantial proportion of glacierized area (Figure 4.6), such as the Hunza River basin, the Shigar River basin and the

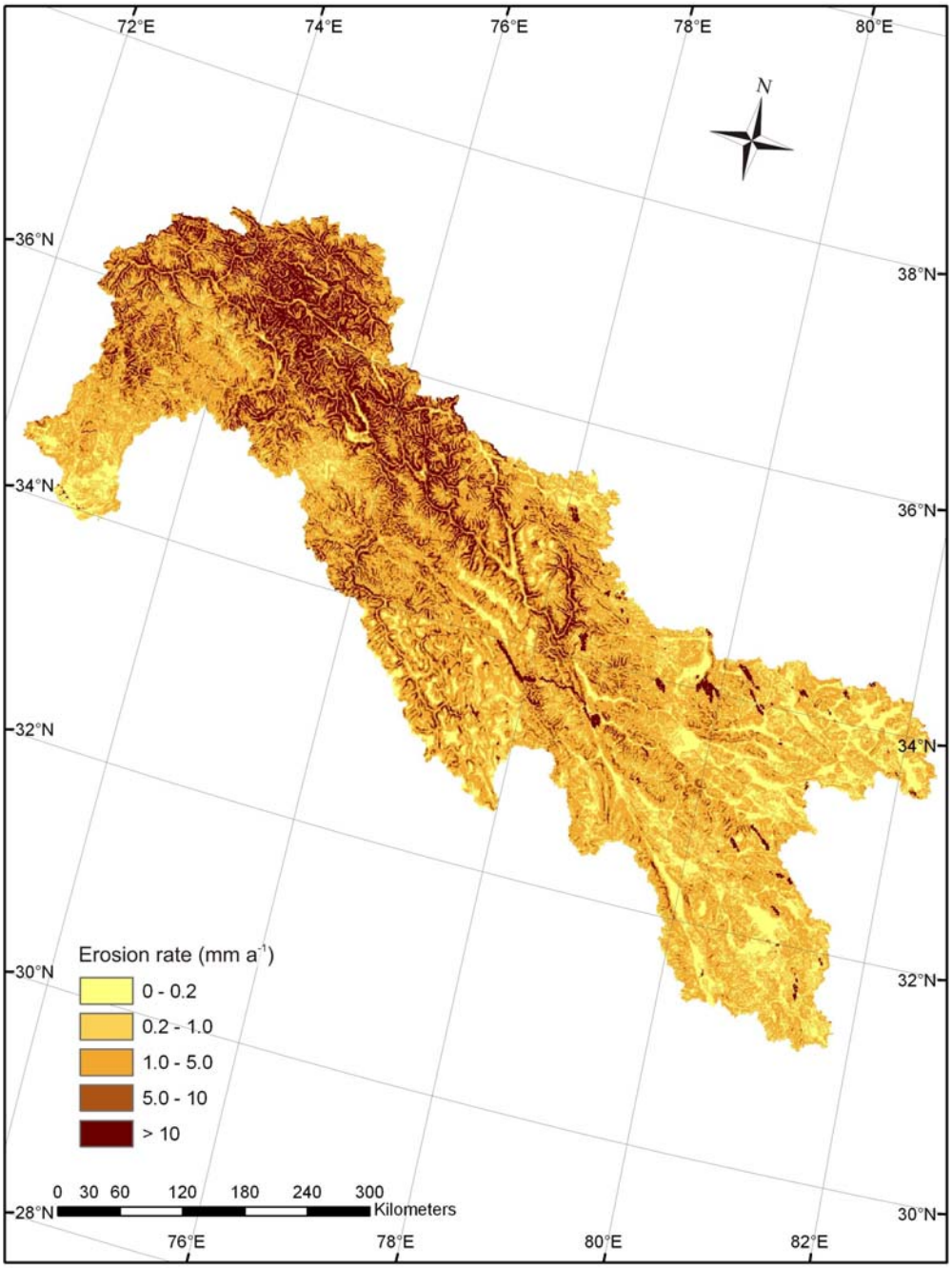

Figure 4.6 Spatial distribution of predicted annual erosion rates

areas around the Nanga Parbat Massif. These sub-regions in the upper Indus River basin are known to have the highest rates of denudation as reported by Ferguson (1984) based on suspended sediment yields, Cornwell *et al*. (2003) based on field measurements, and Garzanti *et al*. (2005) based on a dataset integrating petrographic and mineralogical information. The correspondence of the areas with the highest erosion rates with the glacierized sub-basins is consistent with the findings of Ali and De Boer (2008) that the % snow and ice cover was an important factor affecting sediment yield in the upper Indus River basin. Lower erosion rates (<1.0 mm a^{-1}) are found on the Tibetan Plateau and in the lower part of the basin affected by the monsoon. The Tibetan Plateau is characterized by relatively low slopes (Figure 4.2) and an extremely arid climate with annual precipitation ranging from 100 mm to 300 mm. The monsoon sub-region, on the other hand, receives considerable precipitation. However, the lower erosion rates in this region may be attributed to the dense vegetation cover as seen in Figure 4.3.

The predicted average annual erosion rate of 3.2 mm a^{-1} for the upper Indus River basin is significantly higher than the overall global average erosion rate of 0.38 mm a^{-1} estimated by Yang *et al*. (2003). An average density of 1245 kg m^{-3} for the upper Indus (NEAC Consultants, 2004) was used for converting mean annual erosion rates (mm a^{-1}) to a gross erosion of 868 Mt a^{-1}, which is approximately 4.5 times the long-term sediment yield of the basin determined by Ali and De Boer (2007). Galy and France-Lanord (2001), based on a geochemical budget of the Ganges and Brahmaputra River basins, estimated erosion rates in the eastern Himalayas as 2.9 mm a^{-1} and in the western Himalayas as 2.1 mm a^{-1}. They also estimated that the total Himalayan erosion was approximately twice the measured flux of suspended sediment for these two rivers. A considerably higher potential erosion rate and larger gross erosion magnitude

estimated in the present study indicates the considerably higher rate of degradation in the upper Indus basin compared to the overall Himalayas.

The upper Indus basin is characterized by young, rising mountains with high rates of uplift. According to Summerfield (1991), the overall crustal uplift rates in the Himalayas are currently averaging around 5 mm a^{-1}. This rate is matched by the Andes in Peru and Bolivia. The Southern Alps located on the boundary of the Pacific and Indian plates in New Zealand are experiencing uplift rates of up to 10 mm a^{-1}. A comparison of exhumation and incision rates around the Nanga Parbat Massif suggests that differential bedrock uplift of 1-3 mm a^{-1} has persisted (Leland *et al*., 1998). Dating of abandoned river-cut surfaces by Burbank *et al*. (1996) in the NW Himalayas indicate that the Indus River incises through the bedrock at very high rates of 2-12 mm a^{-1}. The rate of incision is controlled by stream power. Stream power in the upper Indus River basin has been mapped in this study by calculating the product of modeled surface runoff and slopes (Figure 4.7). The pattern of high stream power in the highly glacierized Hunza River basin and in the areas around the Nanga Parbat Massif, and of lower stream power in the relatively flat Tibetan Plateau is consistent with the observed spatial patterns of erosion in the basin.

4.7.3 Validation of Modeled Erosion Rates

A fully quantitative validation of potential erosion rates is difficult for the upper Indus River basin where erosion measurements are very scarce. The model results were therefore validated semi-quantitatively by comparing predicted erosion rates in the basin to published erosion rates from the literature. Some of the problems with this approach are that the temporal and spatial

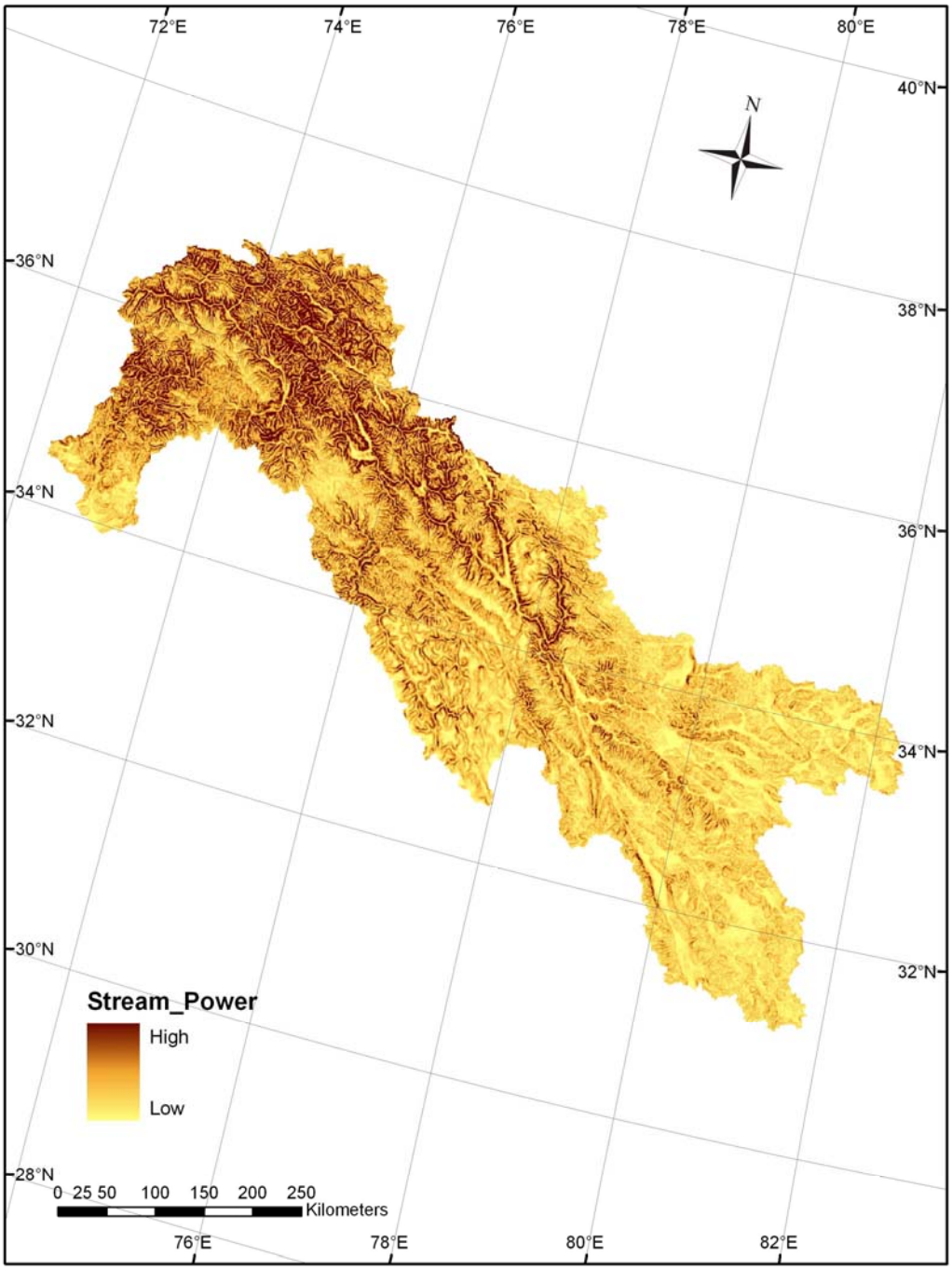

Figure 4.7 Stream power in the upper River basin

scales of the measurements may not correspond to those of the model, and that measured erosion rates depend on the techniques used. Erosion rates reported in the literature for the Indus River basin, the Himalayas and other mountainous region of the world are presented in Table 4.4. A comparison of these rates to modeled erosion rates shows a generally good agreement. The large range of erosion rates (1.5–12 mm a^{-1}) reported for the region around the Nanga Parbat Massif for example by Gardner and Jones (1993), Burbank *et al*. (1996), Hallet *et al*. (1996), Cornwell *et al*. (2003) and Garzanti *et al*. (2005) are in a generally good agreement with the predicted potential erosion rates provided in Table 4.4. The lower erosion rates predicted for the Tibetan Plateau basins like the Shyok River are consistent with the findings of Garzanti *et al*. (2005). There are a few exceptions like the erosion rates of 0.11–0.46 mm a^{-1} measured in the glaciated Nubra Valley, located in Ladakh (Bhutiyani, 2000), which are lower than the rates predicted in this study for the Hunza basin in Western Karakoram. The lower erosion rates measured in the Nubra basin have been attributed to its local geological setting consisting of highly erosion resistant rocks like diorites and granite-gneisses (Bhutiyani, 2000). However, the majority of exposed rocks in the Hunza basin are less erosion-resistant limestones, phyllites and shales, which explains the overall higher erosion rates predicted in the basin found in the present study. The Thornes model gives a few abnormally high values of erosion rates. Similar anomalies were also found by Symeonakis *et al*. (2007) in the Xaló River basin in southeastern mediterranean Spain. The occurrence of such values may be attributed to the exponential nature of the empirical relations used for calculating surface runoff and erosion rates, and to possible quality issues in parts of the spatial datasets.

Table 4.4 An overview of erosion rates reported for the Indus River basin, Himalayas, and other mountainous regions

Location	Erosion rate (mm a^{-1})	Source	Method or technique
Indus River basin			
Upper Indus	3.2	Ali and De Boer (this study)	Spatially distributed modeling
Shyok River sub-basin	2.6		
Shigar River sub-basin	6.3		
Hunza River sub-basin	6.4		
Gilgit River sub-basin (upper)	5.3		
Gilgit River sub-basin (+ Hunza)	5.8		
Astore River sub-basin	4.2		
Gorband River sub-basin	1.7		
Brandu River sub-basin	1.8		
Siran River sub-basin	0.6		
Shigar/Braldu (highest)	4.5±1.7	Garzanti *et al*. (2005)	Petrographic and mineralogical dataset
Nanga Parbat Massif	3.0±1.3		
Karakoram	2.2±0.7		
South Tibet	0.05±0.05		
Hispar	4.0±1.8		
Rupul basin – Raikot and Buldar (Nanga Parbat)	0.2–6.0	Cornwell *et al*. (2003)	Field measurement and computer models
Nanga Parbat near Sichen	0.11–0.46	Bhutiyani (2000)	Suspended sediment yield
Raikot	1.75	Hallet *et al*. (1996)	Glacier sediment yields
Indus crossing Nanga Parbat/Haramosh axis	2.0–12.0	Burbank *et al*. (1996)	Dating of abandoned river cut surfaces
Nanga Parbat Massif (glacier area)	4.6–6.9	Gardner and Jones (1993)	Suspended sediment yield
Himalayas			
Gangotri Glacier, Garhwal Himalaya	1.8	Haritashya *et al*. (2006)	Suspended sediment yield
High Himalayas (upper Ganges)	2.7±0.3	Vance *et al*. (2003)	Cosmogenic isotope inventories
Tibetan Plateau	1.2±0.1		
Foothills to the south of high mountains	0.8±0.3		
Western – Eastern Himalaya in Ganga and Brahmaputra River basins	2.1–2.9	Galy and France-Lanord (2001)	Geochemical budget
On fault bend folds, Nepal	15.0	Lave and Avouac (2000)	Dating of active crustal deformations
Alaknandna near Srinigar	4.0		
Other mountainous regions			
Bolivian Andes in South America	0–128 t ha^{-1} a^{-1}	Saavedra (2005)	Modeling
Taiwan mountain basins	2.2–8.3	Fuller *et al*. (2003)	Suspended sediment yield
Global average	0.38	Yang *et al*. (2003)	Modeling

4.7.4 Erosion Rates and Basin Characteristics

The relationships between potential erosion rates and sub-basin characteristics like slope, runoff, % snow and ice cover, and % vegetation cover have been investigated to gain a better understanding of the controls of sediment yield. The sub-basin erosion rates increase with slope (Figure 4.8a), runoff (Figure 4.8b), and % snow and ice cover (Figure 4.8c), and decreases with increasing vegetation cover (Figure 4.8d). The separate curves for the upper glacierized and lower monsoon sub-basins in Figures 4.8b and Figure 4.8d can be explained by the different characteristics of the upper and lower regions of the basin. For example, the clear distinction between erosion rate-runoff relationships for the upper and lower parts of the basin (Figure 4.8b) can be explained by the difference in vegetation. The sparse vegetation cover in the upper, glacierized and arid sub-basins results in generally higher erosion rates whereas the lower part of the basin affected by the monsoon exhibits lower erosion rates due to a denser vegetation cover (Figure 4.8b). A strong relationship between erosion potential and % snow and ice cover is also consistent with the findings of Ali and De Boer (2008).

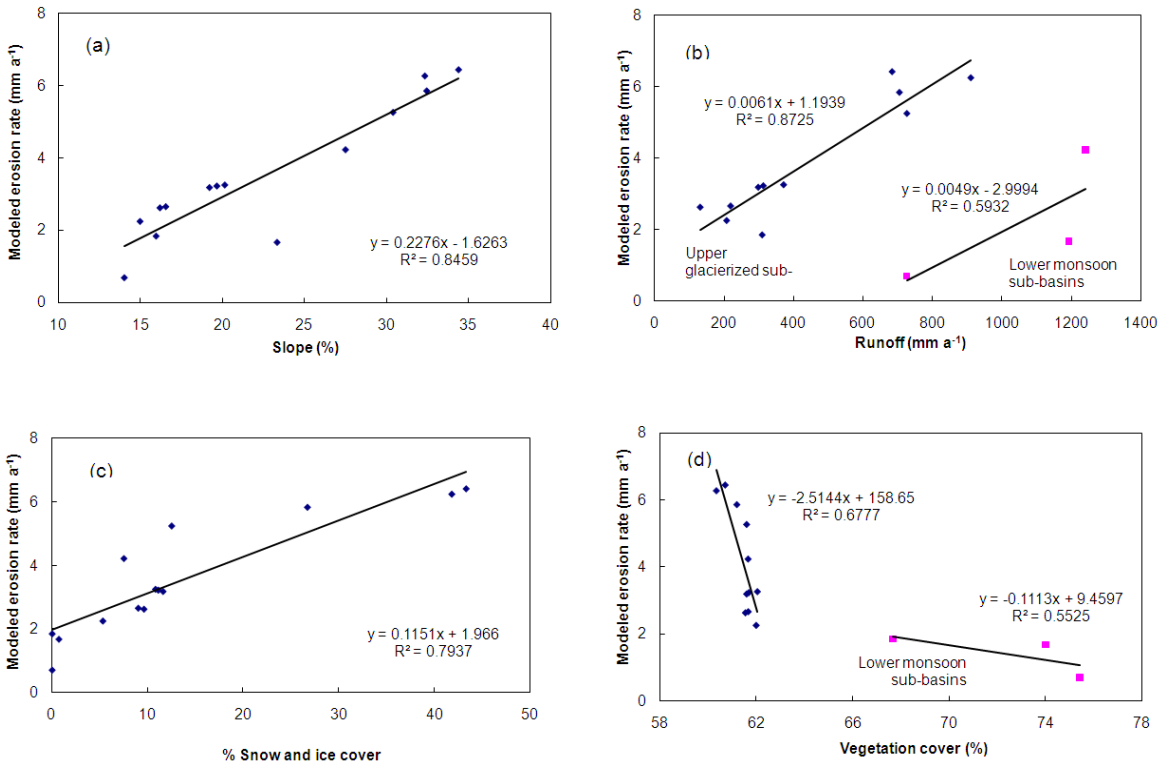

Figure 4.8 Relationship between modeled erosion rates and sub-basin characteristics: (a) slope; (b) runoff; (c) % snow and ice cover; and (d) vegetation cover

4.7.5 Spatial Distribution of Sediment Delivery Ratios

Spatially distributed sediment delivery ratios (*SDR*) have been calculated with Equation (5.5) for each cell in the basin (Figures 4.9). The spatial patterns suggest increasing travel times and decreasing sediment delivery ratios with increasing drainage area and increasing distance from the channel network. Two points located at the same distance from the basin outlet may have different travel times and delivery ratios owing to differences in flow path length and slope. In the upper Indus basin, high delivery ratios (SDR>0.6) are found in 18% of the basin area, mostly located in the high-relief sub-basins like the Shigar, Hunza, Gilgit, and the areas around the Nanga Parbat Massif. The sediment delivery ratio is lower than 0.2 in 70% of the basin area,

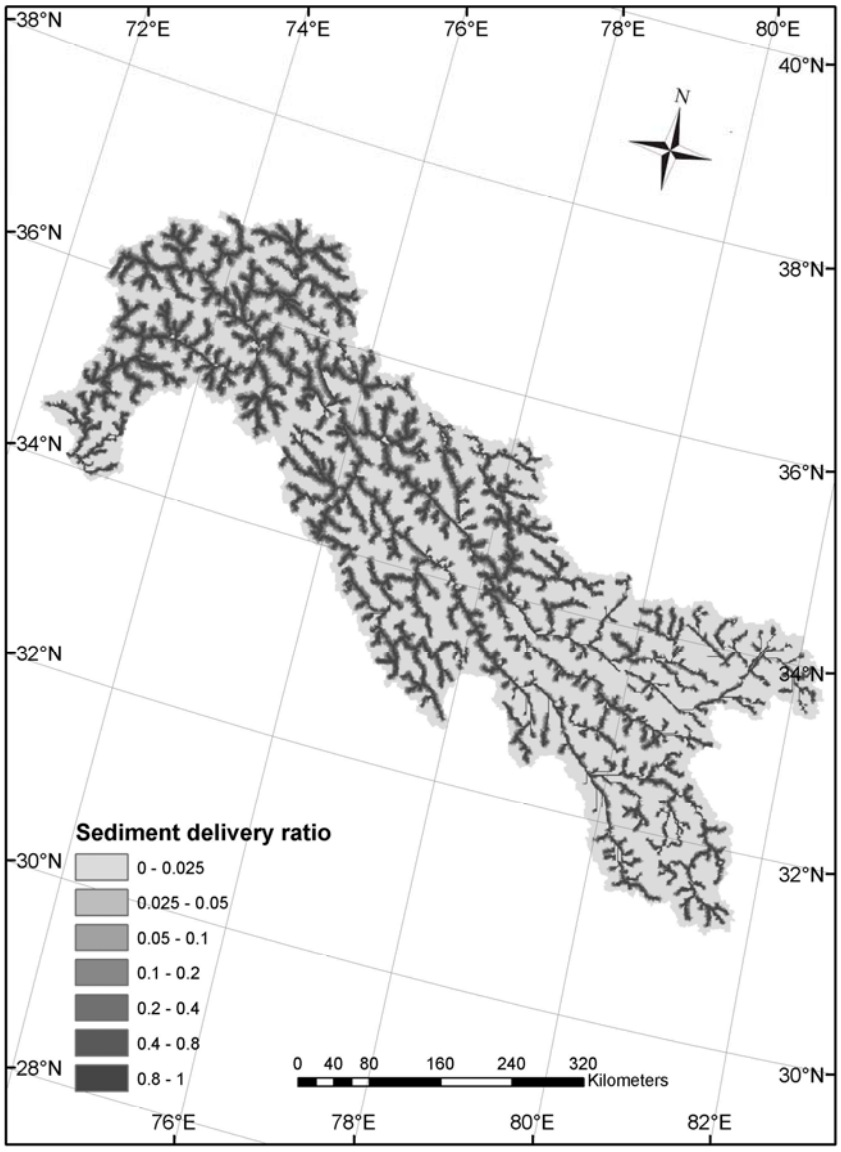

Figure 4.9 Spatial distribution of sediment delivery ratio

mostly found in the low-relief, flat-terrain sub-basins like the Shyok on the Tibetan Plateau, and some portions of the lower monsoon region.

4.7.6 Modeled Annual and Monthly Sediment Yields

Spatially distributed annual sediment yield predictions (Figure 4.10) have been made by coupling sediment delivery ratios and annual erosion rates using equation (4.6). The mean annual sediment yield of the basin was calculated by adding these predicted sediment yields for all the cells as 244 Mt a^{-1}, which compares reasonably with the long-term observed sediment yield of 195.1 Mt a^{-1} for the Indus River at Besham Qila near the basin outlet calculated by Ali and De Boer (2007) and the observed reservoir accumulation of 192.2 Mt a^{-1} obtained from long-term hydrographic surveys of Tarbela Reservoir carried out by Tarbela Dam Project (TDP, 2002). The predicted sediment yield and gross erosion for the basin result in a predicted sediment delivery ratio for the upper Indus River basin of 0.28. This means that a substantial proportion of eroded sediment (72%) is deposited on the slopes. The calculated sediment delivery ratio of 0.28 for the upper Indus River basin is similar to the value of 0.23 for the upper Yangtze River estimated by Wang *et al*. (2007). The average annual specific sediment yield in the basin has been calculated as 1110 t km^{-2} a^{-1} by dividing the predicted mean annual sediment yield of the basin by the total number of basin cells. For a comparison, the specific sediment yields as reported in literature for some other mountainous drainage basins are 524 t km^{-2} a^{-1} in the upper Yangtze (Lu and Higgitt, 1999), 604 t km^{-2} a^{-1} in the Ganges-Brahmaputra (Wasson, 2003), 1400 t km^{-2} a^{-1} in Bolivian Andes (Saavedra, 2005), and 2232 t km^{-2} a^{-1} in the Yellow River basin (Xu and Cheng, 2002). Monthly sediment yields at Besham Qila have also been calculated, and a comparison of predicted monthly mean sediment yields with observed sediment yields of

the Indus River at Besham Qila shows good overall agreement of the distribution pattern (Figure 4.11).

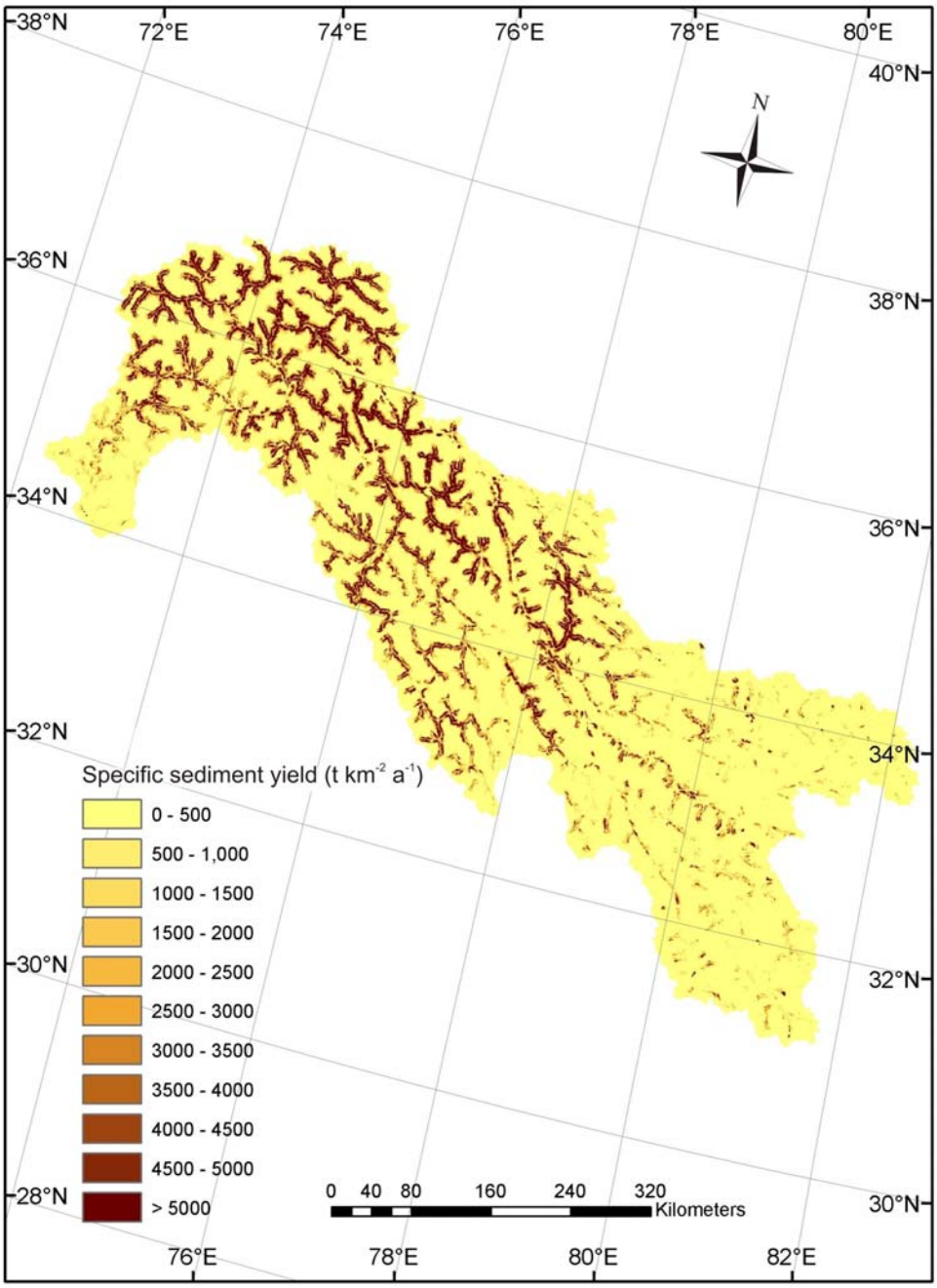

Figure 4.10 Spatial distribution of predicted specific sediment yield

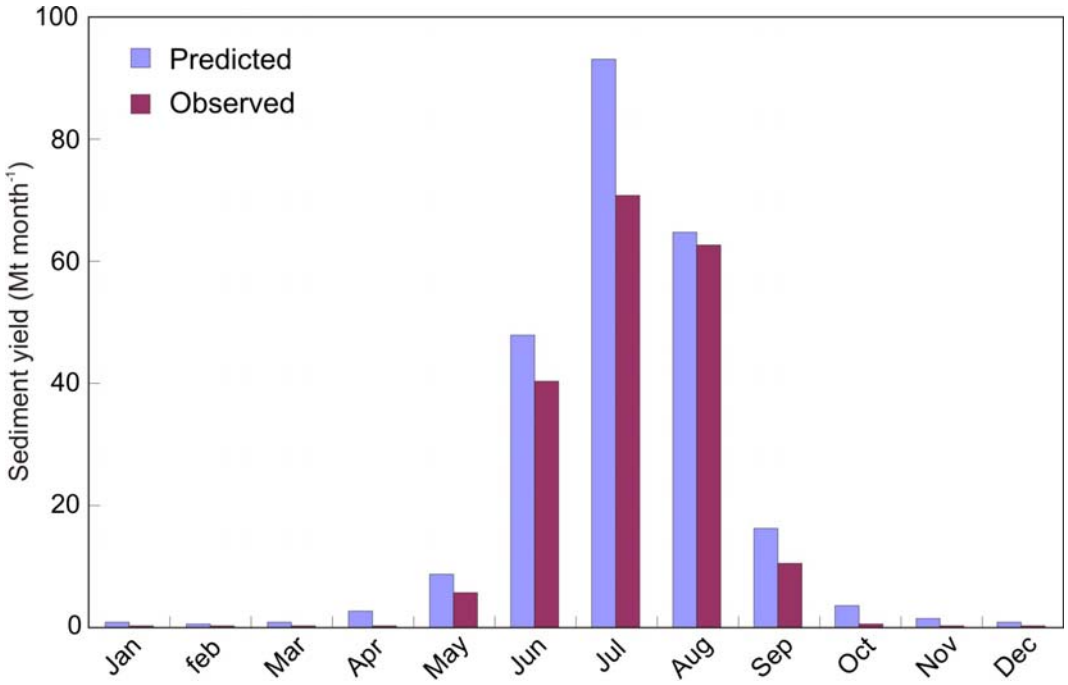

Figure 4.11 Comparison of the predicted and observed monthly sediment yields for the Indus River at Besham Qila

4.7.7 Validation of Modeled Sediment Yields

Moriasi *et al*. (2007) have reviewed a number of quantitative statistics for model evaluation and recommended three for the quantification of accuracy in watershed predictions: (1) the Nash-Sutcliffe efficiency, *NSE* (Nash and Sutcliffe, 1970); (2) the ratio of the root mean square error to the standard deviation of measured data, *RSR* (Legates and McCabe, 1999); and (3) the percent bias, *PBIAS* (Gupta *et al*., 1999). Table 4.5 presents general model evaluation guidelines based on performance ratings for the recommended statistics and project-specific considerations. Model evaluation of predicted monthly sediment yields was carried out in the present study and the computed values of *NSE* = 0.92, *RSR* = 0.29, and *PBIAS* = –26.20% suggest a "very good" to "good" performance rating of predictions for the 12 months. The *PBIAS*

Table 4.5 General performance ratings for accuracy statistics after Moriasi *et al*. (2007)

Performance Rating	*NSE*	*RSR*	*PBIAS* (%)
Very good	$0.75 < NSE \leq 1.00$	$0.00 \leq RSR \leq 0.50$	$PBIAS < \pm 15$
Good	$0.65 < NSE \leq 0.75$	$0.50 < RSR \leq 0.60$	$\pm 15 \leq PBIAS < \pm 30$
Satisfactory	$0.50 < NSE \leq 0.65$	$0.60 < RSR \leq 0.70$	$\pm 30 \leq PBIAS < \pm 55$
Unsatisfactory	$NSE \leq 0.50$	$RSR > 0.70$	$PBIAS \geq \pm 55$

statistic improves to –18.46% for the three summer months of June, July and August, when nearly 90% of the sediment load is transported. The *PBIAS* statistic decreases to 100.73% for the remaining months. Erosion rates and sediment yield in winter are very small, so the discrepancy does not add up to large amounts of sediment.

4.7.8 Modeled Sub-basin Sediment Yields

Potential erosion rates and sediment delivery ratios have also been determined for each of the 17 sub-basins of the upper Indus River basin. The modelling results generally show a good agreement between the predicted and observed sub-basin sediment yields as depicted in Figure 4.12. The observed sediment yields have been determined by Ali and De Boer (2007) by establishing suspended sediment rating curves at hydrological stations in the basin. Computed values of *NSE* = 0.67, *RSR* = 0.58, and *PBIAS* = –36.62% suggest a "good" to "satisfactory" performance rating of predictions for the 17 upper Indus sub-basins. Whereas the accuracy for the larger sub-basins seems to be satisfactory, the *PBIAS* statistics decreases to 84.47% for the small tributaries (<3000 km^2) namely Gorband at Karora, Brandu at Daggar and Siran at Phulra and Thapla located in the lower part of the basin affected by the monsoon. Local factors and extreme conditions seem to have a greater impact in smaller sub-basins due to a relatively coarser resolution of available datasets, whereas local differences tend to be averaged

out in larger basins. As the model parameters have been determined without field calibration, the reliability of the model results can be considered satisfactory for the ungaged sub-basins within the upper Indus.

It is difficult to determine the sediment yield contribution of glaciers in the absence of field data at a large drainage basin scale. Glacier input therefore is not modeled in this study. The sediment yield contribution of glaciers reported in literature is highly variable, ranging from 0.1 mm a^{-1} for Norwegian glaciers, 1.0 mm a^{-1} for glaciers in the Swiss Alps, to 10 mm a^{-1} for glaciers in tectonically active ranges of Alaska (Bogen and Bønsens, 2003; Gurnell *et al*., 1996; Hallet *et al*., 1996). Collins and Hasnain (1995) report that some heavily glacierized streams in the Karakoram contribute up to 60% of the sediment load. Although glacier coverage is not built in the model for predicting erosion and sediment yields in the upper Indus River basin, the model still gives good results. Glacier coverage is important because ice melt drives erosion and sediment yield. On the other hand, ice cover may also indicate an absence of vegetation, i.e., bare soil, resulting in more susceptibility to erosion. It therefore appears that percent snow/ice cover is a proxy for other variables. Nevertheless, the inclusion of percent snow/ice cover may further improve the prediction accuracy.

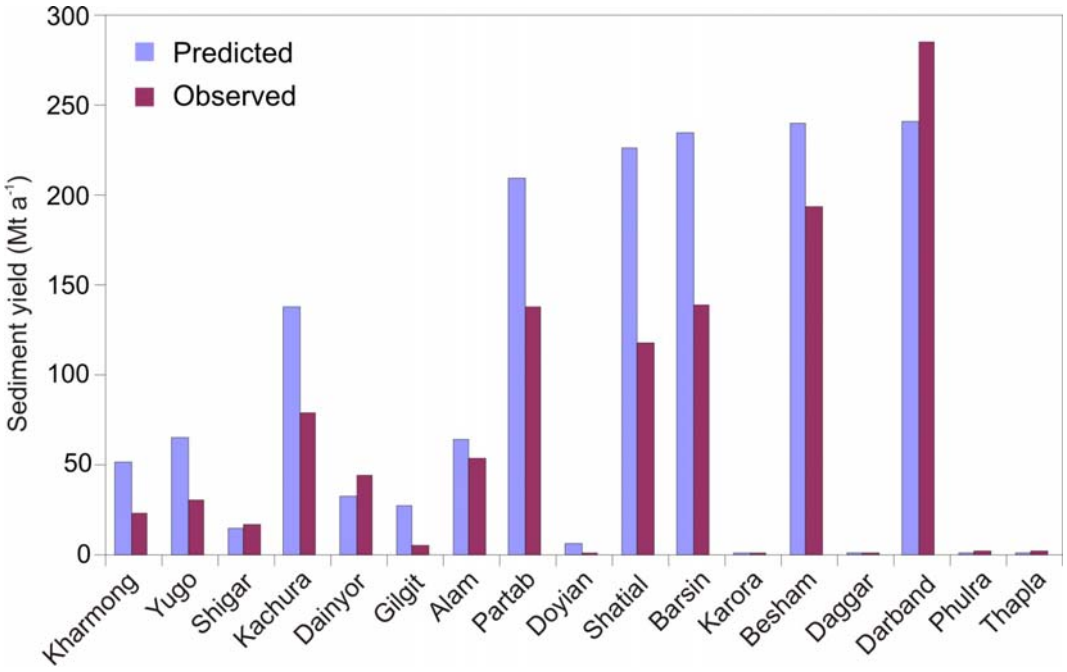

Figure 4.12 Comparison of predicted and observed sub-basin sediment yields in the upper Indus River basin

4.7.9 Relationship Between Sediment Delivery Ratio and Basin Size

Ferro *et al*. (2003) found a strong inverse correlation between basin sediment delivery ratio and basin area for 6 Sicilian basins. This relationship was also investigated for the upper Indus sub-basins in this study, but instead a general trend of increasing sediment delivery ratios with basin area is found for larger sub-basins (>50,000 km^2) (Figure 4.13). Although this trend is contrary to the conventional sediment delivery ratio model, it is consistent with the findings of Ali and De Boer (2007) who discovered a trend of increasing specific sediment yields with drainage area. This follows the same pattern observed by Church and Slaymaker (1989) in British Columbia, De Boer and Crosby (1996) in southeastern prairie region of Saskatchewan, and *Schiefer et al*. (2001) in the Canadian Cordillera. Church *et al*. (1989) attributed the

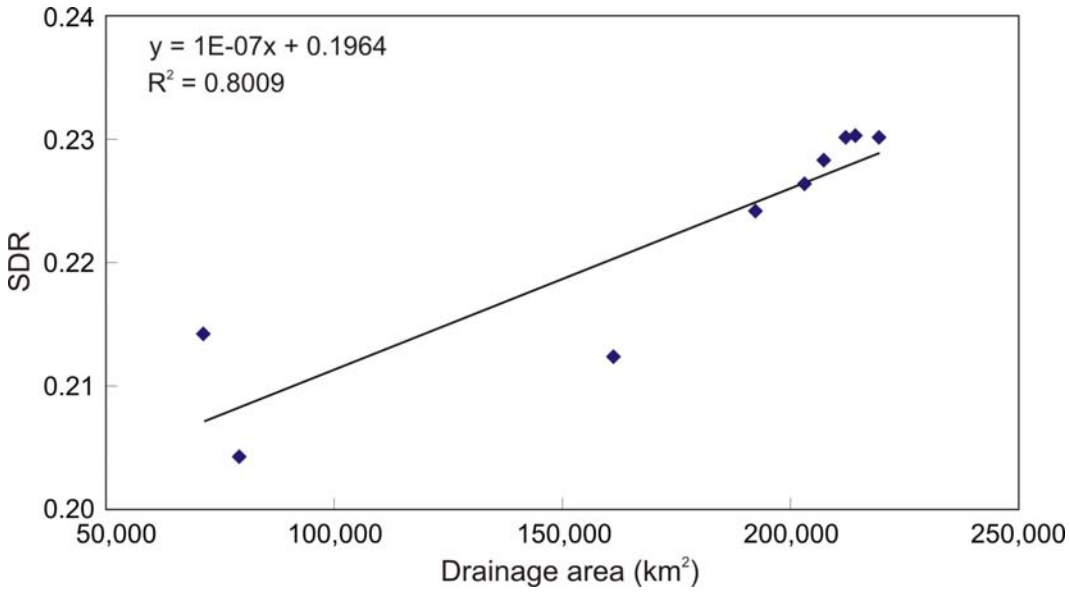

Figure 4.13 Relationship between drainage area and SDR for major Indus basin sub-basins (>50,000 km^2)

increasing specific sediment yields to the dominance of secondary remobilization of Quaternary sediments from stream banks and valley bottom areas over primary denudation of the land surface. Ali and De Boer (2007) explained this increase in specific sediment yields along the Indus River in terms of the predominance of steep straight channels discharging directly into the Indus River.

4.8 Conclusions

This study has presented a modeling framework for predicting large drainage basin scale spatially distributed erosion and sediment yields in the mountainous upper Indus River basin by coupling models of erosion and sediment delivery. Potential erosion rates were calculated by using the Thornes model in combination with a surface runoff model using global environmental

datasets in a GIS environment at a 1-km spatial resolution and a monthly time scale. Predicted erosion rates are consistent with landscape characteristics including slope, altitude and runoff. 87% of the gross annual erosion takes place in the three summer months, following a similar pattern of distribution in the sediment yields of the basin. The large proportion of the basin area experiencing high erosion rates is representative for a large Himalayan basin with exceptional relief and extreme climatic conditions. Lower erosion rates on the Tibetan Plateau can be explained by the arid climate and low relief, and in the lower monsoon sub-region by the dense vegetation and low relief. Analysis of the erosion rates and basin properties reveals that high erosion rates in the basin are associated with high relief, runoff, and low vegetation cover. The model predicts an average annual erosion rate of 3.2 mm a^{-1} for the upper Indus basin which is consistent with other reported values. Total erosion in the basin is calculated as 868 Mt a^{-1}, which is approximately 4.5 times the long-term observed sediment yield of the basin. Although the semi-quantitative validation approach suggests the spatial patterns of predicted erosion to be reliable, quantitative prediction should be interpreted with caution. For obtaining more accurate erosion estimates, a need of finer resolution datasets, consideration of a wider range of processes, and availability of more field data is emphasized.

Higher delivery ratios (SDR>0.6) are found in 18% of the upper Indus basin area, mostly located in the high-relief sub-basins. The sediment delivery ratio is lower than 0.2 in 70% of the basin area, mostly found in the low-relief, flat-terrain sub-basins located on the Tibetan Plateau, and some portions of the lower monsoon region. The Indus basin shows a general increase in sediment delivery ratios with the basin area. Although this trend is contrary to the conventional sediment delivery ratio model, it is consistent with the findings of Ali and De Boer (2007) who

found a trend of increasing specific sediment yields with drainage area in the basin. The mean annual sediment yield of the upper Indus River basin was calculated as 244 Mt a^{-1}, which compares reasonably to the observed sediment yield of the basin. The ratio of the predicted basin sediment yield and the gross basin erosion result in a basin sediment delivery ratio of 0.28. Model evaluation based on accuracy statistics shows "very good" to "satisfactory" performance ratings for predicted monthly and sub-basin sediment yields. The results in this study are based on modeling without calibration and it is envisaged that calibrating model parameters would greatly improve model accuracy.

Satisfactory sediment yield predictions have been made by using the proposed low-data demanding, spatially distributed modeling framework in the large, data-sparse, high mountainous upper Indus River basin, and a better understanding of the basin-wide sediment dynamics has been achieved that can be utilized in constructing a detailed sediment budget for the basin (Ali and De Boer, 2003). The modeling framework presented in this study is based on physiographic characteristics of the basin, and hence it can be used for the estimation of sediment yield in other ungaged drainage basins which have similar hydro-meteorological, topographical and land use conditions.

4.9 Notation

β a catchment specific parameter after Ferro and Minacapilli (1995)
c_i fraction of vegetation cover for the cell for time period i, %
D_i number of precipitation days for the cell for time period i
E basin gross erosion, t km^{-2} a^{-1}
E_i erosion rate for the cell for time period i, mm month^{-1}
ET_{i-1} potential evapotranspiration for the cell for the preceding time period $i–1$, mm
i time period (from 1 to 12 for months)
k soil erodibility coefficient for the cell
l_p flow path length for cell p, m
m total number of cells along a flow path
$NDVI_i$ the Normalized Difference Vegetation Index for the cell for time period i
NSE Nash-Sutcliffe efficiency
p a cell along flow path
P_i total precipitation for the cell for time period i, mm
P_{i-1} total precipitation for the cell for the preceding time period $i–1$, mm
$PBIAS$ percent bias, %
rc potential water storage capacity, mm
RO_i surface runoff for the cell for time period i, mm
RO_{i-1} surface runoff for the cell for the preceding time period $i–1$, mm
RSR ratio of the root mean square error to the standard deviation of measured data
s slope for the cell, m m^{-1}
s_p slope for cell p, m m^{-1}
S_i total initial soil moisture for the cell for time period i, mm
S_{i-1} total initial soil moisture for the cell for the preceding time period $i–1$, mm
SDR sediment delivery ratio for catchment cell
SY basin sediment yield, t km^{-1} a^{-1}
SY_i sediment yield for the cell for the time period i, t km^{-2} month^{-1}
SY_T basin sediment yield for given time period i, t km^{-2} month^{-1}
t travel time of the surface runoff from the cell to the nearest channel, hrs

4.10 References

Ahmad, N. (1993), *Water Resources of Pakistan and Their Utilization.* Shahid Nazir, Lahore, Pakistan.

Ali, K. F., and D. H. De Boer (2003), Construction of sediment budgets in large scale drainage basins: the case of the upper Indus River, in *Erosion Prediction of Ungauged Basins (PUBs): Integrating Methods and Techniques*, edited by D. H. De Boer et al., *IAHS Publ*., *279*, 206–215.

Ali, K. F., and D. H. De Boer (2007), Spatial patterns and variation of suspended sediment yield in the upper Indus River basin, northern Pakistan, *J. Hydrol.*, *334*, 368–387, doi: 10.1016/j.hydrol.2006.10.013.

Ali, K. F., and D. H. De Boer (2008), Factors controlling specific sediment yield in the upper Indus River basin, northern Pakistan, *Hydrol. Processes*, *22*, 3102–3114, doi: 10.1002/hyp.6896.

Bhutiyani, M. R. (2000), Sediment load characteristics of a proglacial stream of Siachen Glacier and the erosion rate in Nubra valley in the Karakoram Himalayas, India, *J. Hydrol.*, *227*, 84–92.

Bogen, J., and T.E. Bønsens (2003) Erosion prediction in ungauged glacierized basins. In *Erosion Prediction in Ungauged Basins: Integrating Methods and Techniques*. Proceedings of symposium held during IUGG2003 at Sapporo. IAHS Publ. *279*, 13-23.

Burbank, D. W., J. Leland, E. Fielding, R. S. Anderson, N. Brozovic, M. R. Reid, and C. Duncan (1996), Bedrock incision, rock uplift and threshold hillslopes in the northwestern Himalayas, *Nature*, *379*, 505–510.

Church, M., and O. Slaymaker (1989), Disequilibrium of Holocene sediment yield in glaciated British Columbia, *Nature*, *337*, 452–454.

Church, M., R. Kellerhals, and T. J. Day (1989), Regional clastic sediment yield in British Columbia, *Can. J. Earth Sci*., *26*, 31–45.

Collins, D. N., and S. I. Hasnain (1995), Runoff and sediment transport from glacierized basins at the Himalayan scale, in *Effects of Scale on Interpretation and Management of Sediment and Water Quality*, edited by W. R. Osterkamp, *IAHS Publ*., *226*, 17–25.

Cornwell, K., D. Norsby, and R. Marston (2003), Drainage, sediment transport, and denudation rates on the Nanga Parbat Himalaya, Pakistan, *Geomorphology*, *55*, 25–43.

De Boer, D. H., and G. Crosby (1996), Suspended sediment yield and drainage basin scale, in *Erosion and Sediment Yield: Global and Regional Perspective*, edited by D. E. Walling and B. W. Webb, *IAHS Publ*., *236*, 333–338.

Drake, N. A., X. Zhang, E. Berkhout, R. Bonifacio, D. Grimes, J. Wainwright, and M. Mulligan (1999), Modelling soil erosion at global and regional scales using remote sensing and GIS techniques, in *Advances in Remote Sensing and GIS Analysis*, edited by P. Atkinson and N. J. Tate, pp. 241–262, John Wiley, New York.

Edwards, T. K., and G. D. Glysson (1999), *Field Methods for Measurement of Fluvial Sediment*, U.S. Geological Survey, TWI 3-C2.

Ferguson, R. I. (1984), Sediment load of the Hunza River, in *The International Karakoram Project*, edited by K. J. Miller, pp. 580–598, Cambridge University Press, Cambridge.

Ferro, V., and M. Minacapilli (1995), Sediment delivery processes at basin scale, *Hydrol. Sci. J.*, *40*(6), 703–717.

Ferro, V., and P. Porto (2000), Sediment delivery distributed (SEDD) model, *J. Hydrol. Engng.*, *5*(4), 411–422.

Ferro, V., C. Di Stefano, M. Minacapilli, and M. Santoro (2003), Calibrating the SEDD model for Sicilian ungauged basins, in *Erosion Prediction in Ungauged Basins (PUBs): Integrating Methods and Techniques*, edited by D. H. De Boer et al., *IAHS Publ*., *279*, 151–161.

Fuller, C. W., S. D. Willett, N. Hovius, and R. Slingerland (2003), Erosion rates for Taiwan Mountain basins: New determinations from suspended sediment records and a stochastic model of their temporal variation, *J. Geol.*, *111*, 71–87.

Galy, A., and C. France-Lanord (2001), Higher erosion rates in the Himalaya: Geochemical constraints on riverine fluxes, *Geology*, *29*(1), 23–26.

Gardner, J. S., and N. K. Jones (1993), Sediment transport and yield at the Raikot Glacier, Nanga Parbat, Punjab Himalaya, in *Himalaya to the Sea: Geology, Geomorphology, and the Quaternary*, edited by J. F. Shroder, pp. 184–197, Routledge, London..

Garzanti, E., G. Vezzoli, S. Andò, P. Paparella, and P. D. Clift (2005), Petrology of Indus River sands: a key to interpret erosion history of the Western Himalayan Syntaxis, *Earth and Planetary Science Letters*, *229*, 287–302.

Golosov, V. (2002), Temporal-spatial variations in the sediment delivery ratio of small drainage basins: the Russian Plain example, in *The Structure, Function and Management Implications of Fluvial Sedimentary Systems*, edited by F.J. Dyer et al., pp. 345–353. *IAHS Publ*., 276.

Gupta, H. V., S. Sorooshian, and P. O. Yapo (1999), Status of automatic calibration for hydrologic models: Comparison with multilevel expert calibration, *J. Hydrologic Eng.*, *4*(2), 135–143.

Gurnell A., Hannah D., Lawler D. (1996) Suspended sediment yield from glacier basins. In *Erosion and Sediment Yield: Global and Regional Perspective*, Walling D.E., Webb B.W. (Eds.) IAHS Publication No. 236. IAHS Press, Wallingford, 97-104.

Hallet, B., L. Hunter, and J. Bogen (1996), Rates of erosion and sediment evacuation by glaciers: A review of field data and their implications, *Global and Planetary Change*, *12*, 213–235.

Haritashya, U. K., P. Singh, N. Kumar, and R. P. Gupta (2006), Suspended sediment from the Gangotri Glacier: Quantification, variability and associations with discharge and air temperature, *J. Hydrol.*, *321*, 116–130.

ISRIC (2008), International Soil and Reference Information Centre (ISRIC), http://www.isric.nl.

IWMI (2008), IWMI World Water and Climate Atlas, http://www.iwmi.cgiar.org.

Jain, M. K., and U. C. Kothyari (2000), Estimation of erosion and sediment yield using GIS, *Hydrol. Sci. J.*, *45*(5), 771–786.

Jain, S. K., S. Kumar, and J. Varghese (2001), Estimation of Soil Erosion for a Himalayan Watershed Using GIS Technique, *Water Resources Management*, *15*, 41–54.

Jain, S. K., P. K. Agarwal, and V. P. Singh (2007), *Hydrology and Water Resources of India*, Springer, Dordrecht.

Jetten, V., G. Govers, and R. Hessel (2003), Erosion models: quality of spatial predictions, *Hydrol. Processes*, *17*, 887–900.

Kothyari, U. C., M. K. Jain, and K. G. Ranga Raju (2002), Estimation of temporal variation of sediment yield using GIS, *Hydrol. Sci. J.*, *47*(5), 693–706.

Lane, L. J., M. Hernandez, and M. Nichols (1997), Processes controlling sediment yield from watersheds as functions of spatial scale, *Environmental Modelling and Software*, *12*(4), 355–369.

Lave, J., and J. P. Avouac (2000), Active folding of fluvial terraces across the Siwaliks Hills, Himalayas of central Nepal, *J. Geophys. Res.*, *B105*, 5735–5770.

Legates, D. R., and G. J. McCabe (1999), Evaluating the use of "goodness-of-fit" measures in hydrologic and hydroclimatic model validation, *Water Resour. Res.*, *35*(1), 233–241.

Leland, J., M.R. Reid, D.W. Burbank, R. Finkel and M. Caffee (1998) Incision and differential bedrock uplift along the Indus River near Nanga Parbat, Pakistan Himalaya, from ^{10}Be and ^{26}Al exposure age dating of bedrock straths. Earth and Planetary Science Letters, 154, 93–107.

Lu, X. X., and D. L. Higgitt (1999), Sediment yield variability in the Upper Yangtze, China, *Earth Surf. Processes and Landforms*, *24*, 1077–1093.

Lu, H., C. J. Moran, and I. P. Prosser (2006), Modelling sediment delivery ratio over the Murray Darling Basin, *Environmental Modelling & Software*, *21*, 1297–1308.

Marston, R. A. (2008), Land, life, and environmental change in mountains, *Annals of the Association of American Geographers*, *98*(3), 507–520.

Meadows, A., and P. S. Meadows (Eds.) (1999), *The Indus River: Biodiversity, Resources, Humankind*, Oxford University Press, Karachi, Pakistan.

Miller, K. J. (Ed.) (1984), *The International Karakoram Project*, Cambridge University Press, Cambridge.

Molnar, P., and P. Tapponnier (1975), Cenozoic tectonics of Asia: Effects of a continental collision, *Science*, *189*, 419–426.

Moriasi, D. N., J. G. Arnold, M. W. Van Liew, R. L. Bingner, R. D. Harmel, and T. Veith (2007), Model evaluation guidelines for systematic quantification of accuracy in watershed simulations, *Transactions of the ASABE, 50*, 885–900.

Nash, J. E., and J. V. Sutcliffe (1970), River flow forecasting through conceptual models: Part 1. A discussion of principles. *J. Hydrol*., *10*(3), 282–290.

NEAC Consultants (2004), *Feasibility Study of the Basha Diamer Dam Hydropower Project*, Lahore, Pakistan.

Nearing, M. A., M. J. M. Romkens, L. D. Norton, D. E. Stott, F. E. Rhoton, J. M. Laflen, D. C. Flanagan, C. V. Alonso, R. L. Binger, S. M. Dabney, O. C. Doering, C. H. Huang, K. C. McGregor, and A. Simon (2000), Measurements and models of soil loss rates, *Science*, *290*, 1300–1301.

Parsons, A. J., J. Wainwright, D. M. Powell, J. Kaduk, and R. E. Brazier (2004), A conceptual model for understanding and predicting erosion by water, *Earth Surface Processes and Landforms*, *29*, 1293–1302.

Parsons, A. J., J. Wainwright, R. E. Brazier, and D. M. Powell (2006) Is sediment delivery a fallacy?, *Earth Surface Processes and Landforms*, *31*, 1325–1328.

Phillips, J. D. (1991), Fluvial sediment delivery to a Coastal Plain estuary in the Atlantic Drainage of the United States, *Marine Geology*, *98*, 121–134.

Pistocchi, A. (2008), An assessment of soil erosion and freshwater suspended solid estimates for continental-scale environmental modelling, *Hydrol. Processes*, *22*, 2292–2314.

Prosser, I. P., I. D. Rutherfurd, J. M. Olley, W. J. Young, P. J. Wallbrink, and C. J. Moran (2001), Large-scale patterns of erosion and sediment transport in river networks, with examples from Australia, *Marine and Freshwater Research*, *52*, 81–99.

Purevdorj, T., R. Tateishi, T. Ishiyama, and Y. Honda (1998), Relationships between percent vegetation cover and vegetation indices, *Int. J. Remote Sens.*, *19*, 3519–3535.

Rantz, S. E., and others (1982), *Measurement and Computation of Streamflow - Volume 1. Measurement of Stage and Discharge*, U. S. Geological Survey Water-Supply Paper 2175.

Ritter, D. F., R. C. Kochel, and J. R., Miller (2002), *Process Geomorphology*, McGraw-Hill, New York.

Saavedra, C. (2005), Estimating spatial patterns of soil erosion and deposition in the Andean region using geo-information techniques: A case study in Cochabamba, Bolivia. ITC Dissertation Number: 128, International Institute for Geo-Information Science and Earth Observation Enschede, The Netherlands.

Saavedra, C., and C. M. Mannaerts (2005), Erosion estimation in an Andean catchment combining coarse and fine resolution satellite imagery, in *Proceedings of the 31st International Symposium on Remote Sensing of Environment*, June 20–24, 2005, Saint Petersburg, Russian Federation.

Schiefer, E., O. Slaymaker, and B. Klinkenberg (2001), Physiographically controlled allometry of specific sediment yield in the Canadian Cordillera: A lake sediment based approach, *Geografiska Annaler Series A: Physical Geography*, *83*(1-2), 55–65.

Searle, M. P. (1991), *Geology and Tectonics of the Karakoram Mountains*, Wiley, New York.

Shroder, J. F. (Ed.) (1993), *Himalaya to the Sea: Geology, Geomorphology and the Quaternary*, Routledge, Chichester.

Smith, H. G. (2008), Estimation of suspended sediment loads and delivery in an incised upland headwater catchment, south-eastern Australia, *Hydrol. Processes*, *22*, 3135–3148, doi: 10.1002/hyp.6898.

Stefano, C. D., V. Ferro, P. Porto, and S. Rizzo (2005), Testing spatially distributed sediment delivery model (SEDD) in a forested basin by cesium-137 technique, *J. Soil Wat. Cons.*, *60*(3), 148–157.

Stone, R. P., and D. Hilborn (2000), Universal Soil Loss Equation (USLE), Ontario Ministry of Agriculture, Food and Rural Affairs Factsheet, http://www.omafra.gov.on.ca/english/engineer/facts/00-001.htm.

Summerfield, M. (1991) *Global Geomorphology*. Prentice Hall Inc., Upper Saddle River, New Jersey 07458

Symeonakis, E., A. Calvo-Cases, and E. Arnau-Rosalen (2007), Land Use Change and Land Degradation in Southeastern Mediterranean Spain, *Environ. Manage.*, *40*, 80–94, doi: 10.1007/s00267-004-0059-0.

TDP (2002), *Reservoir Sedimentation Report 1999*, Survey and Hydrology, Tarbela Dam Project (TDP), Tarbela, Pakistan.

Thornes, J. B. (1985), The ecology of erosion, *Geography*, *70*, 222–234.

Thornes, J. B. (1990), The interaction of erosional and vegetational dynamics in land degredation: spatial outcomes, in *Vegetation and Erosion: Processes and Environments*, edited by J. B. Thornes, pp. 41–53, Wiley, Chichester.

Trimble, S.W. (1977), The fallacy of stream equilibrium in contemporary denudation studies, *Am. J. Sci.*, *277*, 876–887.

Trimble, S. W., (1999), Decreased rates of alluvial sediment storage in the Coon Creek basin, Wisconsin, 1975–93, *Science*, *285*, 1244–1246.

Tucker, C. J. (1979), Red and photographic infrared linear combinations for monitoring vegetation, *Remote Sens. Environ*., *8*, 127–150.

USGS (2008a), EROS Data Centre: Elevation Products, http://edc.usgs.gov/products/elevation.html.

USGS (2008b), Global AVHRR 10-day composite data, http://edc2.usgs.gov/1KM/comp10d.php.

Vance, D., M. Bickle, S. Ivy-Ochs, and P. W. Kubik (2003), Erosion and exhumation in the Himalaya from cosmogenic isotope inventories of river sediments, *Earth and Planetary Science Letters*, *206***,** 273–288.

Wainwright, J., A. J. Parsons, D. M. Powell, R. E. Brazier, (2001), A new conceptual framework for understanding and predicting erosion by water from hillslopes and catchments, in *Soil Erosion Research for the 21st Century. Proceedings of the International Symposium*, edited J. C. Ascough II and D. C. Flanagan, pp. 607–610, American Society of Agricultural Engineers, St Joseph, MI.

Wainwright, J., A. J. Parsons, E. N. Müller, R. E. Brazier, D. M. Powell and B. Fenti (2008), A transport-distance approach to scaling erosion rates: 1. background and model development, *Earth Surface Processes and Landforms*, *33*, 813–826.

Wilkinson, S., A. Henderson, Y. Chen, and B. Sherman (2004), SedNet User Guide, Version 2. Client Report, CSIRO Land and Water, Canberra. www.toolkit.net.au/sednet.

Wilkinson, S. N., I. P. Prosser and A. O. Hughes (2006), Predicting the distribution of bed material accumulation using river network sediment budgets, *Water Resources Research*, *42*, W10419.

Wall, G. J., D. R. Coote, E. A. Pringle, and I. J. Shelton (Eds.) (1997), *RUSLEFAC, Revised Universal Soil Loss Equation for Application in Canada*, Agriculture and Agri-Food Canada, Ottawa. http://sis.agr.gc.ca/cansis/publications/manuals/ruslefac2.pdf

Walling, D.E. (1983), The sediment delivery problem, *J. Hydrol.*, *65*, 209–237.

Walling, D. E., and B. W. Webb (1996), Erosion and sediment yield: a global overview, in *Erosion and Sediment Yield: Global and Regional Perspective*, edited by D. E. Walling and B. W. Webb, *IAHS Publ.*, *236*, 73–84.

Wang, Z. -Y., Y. Li, and Y. He (2007), Sediment budget of the Yangtze River, *Water Resour. Res.*, *43*, W04401, doi: 10.1029/2006WR005012.

Wasson, R.J. (2003), A sediment budget for the Ganga–Brahmaputra catchment, *Current Science*, *84*(8), 1041–1047.

Xu, J., and D. Cheng (2002), Relation between the erosion and sedimentation zones in the Yellow River, China, *Geomorphology*, *48*, 365–382.

Yang, D., S. Kanae, T. Oki, T. Koike, and K. Musiake (2003), Global potential soil erosion with reference to land use and climate changes, *Hydrol*. *Processes*, *17*, 2913–2928

Zhang, X., N. Drake, and J. Wainwright (2002), Scaling land surface parameters for global-scale soil erosion estimation, *Water Resour*. *Res*., *38*(9), 1180, doi: 10.1029/2001WR000356.

CHAPTER 5 – CONSTRUCTION OF A SEDIMENT BUDGET FOR THE UPPER INDUS RIVER BASIN

5.1 Abstract

High rates of soil loss and high sediment loads in rivers necessitate efficient monitoring and quantification methodologies so that effective land management strategies can be designed. Constructing a sediment budget is a useful approach to address these issues. Quantifying a sediment budget using classical field-based techniques is labor intensive, time-consuming and expensive for poorly gauged, large drainage basins. The availability of global environmental datasets in combination with GIS and remote sensing techniques provides an opportunity for studying large basins, and identifying and quantifying the contribution of potential sediment source areas. Following this approach, a framework is presented for constructing sediment budgets for large, data-sparse drainage basins, which is applied to the mountainous upper Indus River basin in northern Pakistan. Sediment source contributions and rates of deposition have been determined based on the analysis of hydrological data, multiple regression analysis, and spatially distributed modelling of erosion and sediment yields in the basin. The long-term mean annual sediment budget, based on mass balance, is characterized by a gross erosion of 762.9, 96.7 and 8.4 Mt and a gross storage of 551.4, 66.1, and 6.5 Mt in the upper, middle, and lower regions of the basin, respectively. The sediment budget indicates that the major sources of eroded sediment are located in the Karakoram, in particular the Hunza basin. Substantial sediment

storage occurs throughout the basin, in particular on the relatively flat Tibetan Plateau and the Indus River valley reach between Partab Bridge and Shatial. The sediment budgeting framework presented in this study has low data requirements and it is therefore useful for large data sparse drainage basins.

5.2 Introduction

Sediments budgets are a useful and powerful conceptual framework for examining the relationships between sources, sinks, fluvial transport and sediment yield, and investigating how these relationships are affected by changes in land use, climate, seismicity and isostatic adjustment (Wasson, 2002). Reid and Dunne (1996, p. 3) have defined a sediment budget as "an accounting of the sources and disposition of sediment as it travels from its point of origin to its eventual exit from a drainage basin." A detailed sediment budget accounts for rates and processes of erosion and sediment transport on hillslopes and in channels, for temporary storage of sediment, and for weathering of sediment while in transport or storage (Dietrich *et al*., 1982). The sediment budget equation in the form:

$$I = O + \Delta S \tag{5.1}$$

where I is input, O is output, and ΔS is the change of storage, can describe the routing of clastic and dissolved sediment over a specified time increment and with respect to a particular storage reservoir (Slaymaker, 1993).

Sediment budget studies have mostly dealt with relatively small drainage basins ranging from a few hectares to a few hundred square kilometers (Phillips, 1991). This is due to the expense and logistical problems associated with the construction of sediment budgets for large river basins, which pose quite a few challenges, including identification and quantification of sediment source areas, measurement of river loads, and data sparsity. Field-based studies of sediment budgets are frequently hampered by the limited availability of data, both in terms of quality and quantity, which raises the question of the representativeness of the dataset for larger or smaller basins over longer periods of time (De Boer and Ali, 2002). Integration of GIS and remote sensing has emerged as a useful tool for studying large basins (e.g. Lu and Higgitt, 1999; Gupta *et al*., 2002) and it provides new insights in constructing sediment budgets (Wasson, 2002). The emerging GIS and remote sensing techniques in combination with historic hydrological records can prove to be very useful for sediment budget studies (Ali and De Boer, 2003; Ramos-Scharrón and MacDonald, 2007; Rustomji *et al*., 2008). Following this approach, the overall objective of this study is to develop a framework for constructing sediment budgets in large data-sparse drainage basins and to apply it to the mountainous upper Indus River basin in Northern Pakistan.

5.3 The Upper Indus River Basin and Sediment Budgeting Issues

The Indus River is one of the longest rivers in southern Asia (Ahmad, 1993; Meadows and Meadows, 2000; Clift, 2002), with a total length of 2880 km and a drainage area of 912,000 km^2 extending across portions of Pakistan, India, China and Afghanistan (Figure 5.1). The upper Indus basin upstream of Tarbela Dam is 1125 km long, with a drainage area of 219,830 km^2.

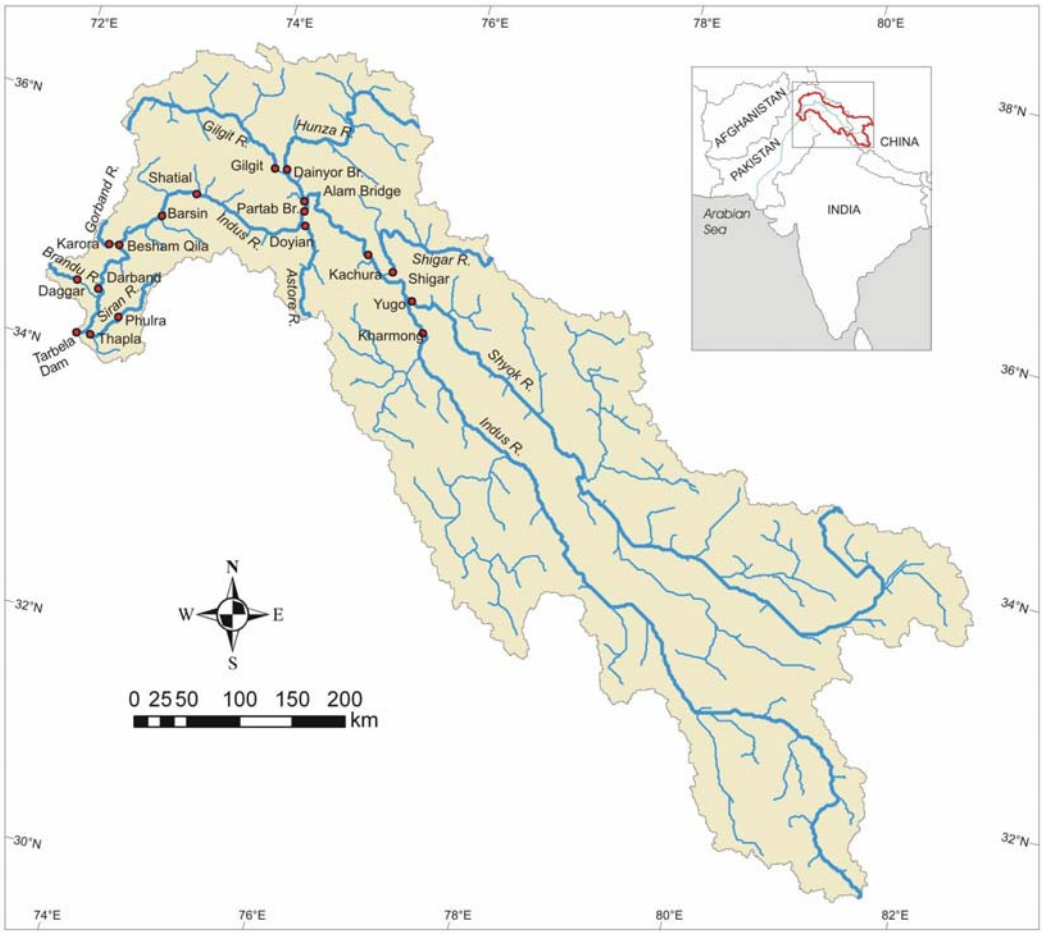

Figure 5.1 The upper Indus River basin

The Indus River rises in the Tibetan Plateau at an elevation of 5486 m on Mount Kailash (Jain *et al*., 2007), follows a well-defined valley parallel to the geologic strike, and descends down to the Arabian Sea. Much of its flow originates in the mountains of the Karakoram and Himalayas. The major Indus tributaries include the Shyok, Shigar, and Gilgit in the upper, glacierized portion; the Astore in the middle reaches; and the Gorband, Brandu, and Siran in the lower, monsoon-affected portion. Major tectonic activity, culminating in the Himalayan orogeny during the mid-Eocene, has shaped the high relief and complex geologic structures observed in the upper Indus basin today (Molnar and Tapponnier, 1975; Miller, 1984). These young mountain ranges of

extreme ruggedness and high elevations are subject to exceptionally rapid degradation by a combination of processes (Searle, 1991; Shroder, 1993, Collins and Hasnain, 1995). The lower, southern part of the basin experiences heavy monsoon rainfall, and rivers in this part of the basin carry large amounts of sediment associated with flash floods. Ali and De Boer (2007) provide a detailed account of the physiography, geology and tectonics, and climate of the basin. The upper Indus represents a unique high mountainous data-sparse large river basin that still exists in its natural condition without any major human impacts and it has not received much attention in the past. In view of recent energy and water crisis in Pakistan where most of the planned water storage and hydro power projects are located in the upper Indus basin, a sediment budget study is timely and desirable.

The sediment budget for the upper Indus River would differ from a downstream river reach type budget like Kesel *et al*. (1992) for the lower Mississippi River, Shi and Zhang (2005) for the lower Yellow River, and Rovira *et al*. (2005) for the lower Tordera River in northeastern Spain. Lower river reaches are characterized by floodplains and river deltas representing major sediment sinks in many drainage basins, and major load transported as bed load. For example Rovira *et al*. (2005) found that 80% of the total load was transported as bed load and only 20% suspended load, whereas only 10–15% is assumed to be transported as bed load for the upper Indus River. A typical basin scale sediment budget would include a number of functional units to investigate the sediment fluxes and for constructing the sediment budget (Rondeau *et al*., 2000). Typically, a river basin can be divided into sections with the upper and middle reaches of the river as the sediment source, and the lower reaches, the delta, and the deep sea as sediment sinks. Kesel *et al.* (1992) partitioned the locations for sediment storage into three categories; the

floodplain, the river channel, and the water column. By contrast, there are few floodplain features along in the upper Indus River where channels are relatively straight and steep; so that there is very little point bar deposition and channel storage.

5.4 Data Sources and the Methodological Framework

Sediment budget construction requires a clear understanding of sediment dynamics in the drainage basin. To gain this understanding, this study has utilized multiple data types and sources including the available hydrological records, erosion rates in the basin compiled from literature, and the recent work in the Indus basin by Ali and De Boer (2007; 2008; in review). Apart from some long-term discharge records for the main Indus River and some of its major tributaries, hydrological data for the upper Indus River basin are very scarce. Long-term, continuous discharge and occasional suspended sediment concentration data are available for only 17 active and discontinued gauging stations in the basin (Figure 5.1). Ali and De Boer (2007) have compiled and processed this database, and calculated mean monthly and mean annual sediment yields by establishing suspended sediment rating curves for all stations. Hydrographic surveys of the Tarbela Reservoir have been carried out on a yearly basis, providing vital information on the storage of sediment at the outlet of the basin. This information has been used for balance calculation at the basin outlet and for checking the results of the sediment budget. Ali and De Boer (2008) have investigated factors affecting specific sediment yields in the basin and have developed multiple regression models for estimating specific sediment yields in the upper Indus River basin. Moreover, Ali and De Boer (in review) have made spatially distributed predictions of erosion and sediment yield in the basin, and the results from these studies have also been used

in constructing the sediment budget.

A simplified methodological framework for constructing a long-term mean annual sediment budget for the upper Indus River is presented in Figure 5.2. This is based on a mass balance approach and consists of analyzing the amount of sediment contributed by different tributaries, on a watershed-by-watershed basis. The methodology presented in this study consists of five

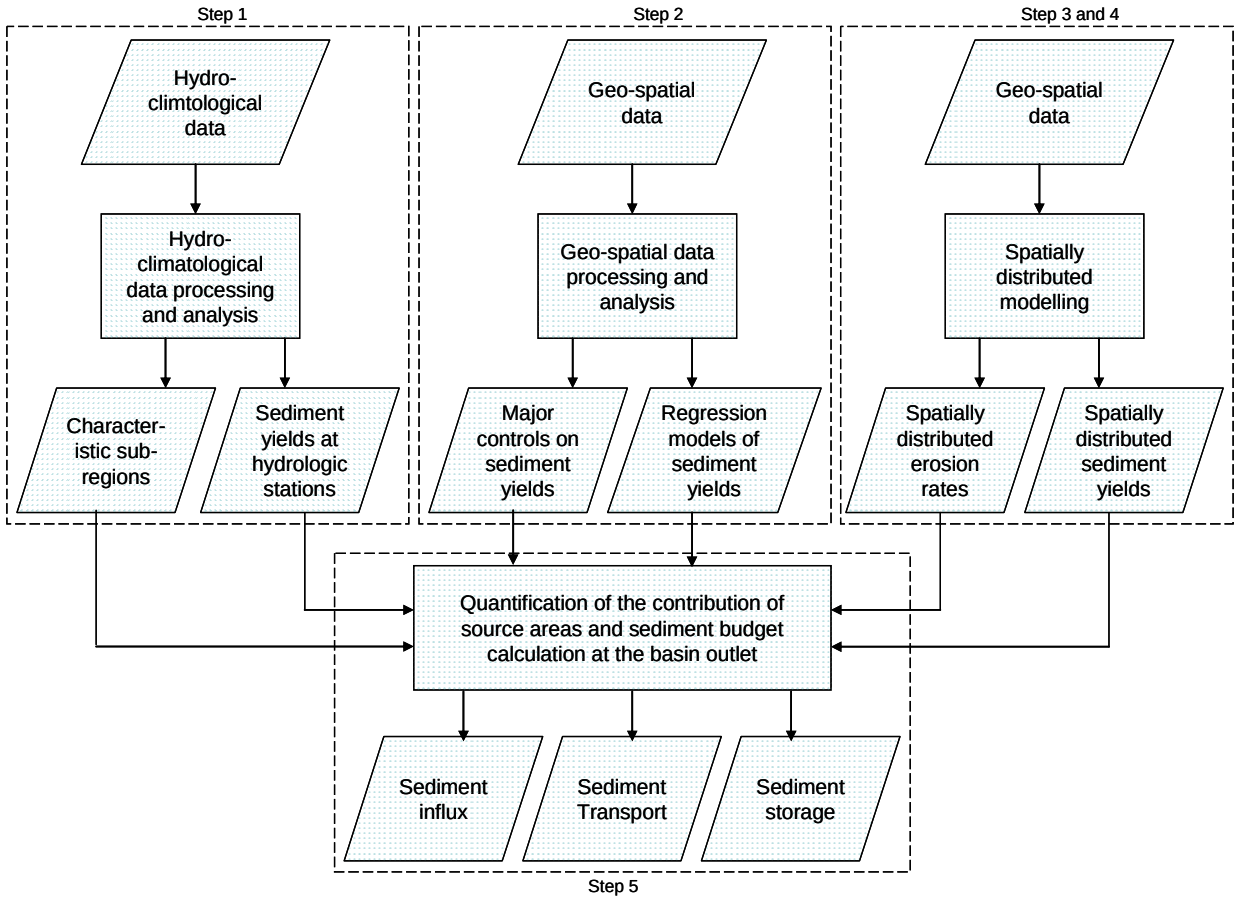

Figure 5.2 Simplified methodological framework of sediment budget construction for the upper Indus River basin

steps: (1) Processing and analysis of the hydro-climatological database for dividing the drainage basin into characteristic regions and calculating sediment yields; (2) Investigation of major controls on sediment yield and constructing multiple regression models for predicting sediment yields; (3) Identification, mapping and quantification of sites that act as sources of sediment from spatially distributed modelling of erosion; (4) Spatially distributed modelling of sediment yield by coupling models of erosion and sediment delivery ratios; and (5) Carrying out the sediment budget balance calculation at the basin outlet based on a mass balance approach by analyzing the amount of sediment contributed by different tributaries, on a watershed-by-watershed basis.

5.5 Hydroclimatic Conditions of the Upper Indus River Basin

Analysis of the available hydro-climatological data by Ali and De Boer (2007) indicates that the upper Indus basin can be subdivided into three characteristic regions based on whether runoff production is controlled by temperature (Region 1, upper, glacierized sub-basins), precipitation caused by the monsoon and western disturbances (Region 3, lower sub-basins), or a combination of the two (Region 2, middle reach sub-basins). Figure 5.3 shows typical climate patterns for these three regions in terms of temperature and precipitation. Region 1 comprises the high elevation, glacierized areas of the Karakoram and the Himalayas located in the northernmost part of the basin. This region extends downstream to Partab Bridge on the Indus River, but does not include the areas around the Nanga Parbat massif. This region is very arid and receives little precipitation. The sediment transport regimes for the Shyok, Gilgit, Hunza and Indus Rivers in this region show the role of melting snow and ice in generating high runoff in the summer months, and a major portion of the annual sediment load is transported in summer months.

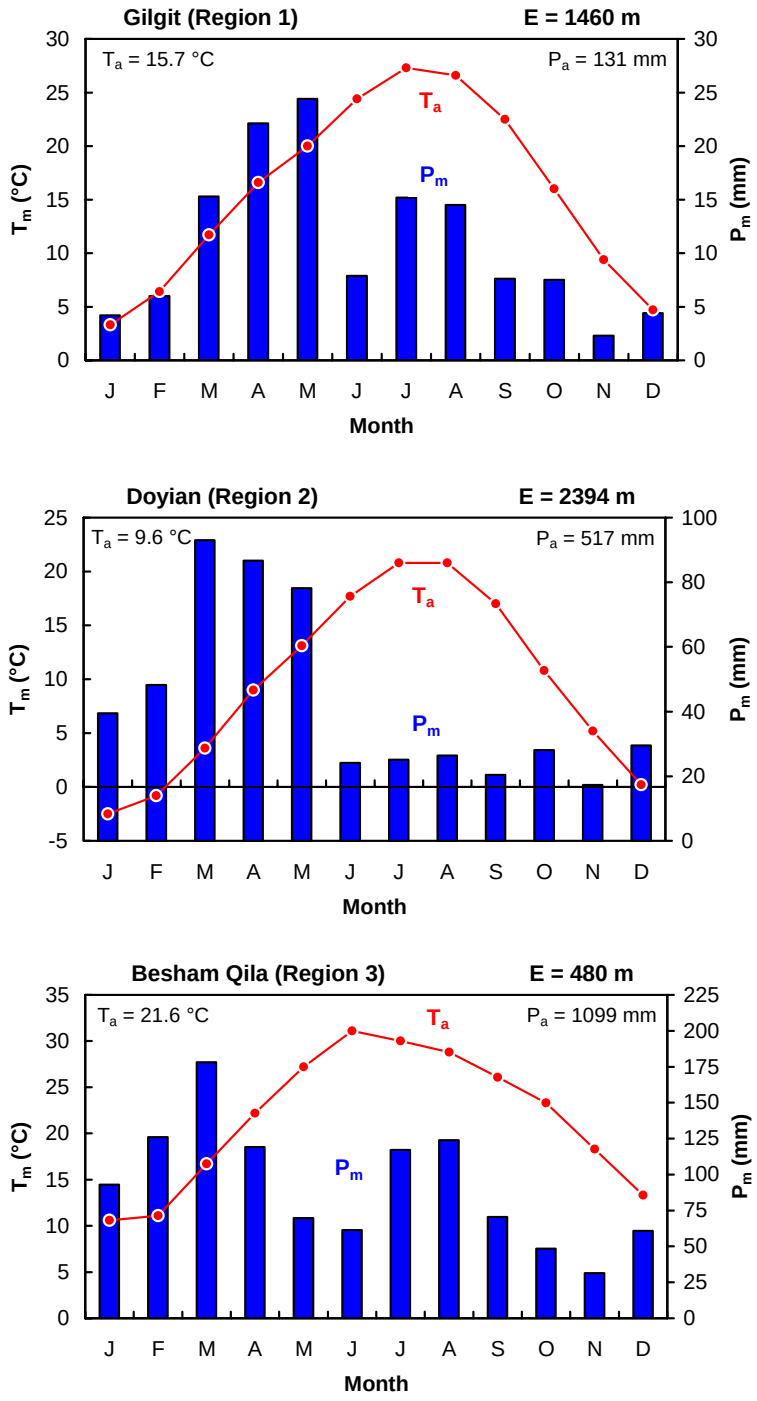

Figure 5.3 Monthly mean temperature, T_m, and monthly mean precipitation, P_m, for the three characteristic regions in the upper Indus River basin (E is elevation of the station, T_a is annual mean temperature, P_a is annual mean precipitation)

Region 2 extends from Partab Bridge to Besham Qila and comprises the area between the upper, glacierized portion of the basin and the lower, monsoon-affected area. The mean annual rainfall recorded in this region at Astore valley is 511 mm, and the seasonal pattern exhibits the influence of western disturbances in producing significant amounts of early spring rainfall. The highest specific discharges in the upper Indus basin are observed from the southeast flanks of Nanga Parbat, where monsoon rain and snowmelt interact and the Astore River at Doyian exhibits one of the highest specific discharges in this region of 1012 mm a^{-1}. The sediment transport regime is also controlled by the interaction of rainfall and lower-elevation snowmelt, which reflects the decreasing contribution of glacier-melt in generating runoff and sediment. Region 3 is the remaining, southernmost part of the basin, and includes the area between Besham Qila and Tarbela Dam. Three of the main tributaries in this region are the Gorband, Siran and Brandu Rivers. This part of the basin is mainly rainfed with little snow, and experiences two types of rainfall: summer monsoon rains, and late winter and early spring rainfall produced by disturbances coming from the west.

5.6 Erosion in the Upper Indus River Basin

A prime step in making a sediment budget for a drainage basin is to identify the processes mobilizing sediment, their controls, and quantifying the contribution from each erosional process (Lehre, 1982). Due to its remote location and lack of development, erosion measurements are very scarce in the upper Indus River basin. Ali and De Boer (in review) used the Thornes erosion model (Thornes, 1985; 1990) in combination with an overland flow sub-model, and calculated spatially distributed erosion rates in the upper Indus River basin at 1-km spatial resolution and

monthly time scales. With a predicted average annual erosion rate of 3.2 mm a^{-1}, gross erosion in the basin is calculated as 868 Mt a^{-1}. The erosion potential map (Figure 5.4) prepared by Ali and De Boer (in review) suggests that areas with the greatest erosion potential are concentrated in the

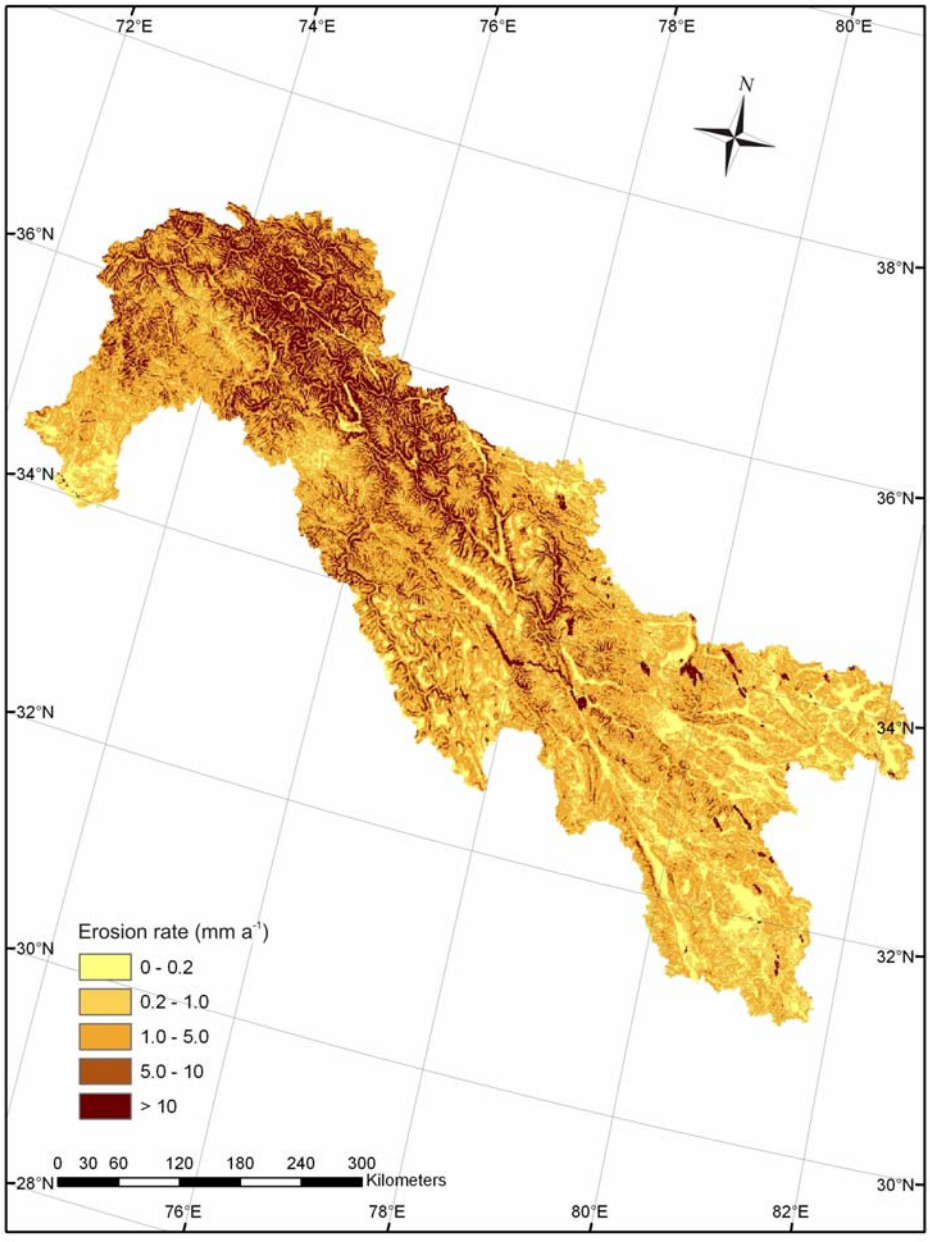

Figure 5.4 Spatial distribution of predicted annual erosion rates (after Ali and De Boer, in review)

sub-basins having a high relief and a substantial proportion of glacierized areas, such as the Hunza River basin, the Shigar River basin, and the areas around the Nanga Parbat Massif. Lower erosion rates can be explained by the arid climate and low relief on the Tibet Plateau, and by the dense vegetation and lower relief in the lower monsoon sub-region. In the present study, the gross erosion has been calculated for various sub-basins of the upper Indus River basin (Table 5.1).

Table 5.1 Erosion characteristics of the upper Indus River sub-basins

Station	Sub-basin	Area (km^2)	Erosion rate ($mm\ a^{-1}$)	($t\ km^{-2}\ a^{-1}$)	Gross Erosion ($Mt\ a^{-1}$)
Kharmong	Indus	71,685	2.2	2796	200.5
Yugo	Shyok	79,586	2.6	3263	259.7
Shigar	Shigar	6,891	6.3	7789	53.7
Kachura	Indus	161,651	2.7	3303	533.9
Dainyor	Hunza	13,576	6.4	8002	108.6
Gilgit	Gilgit	12,379	5.3	6539	80.9
Alam	Gilgit	27,953	5.8	7276	203.4
Partab	Indus	192,701	3.2	3959	762.9
Doyian	Astore	3,891	4.2	5256	20.5
Shatial	Indus	203,430	3.2	4011	816.0
Barsin	Indus	207,823	3.3	4059	843.5
Karora	Gorband	567	1.7	2079	1.2
Besham	Indus	212,447	3.3	4046	859.6
Daggar	Brandu	634	1.8	2293	1.5
Darband	Indus	214,505	3.2	4025	863.4
Phulra	Siran	1,035	0.7	864	0.9
Thapla	Siran	2,766	0.6	792	2.2
Tarbela	Indus	219,793	3.20	3947	867.4

5.7 Sediment Transport and Storage Characteristics of the Upper Indus River Basin

Sediment production is the amount of mobilized sediment reaching a channel, and sediment yield is the amount of sediment actually discharged from the drainage basin. In order to construct

the sediment budget, sediment yield values have been derived for the 17 upper Indus sub-basins that are based upon: (1) relationships developed between discharge and suspended sediment concentrations by Ali and De Boer (2007); (2) multiple regression models for predicting specific sediment yields by Ali and De Boer (2008); and (3) spatially distributed sediment yield modelling (Figure 5.5) by coupling of erosion rates and sediment delivery ratios by Ali and De Boer (in review). The specific sediment yields calculated from sediment rating curves along the main stem of the Indus River range from 496 t km^{-2} a^{-1} at Kharmong to 1345 t km^{-2} a^{-1} at Besham Qila, showing a general increase of sediment yields with basin area (Figure 5.6). Among the main tributaries, the Hunza River at Dainyor shows the highest specific sediment yield of 3375 t km^{-2} a^{-1}, which is amongst the largest in the world for a drainage basin of its size, mainly because of very high suspended sediment concentrations in summer meltwater discharges. The channel system in the upper Indus River basin is deeply incised, resulting in narrow or no floodplains, and little opportunity for sediment storage. Runoff and sediment yield data drawn from the available hydrological database for the three typical hydrological stations in each of the three hydro-climatological regions of the upper Indus River basin are presented in Figure 5.7. The long-term annual distribution of runoff and sediment yield appears to be closely associated and shows a strong dependence of sediment transport on runoff at the representative locations for the three regions of the basin.

The sediment storage is the most poorly understood component of sediment budgets (Sutherland and Bryan, 1991) and it varies substantially over time. The total erosion from the upper Indus basin is 868 Mt a^{-1}, but the long-term mean annual sediment yield at Besham Qila just upstream of Tarbela Reservoir is 195.1 Mt a^{-1}. The difference between the

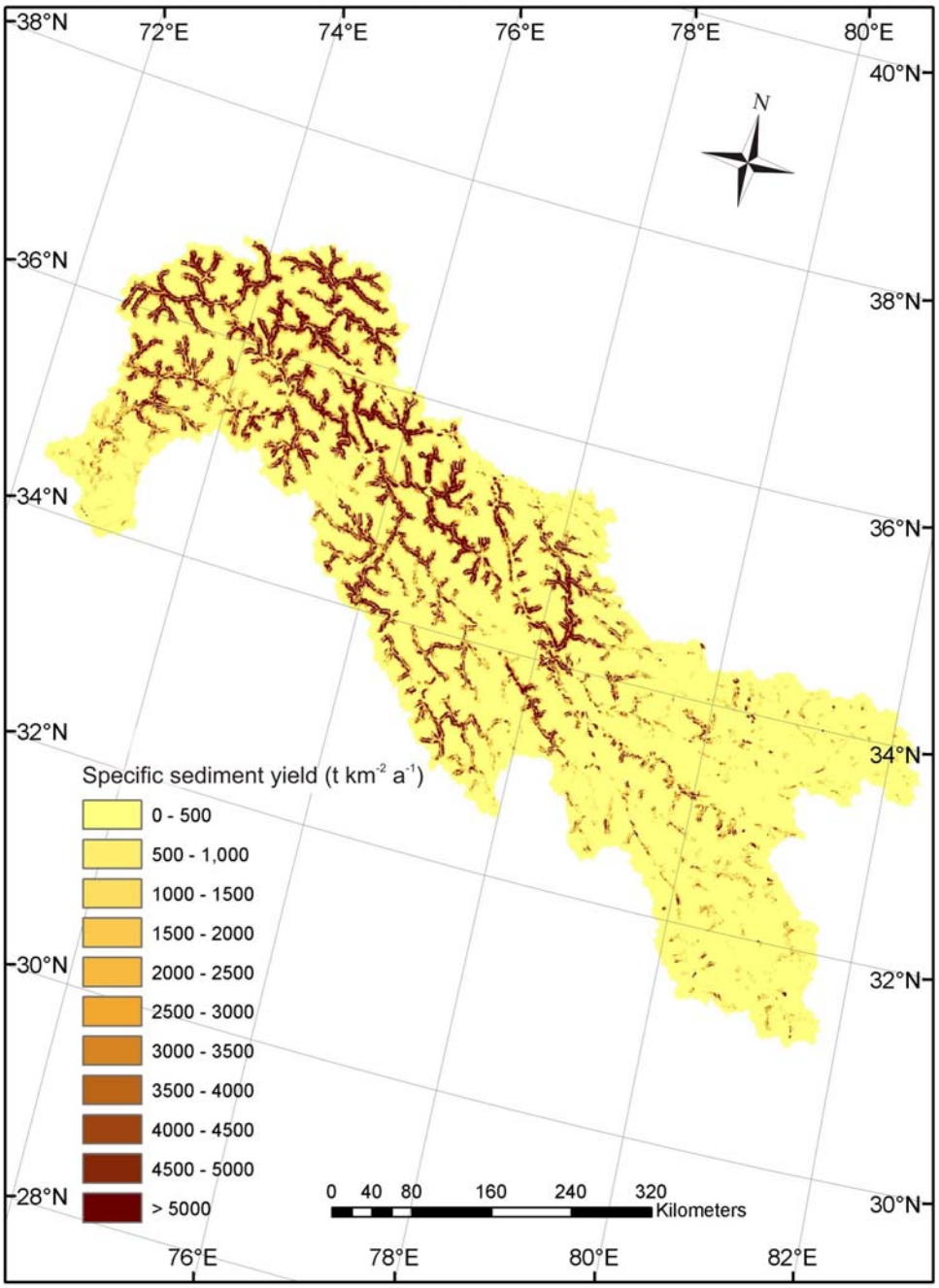

Figure 5.5 Spatial distribution of predicted specific sediment yield (after Ali and De Boer, in review)

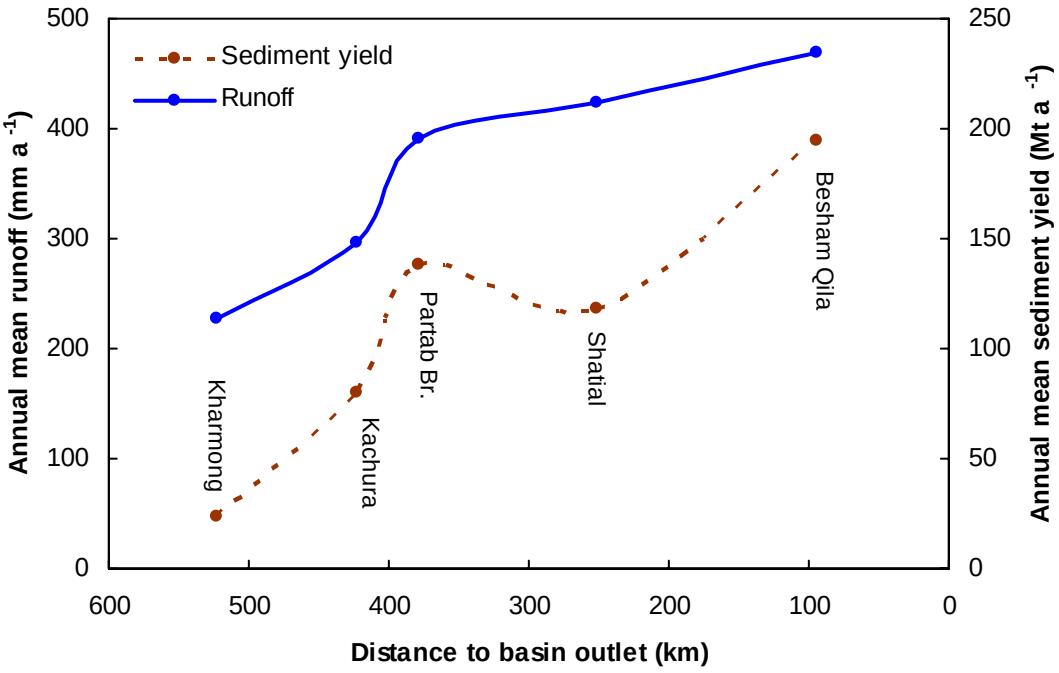

Figure 5.6 Distribution of annual mean sediment yield and runoff along the main Indus River

volumes of the total erosion and sediment yield at Besham Qila is 672.9 Mt a^{-1}. In other words, only 23 % of the eroded sediment is transported to Besham Qila and 77 % is stored in the basin. The spatial distribution of sediment storage in the basin (Figure 5.8) has been determined by calculating the difference between erosion and sediment yield for each cell of the basin. Storage of eroded sediment appears to be widely distributed in the basin and somewhat proportional to erosion as well. It means that the areas undergoing more erosion like the Hunza River basin are also experiencing more storage. The relatively flat Tibetan Plateau which constitutes a major portion of the upper half of the basin is a substantial sediment storage area. Sediment transport characteristics of the upper Indus River investigated by Ali and De Boer (2007) suggested a significant storage on the valley floors along a stretch of 150 km between Partab Bridge and Shatial. This storage is also confirmed from Figure 5.8.

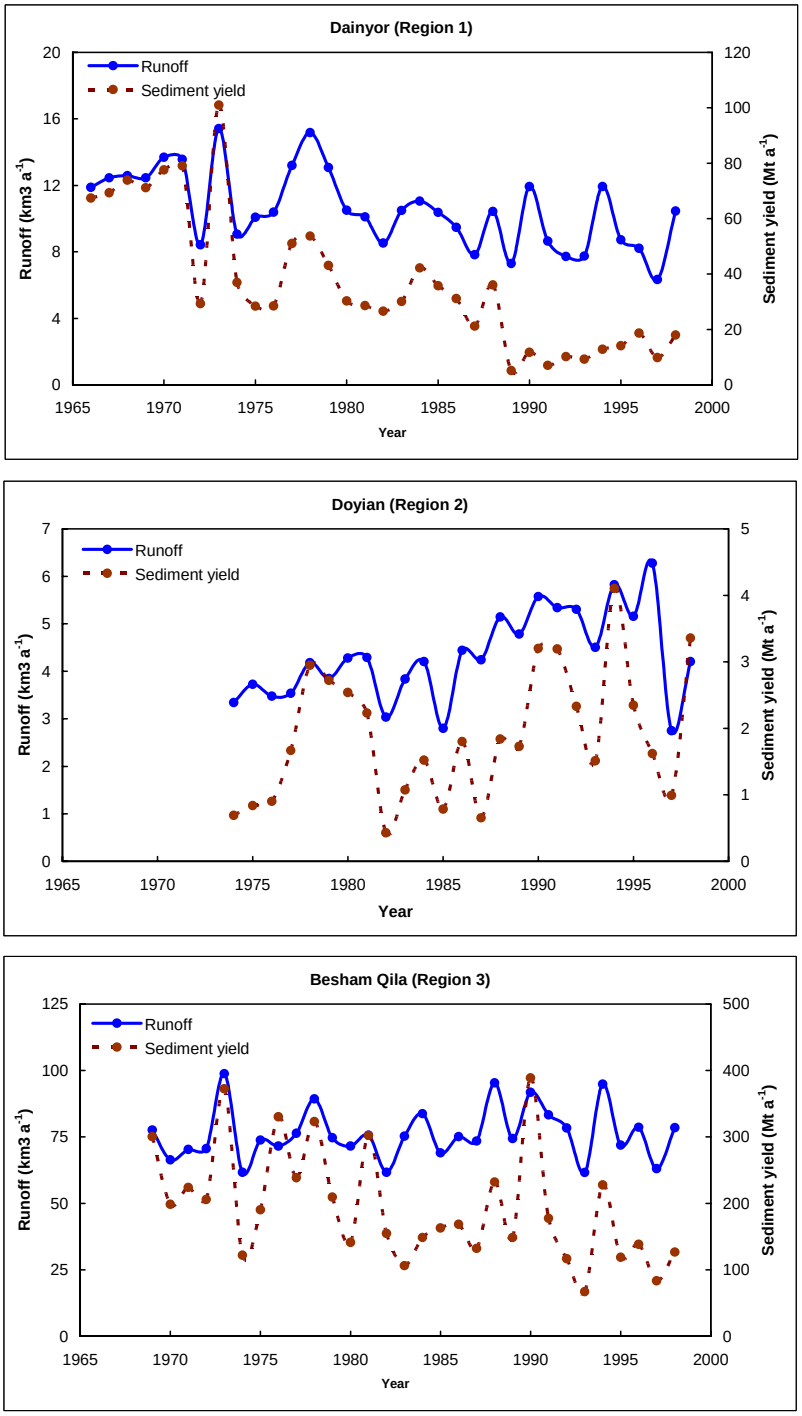

Figure 5.7 Runoff and sediment yield data of three typical hydrological stations in three characteristic regions of the upper Indus River basin

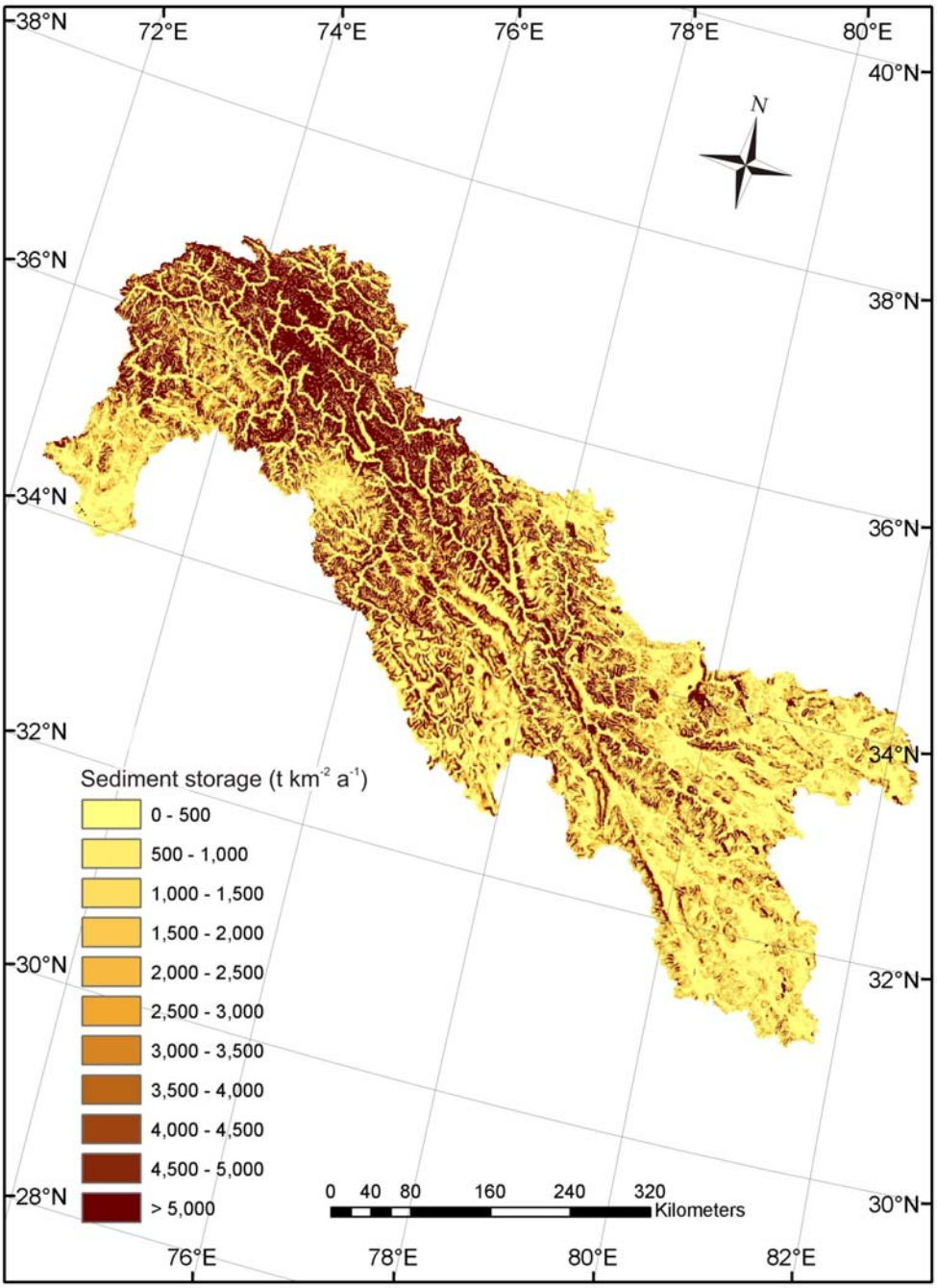

Figure 5.8 Sediment storage in the upper Indus River basin

5.8 The Sediment Budget of the Upper Indus River Basin

Reconciliation is the final step in the construction of sediment budget and this involves setting up a balance sheet showing mobilization on slopes, production to channels, sediment yield, and storage changes. In other words, it consists of quantifying the contribution of sediment source areas and carrying out the sediment budget balance calculation at the basin outlet. Sediment from the upper Indus basin is deposited in the Tarbela Reservoir. The sediment budget of the upper Indus basin is displayed in Figure 5.9 which shows the basin divided into three regions, based on hydro-climatic conditions as discussed in section 5.5. This schematic diagram (Figure 5.9) also represents a balance sheet in terms of the erosion contribution of the upper Indus sub-basins, their respective sediment yield, and their contribution to sediment storage in the basin. The values of sub-basin scale erosion are deduced from spatially distributed modelling (Section 5.6). Sub-basin sediment yields have been calculated based on discharge-sediment concentration relationships. Sediment storage values for the regions have been calculated from the difference of erosion and sediment yields. The upper Indus basin sediment budget (Figure 5.9) is characterized by a gross modelled erosion of 868 Mt a^{-1}, a gross modeled storage of 624 Mt a^{-1}, and basin sediment yield of 244 Mt a^{-1}. This sediment budget is exclusively based on modelling results. For the sake of comparison, Figure 5.9 also includes observed sediment yields. A detailed comparison of modelled and observed sediment yields is presented in section 4.7.8 (Figure 4.11) where model evaluations based on accuracy statistics suggest good to satisfactory performance rating for predicted sediment yields. Figure 5.9 presents a balance sheet of 'predicted' sediment input, transport and storage for a large scale drainage basin divided into three characteristic regions. This sediment budget is different from a typical small scale budget.

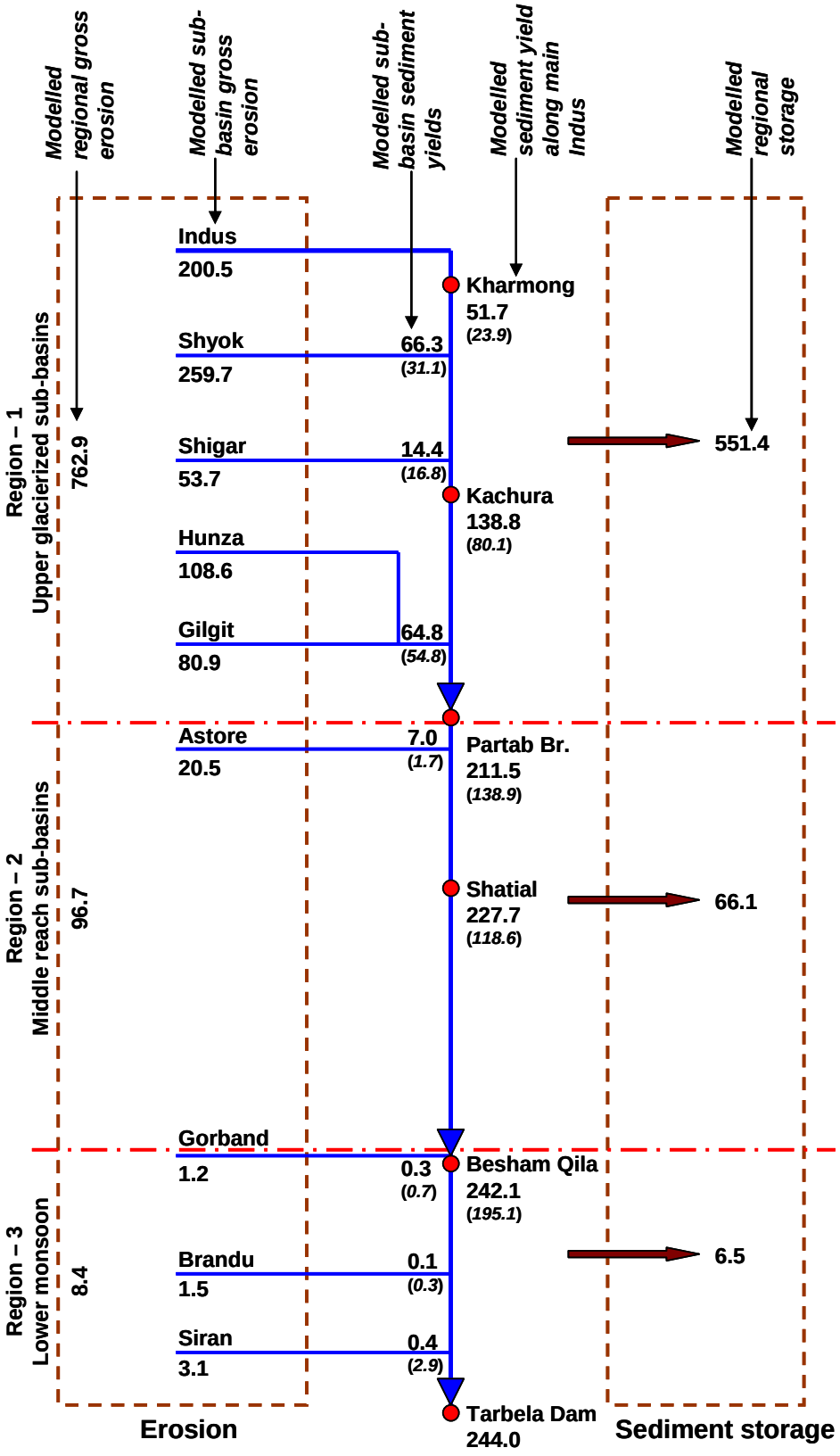

Note: All values in Mt a^{-1}. Values in brackets are observed sediment yields.

Figure 5.9 Schematic representation of the sediment budget of the upper Indus River basin

For example, Dietrich and Dunne (1978) constructed a detailed sediment budget for 16.2 km^2 Rock Creek basin in the Coast Range of Oregon, which is based on the different erosional and depositional processes involved.

Region (1) occupies the major part (87.6%) of the basin area in the Himalayas, Karakorum and Hindu Kush mountains. It accounts for 762.9 Mt a^{-1} (or 87.9%) of total basin erosion, 551.4 Mt a^{-1} (or 88.4%) of the total basin storage, and 211.5 Mt a^{-1} (or 86.6%) of the total basin sediment yield. The large proportion of sediment storage in the region can be explained by the flat, low relief upper Indus and Shyok River basins located on the Tibet Plateau, upstream of the confluence of the Indus and Shyok Rivers, which constitute a substantial part of the region. Major contributions come from the Karakoram (Hunza) part of the basin, which contributes disproportionately higher sediment yield (22.8%) than the relative basin area (8.1%) would indicate (Ali and De Boer, 2007). Based on an analysis of Nd isotopes, Foster and Carter (2007) also concluded that major erosion in the Western Himalaya occurs predominantly in the Karakoram Belt and contributes significantly to the sediment flux delivered to the Indian Ocean by the Indus. This is also reflected in the very high suspended sediment concentrations in summer melt-water discharges of the Hunza River (Ferguson, 1984).

Region (2) occupies the central part of the basin and covers 9% of the basin area. It is responsible for 96.7 Mt a^{-1} (or 11.1%) of total basin erosion and 66.1 Mt a^{-1} (or 10.6%) of total basin storage. The decrease in sediment yield between Partab Bridge and Shatial is likely an artifact caused by the low frequency of sampling and site specific, uneven distribution of sediments concentration near one bank of the river. The Nanga Parbat Massif is an important

feature in this region. Clift *et al*. (2000, 2001) demonstrated that sediment in the Indus system is preferentially eroded from the western Tibetan Plateau and the Karakoram, and erosion from rapidly uplifting massifs, most notable the Nanga Parbat-Harramosh Massif, does not represent a major source of fan sediment. Lee *et al*. (2003) studied the trace element composition of detrital amphibole grains of the Indus River and concluded that the rapidly exhuming Southern Karakoram Metamorphic Complex is the dominant sediment source to the deep-sea Indus Fan. Although the Nanga Parbat Massif, located adjacent to the river's course is also rapidly exhuming, it is not an important source of sediment despite the high erosion rate, probably because of its relatively small contributing area.

Region (3) covers only 3.4% of the basin and is responsible for 8.4 Mt a^{-1} (or 1%) of total basin erosion and 6.5 Mt a^{-1} or (1.0%) of total basin storage. This region is characterized by an immediate and large response to monsoon rainstorms and most of the eroded sediment is transported as a result of flashfloods.

5.9 Conclusions

This paper has demonstrated a methodological framework for developing a sediment budget for a large drainage basin using a combination of multiple data sources. The division of the basin into three characteristic regions (i.e., the upper glacierized sub-basins, middle reach sub-basins, and lower monsoon sub-basins) based on hydro-climatological data analysis provides a basis for understanding the sediment dynamics of the basin. Sediment fluxes from the sources and amounts of deposition in the basin estimated by analyzing a variety of hydrological and

geospatial data, and by spatially distributed modelling of erosion and sediment yield provide the sediment budget for the upper Indus River basin. The long-term mean annual sediment budget of the upper Indus River basin is characterized by sediment inputs of 762.9, 96.7 and 8.4 million tons, and sediment storages of 551.4, 66.1 and 6.5 million tons for the upper, middle, and lower regions of the basin, respectively. The sediment budget indicates that the major source of eroded sediment is located in the Karakoram part of the basin, drained by the Hunza River, that contributes a sediment yield disproportionate to its drainage area. Substantial sediment storage occurs on the relatively flat Tibetan Plateau, and in the reach between Partab Bridge and Shatial. The relatively low data demanding framework for sediment budget construction of large drainage basins presented in this study is mainly dependent on the global geospatial environmental datasets available in the public domain and therefore it can be applied to other large data sparse drainage basins of the world.

5.10 References

Ahmad, N. (1993), *Water Resources of Pakistan and Their Utilization.* Shahid Nazir, Lahore, Pakistan.

Ali, K. F., and D. H. De Boer (2003), Construction of sediment budgets in large scale drainage basins: the case of the upper Indus River, in *Erosion Prediction of Ungauged Basins (PUBs): Integrating Methods and Techniques*, edited by D. H. De Boer et al., *IAHS Publ*., *279*, 206–215.

Ali, K. F., and D. H. De Boer (2007), Spatial patterns and variation of suspended sediment yield in the upper Indus River basin, northern Pakistan, *J. Hydrol.*, *334*, 368–387, doi: 10.1016/j.hydrol.2006.10.013.

Ali, K. F., and D. H. De Boer (2008), Factors controlling specific sediment yield in the upper Indus River basin, northern Pakistan, *Hydrol. Processes*, *22*, 3102–3114, doi: 10.1002/hyp.6896.

Ali, K. F., and D. H. De Boer (in review), Spatially distributed erosion and sediment yield modeling in the upper Indus River basin.

Clift, P. D. (2002), A brief history of the Indus River, in *The Climatic and Tectonic Evolution of the Arabian Sea Region*, edited by P. D. Clift et al., *Geological Society, London, Special Publications*, *195*, 237–258, doi: 10.1144/GSL.SP.2002.195.01.13.

Clift, P. D., C. Gaedicke, N. Shimizu, G. Layne, and M. Clark (2000), 55 million years of Tibetan and Karakoram evolution recorded in the Indus Fan, *EOS, 81*, 277–282.

Clift, P. D., N. Shimizu, G. Layne, C. Gaedicke, H. U. Schlüter, M. Clark, and S. Amjad (2001), Development of the Indus Fan and its significance for the erosional history of the western Himalaya and Karakoram, *Geological Society of America Bulletin*, *113*, 1039–1051.

Collins, D. N., and S. I. Hasnain (1995), Runoff and sediment transport from glacierized basins at the Himalayan scale, in *Effects of Scale on Interpretation and Management of Sediment and Water Quality*, edited by W. R. Osterkamp, *IAHS Publ*., *226*, 17–25.

De Boer, D.H., and K. F. Ali (2002), Sediment budgets and self-organization in a cellular landscape model, in *The Structure, Function and Management Implications of Fluvial Sedimentary Systems*, edited by F. J. Dyer et al., IAHS Publ., *276*, 365–372.

Dietrich, W. E., and T. Dunne (1978), Sediment budget for a small catchment in mountainous terrain, *Geomorphology*, *29*, 191–206.

Dietrich, W. E., T. Dunne, N. F. Humphrey, and L. M. Reid, (1982), Construction of sediment budgets for drainage basins: in *Sediment Budgets and Routing in Forested Drainage Basins*, edited by F. J. Swanson et al., pp. 5–23, U.S.D.A. Forest Service General Technical Report PNW–141.

Ferguson, R. I. (1984), Sediment load of the Hunza River, in *The International Karakoram Project*, edited by K. J. Miller, Cambridge University Press, Cambridge, 580–598.

Foster, G. L., and A. Carter (2007), Insights into the patterns and locations of erosion in the Himalaya – A combined fission-track and in situ Sm–Nd isotopic study of detrital apatite, *Earth and Planetary Science Letters*, *257*, 407–418

Gupta, A., L. Hock, H. Xiaojing, and C. Ping (2002), Evaluation of part of the Mekong River using satellite imagery, Geomorphology, *44*, 221–239.

Jain, S. K., P. K. Agarwal, and V. P. Singh (2007), *Hydrology and Water Resources of India*, Springer, Dordrecht.

Kesel, R. H., E. G. Yodis, and D. J. McCraw (1992), An approximation of the sediment budget of the lower Mississippi River prior to human modification, *Earth Surface Processes and Landforms*, *17*, 711–722.

Lee, J. I., P. D. Clift, G. Layne, B. Blum, and A. A. Khan (2003), Drainage, sediment transport, and denudation rates on the Nanga Parbat Himalaya, Pakistan, *Geomorphology*, *55*, 25–43.

Lehre, A. K. (1982), Sediment budget of a small coast range drainage basin in North-Central California, in *Sediment Budgets and Routing in Forested Drainage Basins*, edited by F. J. Swanson et al., pp. 67–77, USDA Forest Service, General Technical Report PNW-141.

Lu, X. X., and D. L. Higgitt (1999), Sediment yield variability in the Upper Yangtze, China, *Earth Surf. Processes and Landforms*, *24*, 1077–1093.

Meadows, A., and P. S. Meadows (Eds.) (1999), *The Indus River: Biodiversity, Resources, Humankind*, Oxford University Press, Karachi, Pakistan.

Miller, K. J. (Ed.) (1984), *The International Karakoram Project*, Cambridge University Press, Cambridge.

Molnar, P., and P. Tapponnier (1975), Cenozoic tectonics of Asia: Effects of a continental collision, *Science*, *189*, 419–426.

Phillips, J. D. (1991), Fluvial sediment budgets in North Carolina Piedmont, *Geomorphology*, *4*(3/4), 231–242.

Ramos-Scharrón C. E., and L. H. MacDonald (2007), Development and application of a GIS-based sediment budget model, *Journal of Environmental Management*, *84*(2), 157–172.

Reid, L. M., and T. Dunne (1996), *Rapid Evaluation of Sediment Budgets*, Catena Verlag GMBH, Reiskirchen, Germany.

Rondeau, B., D. Cossa, P. Gagnon, and L. Bilodeau (2000), Budget and source of suspended sediment transport in St. Lawrence River in Canada, *Hydrol. Processes*, *14*(1), 21–36.

Rovira, A., R. J. Batalla, and M. Sala (2005), Fluvial sediment budget of a Mediterranean river: the lower Tordera (Catalan Coastal Ranges, NE Spain), *Catena*, *60*(1), 19–42.

Rustomji, P., G. Caitcheon, P. Hairsine (2008), Combining a spatial model with geochemical tracers and river station data to construct a catchment sediment budget, *Water Resour. Res*., *44*, W01422, doi:10.1029/2007WR006112.

Searle, M. P. (1991), *Geology and Tectonics of the Karakoram Mountains*, Wiley, New York.

Shi, C., and D. D. Zhang (2005), A sediment budget of the lower Yellow River, China, over the period from 1855 to 1968, *Geografiska Annaler, Series A: Physical Geography*, *87*(3), 461–471, doi:10.1111/j.0435-3676.2005.00271.x.

Shroder, J. F. (Ed.) (1993), *Himalaya to the Sea: Geology, Geomorphology and the Quaternary*, Routledge, Chichester.

Slaymaker, O. (1993), The sediment budget of the Lillooet River basin, British Columbia, *Physical Geography*, *14*(3), 304–320.

Sutherland, R. A., and R. B. Bryan (1991), Sediment budgeting: a case study in Katiorin drainage basin, Kenya, *Earth Surf. Processes and Landforms*, *16*(5), 383–398.

Thornes, J. B. (1985), The ecology of erosion, *Geography*, *70*, 222–234.

Thornes, J. B. (1990), The interaction of erosional and vegetational dynamics in land degredation: spatial outcomes, in *Vegetation and Erosion: Processes and Environments*, edited by J. B. Thornes, pp. 41–53, Wiley, Chichester.

Wasson, R. J. (2002), Sediment budgets, dynamics, and variability: new approaches and techniques, in *The Structure, Function and Management Implications of Fluvial Sedimentary Systems*, edited by F.J. Dyer et al., *IAHS Publ.*, *276*, 471–478.

CHAPTER 6 – SYNTHESIS AND SUMMARY

The magnitude and frequency of sediment transport depend not only on the hydraulics of the river system, but also on the complex pattern of sediment availability from the sources in the basin. A true picture of sediment dynamics therefore can only be presented by constructing a sediment budget since it provides a comprehensive accounting of the sources and disposition of sediments in the drainage basin (Walling and Horowitz, 2005). Quantifying a sediment budget using classical field-based techniques is labour intensive, time-consuming and expensive for poorly gauged, large drainage basins. The availability of global environmental datasets in combination with GIS and remote sensing techniques provides an opportunity for identifying potential sediment source areas and quantifying their respective contributions in large basins. Following this approach, a framework is presented for constructing sediment budgets for large, data-sparse drainage basins. The methodological framework consists of five steps: (1) analyzing hydro-climatological data for dividing the drainage basin into characteristic regions, and calculating sediment yields; (2) investigation of major controls on sediment yields; (3) identification and mapping of sediment source areas by spatially distributed modelling of erosional processes; (4) spatially distributed modelling of sediment yields; and (5) carrying out the sediment budget balance calculation at the basin outlet. The next section presents the synthesis and summary of conclusions drawn following the implementation of this sediment budget framework in the mountainous upper Indus River basin in northern Pakistan.

6.1 Conclusions

6.1.1 Spatial Patterns and Variation of Suspended Sediment Yield in the Upper Indus River Basin

A sediment budget presents an accounting of the sources and disposition of sediment as it travels from its point of origin to its eventual exit from a drainage basin. The hydro-climatic conditions change significantly in a large drainage basin. Therefore, at the starting point of the construction of a sediment budget for a large drainage basin, it is important to divide the basin into smaller characteristic regions for an effective accounting of rates and processes of erosion and sediment transport in the basin.

The upper Indus River basin is over 200,000 km^2 in size and therefore the sediment transport characteristics in the basin show considerable variation due to differences in physiography, climate, hydrologic regime, and drainage area. Following the hydrologic regimes observed by Archer (2003), the basin was subdivided into three characteristic regions based on whether runoff production is controlled by temperature (Region 1, upper, glacierized sub-basins), precipitation (Region 3, lower sub-basins), or a combination of the two (Region 2, middle reaches). The nature of the hydrological response is very different in the monsoon-affected southern part of the basin and in the non-monsoon, glacierized northern part of the basin. In the monsoon basins, the discharge can vary significantly over a few days, with an immediate and

large response in the sediment concentration. Conversely, the non-monsoon basins are predominantly fed by snowmelt, and therefore do not show such high variability.

The seasonal sediment transport regimes for the Shyok, Gilgit, Hunza and Indus Rivers in the glacierized northern Region 1 show the effect of melting snow and ice on generating high runoff in the summer months. In Region 1, 80 to 85% of the annual sediment load is transported in July and August. The seasonal distribution in Region 2 is influenced by the interaction of snowmelt and rainfall. In this region, the Astore River at Doyian shows an early increase in sediment yield starting in May due to snowmelt at lower elevations, and a comparatively lower sediment yield in August due to a decreased importance of ice-melt. Region 3 is mainly rainfed and experiences two types of rainfall: summer monsoon rains, and late winter to early spring rainfall produced by western disturbances. Consequently, two separate peaks of sediment discharge are observed for the Gorband River at Karora in April and July.

The upper Indus basin exhibits distinct patterns of suspended sediment yield along the main Indus River and in each of the three regions. The mean annual sediment yield increases downstream along the Indus River. The Hunza River contributes a much greater proportion of sediment than its drainage area would indicate. The sediment yield decreases between Partab Bridge and Shatial Bridge, possibly reflecting deposition in the valley. The section between Partab Bridge and Besham Qila provides a major contribution to the sediment load at Besham Qila. This can be attributed to the presence of a large number of small, relatively steep catchments that discharge straight in to the Indus River without much opportunity for sediment storage in the narrow valleys.

The specific sediment yield of the main Indus River increases with drainage area, from 355 t km^{-2} yr^{-1} at Kharmong to 1197 t km^{-2} yr^{-1} at Besham Qila. This is contrary to the conventional sediment yield model which holds that specific sediment yield generally decreases with drainage area due to the increased opportunity for sediment storage as drainage area increases. The increase in specific sediment yield along the Indus River can be explained by the predominance of channel erosion as compared to slope (sheet, gully) erosion, and the steep straight channels discharging directly into the Indus River.

An analysis of the magnitude-frequency characteristics of sediment transport in the basin reveals a trend of transporting most sediment during extreme events. The percentage of sediment transported at high discharges decreases downstream. The sediment discharge histograms reveal a variety of forms and a wide range of effective discharges. The effective discharges for tributaries range from 1.5-2.0 to 5.5-6.0 times the average discharge, and decrease downstream. The main Indus River, however, shows a consistent effective discharge in the range of 2.5-3.0 times the average discharge.

6.1.2 Major Controls on Specific Sediment Yield and Construction of Multiple Regression Models for Predicting Specific Sediment Yields

The division of the basin into three characteristic regions based on hydro-climatic data analysis is useful in understanding the sediment dynamics in terms of the spatial patterns and variation of suspended sediment yields in the basin. In order to obtain a more comprehensive

knowledge of the rates and processes of sediment transport component of a sediment budget, it is important as a next step to investigate the major controls on sediment yield in the basin.

The availability of high resolution, global datasets provides an opportunity for examining major controls of specific sediment yield by using modern GIS techniques at a regional scale in large, data-sparse drainage basins. The hydrologic, topographic, climatic, and land use variables extracted from these datasets can provide the detailed spatial patterns of the various environmental characteristics of a basin. Twenty nine variables were derived from geo-spatial datasets available in the public domain and their correlation with specific sediment yield in the upper Indus River basin basin was investigated. Reduction of scatter was obtained by dividing the basin into characteristic regions, and multiple regression models were constructed for estimating sediment yield in the basin. These models of specific sediment yield provide a linkage between hydrological variables and environmental characteristics on a regional scale, and allow the prediction of specific sediment yield at ungauged sites within the basin. For the whole basin, a model incorporating percent snow/ice cover (LC_s), maximum monthly precipitation (P_{max}), hypsometric integral (HI), upstream channel elevation (EL_{ch}), and relief peakedness (R_{pk}) explains 93.7% of the variance in observed specific sediment yield. The diversity of variables in the model indicates considerable variability and complexity of the controls of suspended specific sediment yield in the basin. A regression model with LC_s as a single independent variable, however, explains 73.4 % of the variance, after excluding two outliers from the dataset. Percent snow/ice cover (LC_s), therefore, emerges as the major control of specific sediment yield in the basin.

Subdivision of the hydrologic stations into smaller groups improves the prediction of specific sediment yield in terms of variance explained by the multiple regression models (98.5% in the upper, glacierized sub-basins, 99.4% in the lower, monsoon basins, and 92.4% along the main Indus River). The variables used in the models reflect the different processes of sediment load generation in the various regions. The major role of percent snow/ice cover (LC_s) in predicting specific sediment yield in the upper, glacierized basins reflects the importance of glacial and glaciofluvial processes for generating the sediment load. Mean annual rainfall (P) is the main controlling variable for the lower, monsoon part of the basin. This part of the basin has less relief but is subjected to heavy monsoon rainfall which becomes the dominant factor in controlling erosional processes and in transporting the sediment along the Himalayan topographic front. The importance of relief is well documented in the literature in producing abnormally high sediment yields in mountain areas and basin relief (R) is also the dominant control along the main Indus River. The validation parameters, in terms of positive paired t-test results and model efficiency (ME) values close to 1.0, show that the models present useful tools for predicting specific sediment yield in the upper Indus River basin.

6.1.3 Spatially Distributed Modelling of Erosion and Sediment Yields in the Upper Indus River basin

The expense and logistical problems associated with the construction of sediment budgets for large river basins pose quite a few challenges, including identification and quantification of sediment source areas, and this remains a major challenge in constructing a sediment budget for a large river basin (Brown *et al*., 2009; Wilkinson *et al*., 2009). In addition, the multiple

regression models do not explain all the observed variation in specific sediment yield in the basin, which emphasizes the importance of the need for physically-based, spatially distributed models. Therefore, to complete the 3rd and 4th steps of sediment budget construction, a modeling framework was developed for predicting spatially distributed erosion and sediment yields. Potential erosion rates were calculated with the Thornes model in combination with a surface runoff model using global environmental datasets in a GIS environment at a 1-km spatial resolution and a monthly time scale. Predicted erosion rates are consistent with landscape characteristics including slope, altitude and runoff. 87% of the gross annual erosion takes place in the three summer months, following a similar pattern of distribution in the sediment yields of the basin. The large proportion of the basin area experiencing high erosion rates is representative for a large Himalayan basin with exceptional relief and extreme climatic conditions. Lower erosion rates on the Tibetan Plateau can be explained by the arid climate and low relief, and in the lower monsoon sub-region by the dense vegetation and low relief. Analysis of the erosion rates and basin properties reveals that high erosion rates in the basin are associated with high relief, runoff, and low vegetation cover. The model predicts an average annual erosion rate of 3.2 mm a^{-1} for the upper Indus basin, which is consistent with other reported values. Total erosion in the basin is calculated as 868 Mt a^{-1}, which is approximately 4.5 times the long-term observed sediment yield of the basin.

Spatially distributed sediment yields were predicted by coupling models of erosion and sediment delivery. Higher delivery ratios (SDR>0.6) are found in 18% of the upper Indus basin area, mostly located in the high-relief sub-basins. The sediment delivery ratio is lower than 0.2 in 70% of the basin area, mostly found in the low-relief, flat-terrain sub-basins located on the

Tibetan Plateau and in some portions of the lower monsoon region. The Indus basin shows a general increase in sediment delivery ratio with basin area. Although this trend is contrary to the conventional sediment delivery ratio model, it is consistent with the findings of Ali and De Boer (2007) who identified a trend of increasing specific sediment yields with drainage area in the basin. The mean annual sediment yield of the upper Indus River basin was calculated as 244 Mt a^{-1}, which compares reasonably well to the observed sediment yield of the basin of 195.1 Mt a^{-1}. The ratio of predicted basin sediment yield and gross basin erosion result in a basin sediment delivery ratio of 0.28. Model evaluation based on accuracy statistics shows "very good" to "satisfactory" performance ratings for predicted monthly and sub-basin sediment yields. The results in this study are based on modeling without calibration and it is envisaged that calibrating model parameters would greatly improve model accuracy.

Percent snow/ice cover emerged as an important variable explaining sediment yields in the basin in the earlier part of the study. Although snow and ice coverage is not built in the model for predicting erosion and sediment yields, the model still gives good results. Percent snow/ice cover is important because snow and ice melt drives erosion and sediment yield. On the other hand, snow and ice cover may also indicate an absence of vegetation, i.e., bare soil resulting in more susceptibility to erosion. Therefore, it appears that percent snow/ice cover is also a proxy for other variables. Perhaps the inclusion of percent snow/ice cover may further improve the prediction accuracy. Moreover, the regions are also not built in the model. Nevertheless, regions are confirmed by the hydro-climatological data analysis and they facilitate the construction and interpretation of the sediment budget as explained in the 5th step of the study in the next section.

6.1.4 Construction of Sediment Budget for the Upper Indus River basin

This part of the study accomplishes the last step of sediment budget construction and illustrates the practical applicability of the proposed methodological framework by implementing it in the upper Indus River basin. This involves carrying out sediment budget calculations at the basin outlet based on a mass balance approach by analyzing the amount of sediment contributed by different sub-basins. The division of the basin into three characteristics regions (i.e., the upper glacierized sub-basins, middle reach sub-basins, and lower monsoon sub-basins) based on the hydro-climatological data analysis provides a basis for understanding the sediment dynamics of the basin. Sediment fluxes from the sources and amounts of deposition in the basin estimated by analyzing a variety of hydrological and geospatial data, and by spatially distributed modelling of erosion and sediment yield provide the contribution from basin to basin for compiling a balance sheet at the basin outlet. The long-term mean annual sediment budget of the upper Indus River basin is characterized by a sediment input of 762.9, 96.7 and 8.4 Mt a^{-1}, and sediment storage of 551.4, 66.1 and 6.5 Mt a^{-1} for the upper, middle, and lower regions of the basin, respectively. The sediment budget indicates that the major source of eroded sediment is located in the Karakoram (Hunza) part of the basin that contributes disproportionately higher amount of sediment than its relative basin area would indicate. Substantial sediment storage occurs on the relatively flat Tibetan Plateau, and in the reach between Partab Bridge and Shatial.

6.2 Significance of the Study

A major scientific contribution of this study is that it has resulted in an advancement of the knowledge of constructing sediment budgets by proposing a framework for large data sparse drainage basins. The relatively low data demanding framework for sediment budget construction of large drainage basins presented in this study is mainly dependent on the global geospatial environmental datasets available in the public domain, which offers possibility of applying it to other large data sparse drainage basins of the world with similar topographic, seismotectonic and hydrologic conditions.

The practical significance and technical contribution of this study has been demonstrated by a successful implementation of the proposed framework of sediment budget construction to the upper Indus basin. Satisfactory predictions of large scale erosion and sediment yield have been made in the basin, and a better understanding of the basin-wide sediment dynamics has been achieved. This is also an example of innovative application of existing knowledge in terms of spatially distributed implementation of erosion, sediment delivery, sediment yield, and sediment storage models. Identification of large sediment source areas with the application of multidata type analysis in the GIS environment rather than field survey methods is an economic application of this study in presenting a cost-effective and efficient way of studying sediment dynamics of a large drainage basin. This approach is thus helpful to understand not only the geomorphologic processes in headwater regions, but also to ensure a better future planning of water uses and their design and operation in a more economical way.

This study is useful to ensure the basic requirements of water for drinking, irrigation and hydropower for the fast growing population in remote areas of Himalayan and Karakoram

mountains. The results of this study can also be utilized when remedial measures as well as new development projects are started for sustainable development in these areas. Further application include improving forecasting of food availability and living conditions of poor and marginalized groups living mainly in these upland high mountain areas of the Indian Subcontinent, in relation to water resources management strategies. In addition to the population of the project area, a number of agencies and organizations such as Pakistan like the Water and Power Development Authority (WAPDA), irrigations departments and water supply boards may benefit from this research.

6.3 Possible Future Steps

This study has addressed the research gap in presenting a methodological framework for constructing sediment budgets for large scale drainage basins. However, some limitations are identified that need to be addressed in future studies.

(1) Availability and accuracy of geo-spatial datasets

Recent development and increased availability of geospatial datasets (e.g., topography, hydrology, climatology, soil, lithology, tectonics, population) in the public domain has provided an opportunity for spatially distributed modelling of Earth surface processes. However, the available datasets differ in spatial and time scales, and give rise to compatibility issues in overlay analysis in a GIS environment. Moreover, there is a lack of information regarding the accuracy of the datasets as well. The inconsistency of the spatial and temporal scales in different datasets,

and the doubts regarding the accuracy of the datasets increase the uncertainty of the model results based on these datasets.

(2) Availability of field measurements

Model validation is extremely important for the reliability of predictions. This, however, requires a comparison between the measured and predicted values from the model. The scarcity of field observations (e.g., erosion measurements in the Himalayas) is another source of uncertainty for the modelling results.

(3) Increasing complexity of erosion processes in the modelling framework

The spatially distributed modelling framework has made satisfactory predictions of erosion and sediment yield in the upper Indus River basin. This framework is relatively simple and it is envisaged that the inclusion of additional processes of erosion and sediment yield would further improve the accuracy of predictions from the modelling framework. As a next step in this study, the modelling framework could be expanded to include snow and ice coverage, bank and channel erosion processes, and mass movements resulting from seismic activities.

(4) Sediment budget of the entire Indus River basin

The present study is based on the upper stretch of the Indus River up to Tarbela Dam. Downstream of Tarbela Dam, the Indus River travels another 1800 km and descends to the Arabian Sea. This stretch of the River, characterized by a number of barrages and inter-basin diversion canals, represents one of the most complex irrigation systems of the World. Another possible step in this study is a sediment budget construction for the entire Indus River basin

which would take into account the complex anthropogenic affects in the lower part of the basin. A body of literature available on the source of sediment found in the Indus Delta (Clift *et al.*, 2002; Lee *et al., 2003*) could prove to be useful in developing this sediment budget.

(5) Application of the developed framework to other data-sparse basins of the world

The developed framework for the construction of sediment budgets for large drainage basins is mainly dependent on global datasets available in the public domain. Therefore, it can be used to constructed sediment budgets for other large, data-sparse and remote drainage basins of the world.

(6) Impact of climate change in the high mountainous Himalayan drainage basins

Climate change models predict strong surface warming in winter in high mountainous regions and significant increase of summer precipitation in monsoon areas (Li *et al*., 1995; IPCC, 2007). The Indus River is included in the World's top 10 rivers at risk due to climate change (WWF, 2007). Climate change will have important implications in the upper Indus River basin in terms of increasing discharges and sediment yields as a result of rapidly melting glaciers. Increasing monsoon precipitation may intensify erosion in the lower part of the basin at first, but may also result in reduced erosion rates due to vegetation growth according to the Langbein and Schumm (1958) model. One billion people are dependent on the snow and ice-melt flows originating from the Himalayas. An investigation of different climate change scenarios affecting the sediment budget dynamics in these high mountainous areas presents yet another possible next step for this study.

6.4 References

Ali, K. F., and D. H. De Boer (2007), Spatial patterns and variation of suspended sediment yield in the upper Indus River basin, northern Pakistan, *J. Hydrol.*, *334*, 368–387, doi: 10.1016/j.hydrol.2006.10.013.

Archer, D. (2003), Contrasting hydrological regimes in the upper Indus basin, *J. Hydrol*. *274*, 198–210. DOI: 10.1016/S0022-1694(02)00414-6.

Brown, A. G., C. Carey, G. Erkens, M. Fuchs, T. Hoffmann, J–J. Macaire, K–M, Moldenhauer, and D. E. Walling (2009), From sedimentary records to sedimentary budgets: Multiple approaches to catchment sediment flux, *Geomorphology*, *108*, 35–47.

Clift, P. D., C. Gaedicke, R. Edwards, J. I. Lee, P. Hildebrand, S. Amjad, R. S. White, and H. U. Schülter (2002), The stratigraphic evolution of the Indus Fan and the history of sedimentation in the Arabian Sea, *Marine Geophysical Researches*, *23*, 223–245.

IPCC (2007) IPCC Fourth Assessment Report (AR4). Climate Change 2007: Impacts, Adaptation and Vulnerability. Contribution of Working Group II to the Fourth Assessment Report of the Intergovernmental Panel on Climate Change. M.L. Parry, O.F. Canziani, J.P. Palutikof, P.J. van der Linden and C.E. Hanson, Eds. Cambridge University Press, Cambridge, UK, 976 pp

Langbein, W.B., and S.A. Schumm (1958) Yield of sediment in relation to mean annual precipitation. *Trans. Am. Geophys. Un*, *39*, 1076-1084.

Lee, J. I., P. D. Clift, G. Layne, J. Blum, and A. A. Khan (2003), Sediment flux in the modern Indus River traced by the trace element composition of detrital amphibole grains, *Sedimentary Geology*, *160*, 243–257.

Li, X.D., Z.C. Zhao, S.W. Wang, and Y.H. Ding (1995) Evaluation of CGCM and simulation of regional climate change in east Asia. *Acta-Meteorologica-Sinica*, *9*(4), 385-401.

Walling, D. E., and A. J. Horowitz (2005), *Sediment Budgets 1*, Proceedings of Foz do Iguaçu Symposium April 2005, Brazil, *IAHS Publ*., *291*.

WWF (2007) World's top 10 rivers at risk. WWF Global Freshwater Programme. Zeist, the Netherlands.

Wilkinson, S. N., I. P. Prosser, P. Rustomji, and A. M. Read (2009), Modelling and testing spatially distributed sediment budgets to relate erosion processes to sediment yields, *Environmental modelling & Software*, *24*, 489–501.